THE ROLE OF PROTEIN CARBONYLATION IN THE ADIPOCYTE NUCLEUS

A DISSERTATION
SUBMITTED TO THE FACULTY OF
UNIVERSITY OF MINNESOTA
BY

AMY KATHERINE HAUCK

IN PARTIAL FULFILLMENT OF THE REQUIREMENTS
FOR THE DEGREE OF
DOCTOR OF PHILOSOPHY

DR. DAVID A BERNLOHR, ADVISOR

NOVEMBER 2017

Acknowledgements

The work described herein was only possible through the combined efforts of many people who I have been lucky to work with. First and foremost, I would like to thank my advisor, Dr. David Bernlohr, for sharing his vision, intellect, optimism, and enthusiasm for the scientific process. Your mentorship, encouragement, and criticism have been incalculably valuable.

The Bernlohr laboratory is an exceptional group of scientists that have assisted me in many ways throughout my graduate studies. Specifically, my fellow graduate students Kaylee, Dalay, Ajeetha, and Arthur have become both cherished friends and colleagues. I would like to acknowledge Rocio, whose kind heart, patience, and intelligence are something to strive for. I would especially like to thank Wendy Hahn, whose experimental prowess is unmatched. I have learned so much from you. Finally, I would like to acknowledge Dr. Yue Chen and Dr. Tong Zhou for their collaboration and significant contribution to this work.

In addition, I would like to thank the members of my thesis committee, Anja Bielinsky, Lincoln Potter, Edgar Arriaga, and David LaPorte for their guidance and insight.

I am particularly grateful to my peers in the BMBB and MCDB&G programs for their friendship, encouragement, collaboration, and wisdom. It has been a complete joy to be a part of this community. Thank you for making me think deeper and laugh louder.

Finally, I would like to thank my family. To my parents Mary and Rolf, for being brilliant examples of the type of person and professional I hope to be. To my sisters Kari and Sarah for their support, friendship, and compassion. To Tim, who inspires me every day.

Dedication

This thesis is dedicated to Elaine, Jaran, Ruth, Rod, Mary, & Rolf who taught me to work hard to chase my dreams.

Abstract

As the incidence of obesity rises globally, it has become increasingly imperative to identify the mechanisms that cause obesity-related metabolic disease. In particular, oxidative stress in the adipose tissue is known to cause metabolic dysfunction, but the mechanisms that contribute to this process remain unclear.

Protein carbonylation refers to the post-translational modification of lysine, cysteine, and histidine residues by diffusible electrophilic lipids. Specifically, 4-hydroxy-2-nonenal (4-HNE) and 4-hydroxy-2-hexenal (4-HHE) are produced at high levels in obese adipose tissue as a direct result of increased oxidative stress. The studies herein focus on the hypothesis that protein carbonylation is a mechanistic link between elevated oxidative stress and metabolic dysfunction in obese adipose tissue.

We found that protein carbonylation is elevated specifically in the nucleus of adipocytes as a consequence of obesity and of aging. Proteomic evaluation of these modifications revealed that the core histones and zinc finger proteins are major targets of carbonylation. Since these proteins are critical regulators of transcriptional mechanisms, these data describe a potential link between oxidative stress and altered expression of metabolic pathways in adipose tissue.

TABLE OF CONTENTS

List of Tables

List of Figures

Chapter 1

Adipose carbonylation and mitochondrial dysfunction

Chapter 2

Redox regulation of DNA binding proteins in adipocytes and the role of nuclear protein carbonylation

Chapter 3

Histone carbonylation is a novel redox-regulated epigenomic modification that accumulates with obesity and aging

CHAPTER ONE

Adipose Carbonylation and Mitochondrial Dysfunction

Amy K. Hauck, Dalay M. Olson, Joel S. Burrill, and David A. Bernlohr.

Department of Biochemistry, Molecular Biology, and Biophysics, University of Minnesota, Minneapolis, MN 55455

This chapter contains an original research article previously published.

Introduction

Dramatic increases in obesity and associated metabolic disease in modern culture have spurred great interest in defining molecular mechanisms underlying obesity-induced metabolic syndrome. While decades of work have contributed to a general model of obesity-induced insulin resistance, there remain many open questions in the field. Importantly, a primary goal both from a basic science perspective as well as from a clinical point of view is to identify the *initiating factors* that drive metabolic dysfunction in the obese state.

At the molecular level, obesity-linked metabolic disease can be described as a chronic low-grade pro-inflammatory state in which immune cell-derived cytokines such as tumor necrosis factor alpha (TNF-α), interleukin 1 beta (IL-1β), interleukin 6 (IL-6) and interferon gamma (IFNγ) initiate a cascade of molecular events in adipocytes leading to increased oxidative stress, impaired mitochondrial function and endoplasmic reticulum (ER) stress that alter adipokine secretion and result in local and systemic insulin resistance. However, despite advances in this mechanistic understanding, the molecular pathways that connect oxidative stress to mitochondrial dysfunction and ER stress remain unclear. Oxidative protein damage via carbonylation, particularly in the mitochondrion, represents an attractive mechanistic target behind this process and has garnered much attention over the last decade.

Protein carbonylation refers to oxidative protein damage that results from post-translational modification of proteins with reactive lipid aldehydes such as 4-hydroxy *trans* 2,3 nonenal (4-HNE), 4-hydroxy trans 2,3 hexenal (4-HHE), and 4-oxo *trans* 2,3 nonenal (4-ONE). Lipid aldehydes are formed at high levels under conditions of increased oxidative stress and as such, protein carbonylation has long been considered a biomarker of oxidative stress in adipocytes, neurons, and muscle cells. It is now appreciated that protein carbonylation plays a major role in a wide array of cellular processes including the oxidative stress response, apoptosis, mitochondrial function, and cell proliferation[1]. Moreover, numerous studies suggest that protein carbonylation may serve as an initiating factor that contributes to the development of various metabolic disease states including neurodegeneration, aging, and insulin resistance[2-6].

Protein carbonylation is acutely relevant to the field of adipose biology for oxidative stress is a major effector of metabolic disease in the obese state in humans and can be studied readily in a number of mouse and cell-based systems[7,8]. Furthermore, the adipocyte contains very high levels of fatty acyl groups in the form of triacylglycerol, making the fat droplet a rich potential source for aldehyde synthesis, a quality that renders adipose tissue particularly susceptible to lipid oxidation and protein carbonylation. Herein we describe oxidative stress in adipose tissue, its linkage to protein carbonylation, the current methods used to detect and analyze carbonylated proteins as well as provide a

comprehensive evaluation of known proteins and pathways that are targets of these modifications in adipose biology.

Reactive Oxygen Species (ROS)

Classically, oxidative stress is defined as an imbalance between the production of oxidants and the presence and activity of the antioxidant defense system. Although the term oxidative stress encompasses many forms of reactive oxidants, the production and signaling mechanisms of reactive oxygen species are the best characterized and will be the focus of this chapter[7,9].

Within the cellular environment three main reactive oxygen species dominate: superoxide anion ($^{\bullet}O_2^-$), hydrogen peroxide (H_2O_2) and the hydroxyl radical ($^{\bullet}OH$). All ROS forms are generated under basal conditions as products of various metabolic functions within the cell. Due to their high reactivity, each ROS is capable of non-enzymatically modifying proteins, DNA, RNA, carbohydrates and lipids in their biological environment. This quality enables them to act as signaling molecules in metabolic pathways, and in fact, modest production of ROS is required for many cellular functions, including adipogensis[1,10-12]. The high reactivity of these species also renders them toxic to the cell at high levels. As such, the production and metabolism of ROS is tightly controlled by antioxidant enzymes whose role is to reduce the pool of ROS such that oxidative damage to cellular machinery is minimized.

There are several metabolic systems that produce ROS as a consequence of normal enzymatic function. For example, xanthine oxidase, lipoxygenases, cyclooxygenases, nitric oxide synthases and the NADPH oxidase have all been shown to catalyze ROS production[13]. Beyond individual ROS-producing enzymes, the mitochondria contribute greatly to ROS pools, particularly under diseased states and in response to inflammatory stimuli. Strikingly, there are eight known enzymes of ROS production within the mitochondria alone[14,15].

Within the mitochondria, electron leak from the electron transport chain is the most well studied source of ROS. Under physiological conditions NADH and $FADH_2$ oxidation by Complex's I and II, respectively, liberate electrons that are passed between numerous carriers, releasing energy that is used to pump protons into the inter-mitochondrial membrane space. The electrochemical potential created by the proton gradient is then utilized by the F_oF_1 ATP synthase, coupling its energy release to the formation of ATP. However, compared to cardiac or skeletal muscle, adipocytes have very little work function and thus maintain high levels of ATP mostly for triacylglycerol synthesis. Moreover, under conditions where ATP levels are high and NADH oxidation is needed for glucose metabolism to facilitate triacylglycerol synthesis, electrons can leak from the electron transport chain (ETC), most likely at Complexes I and III, to form superoxide anion.

The one electron reduction of molecular oxygen occurs virtually instantaneously as electrons leak from the electron transport chain. Due to the unpaired electron, superoxide anion is unable to pass through lipid membranes and a result, if not enzymatically detoxified, will react and modify biomolecules in its immediate environment. To prevent accumulation of superoxide anion, the mitochondria contain high levels of superoxide dismutase (SOD) for production of hydrogen peroxide (**Figure 1**).

Hydrogen peroxide (H_2O_2) is the least reactive but most stable of the three major ROS forms. Due to its chemical nature, hydrogen peroxide is capable of both transmembrane diffusion as well as facilitated movement through aquaporins[16,17]. As such, its diffusibility allows it to traverse multiple compartments within the cell and interact with a wide variety of biomolecules distal from its site of formation. Thus, unlike superoxide anion that reacts within its immediate environment, the combined qualities of stability and diffusibility allow for a much broader functional boundary for H_2O_2.

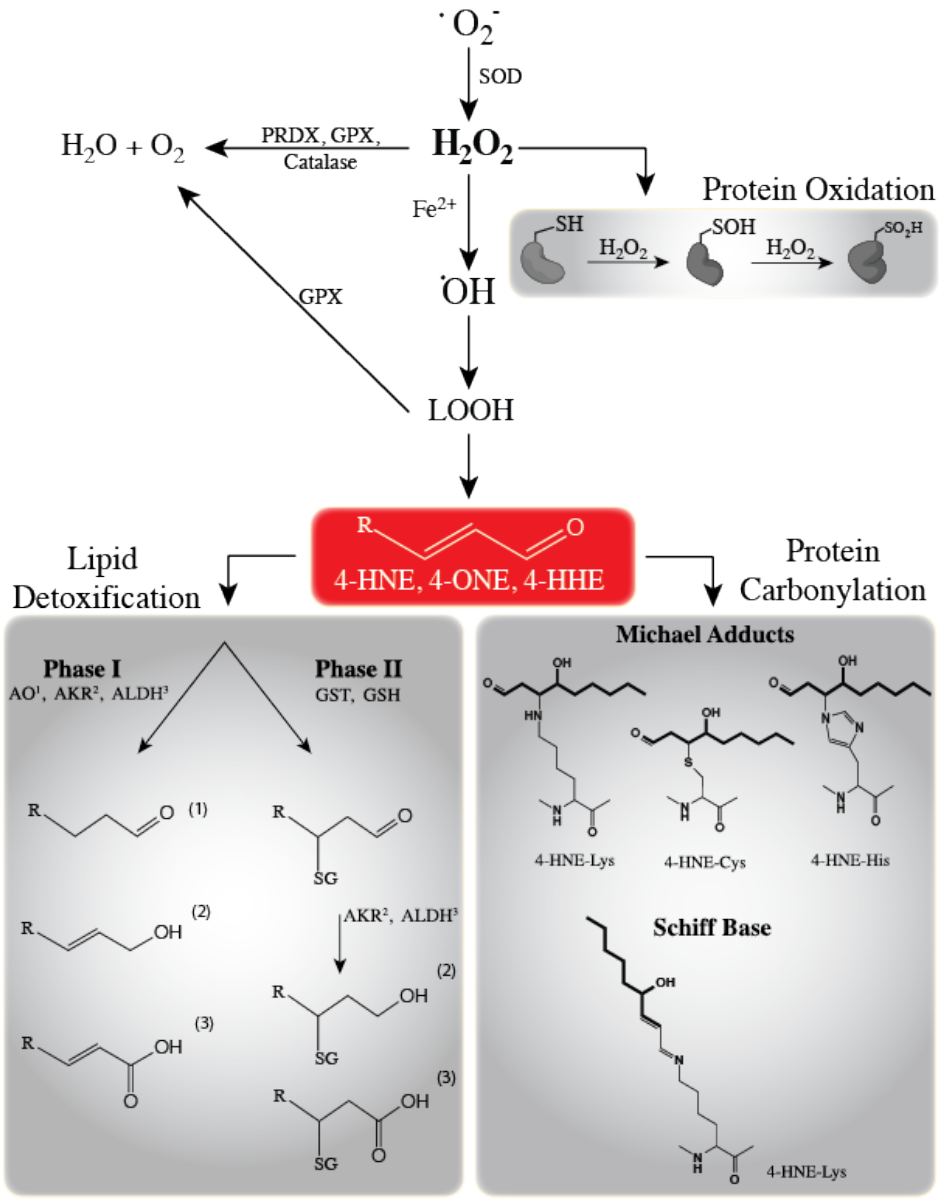

Figure 1. Metabolism of ROS and outcomes of oxidative stress. Superoxide is metabolized via SOD to yield hydrogen peroxide that is subsequently detoxified by PRDX, GPX or Catalase. Alternatively, hydrogen peroxide can undergo Fenton chemistry forming hydroxyl radicals leading to the production of reactive lipid aldehydes. Upon formation, reactive aldehydes can either undergo detoxification by Phase I and Phase II enzymes or can covalently modify protein side chains (Lys, His, Cys) leading to protein carbonylation.

In general, H_2O_2 follows one of three paths in the adipocyte: detoxification by antioxidant enzymes, direct oxidation of biomolecules, or generation of the hydroxyl radical. There are many enzymes that metabolize hydrogen peroxide to water and molecular oxygen including peroxidredoxin, glutathione peroxidase and catalase (**Figure 1**)[18]. These enzymes are present at high levels in the mitochondrion, but are also found throughout other cellular compartments and function to regulate the pool of H_2O_2 to prevent it from reaching toxic levels. If H_2O_2 is not metabolized by antioxidants, it can oxidize a variety of targets and even at low levels is capable of oxidizing sulfur atoms of either cysteine or methionine, thereby altering protein function and affecting signaling pathways.

Alternatively, in cells with high levels of H_2O_2 (potentiated by superoxide dismutase) and a diminished capacity for its metabolism (attenuated glutathione peroxidase, peroxiredoxin), free Fe^{+2} can readily oxidize hydrogen peroxide to the hydroxyl radical through Fenton chemistry[19]. The hydroxyl radical is the most reactive ROS. Unlike superoxide anion and H_2O_2, it is not readily metabolized and is only consumed through the removal of hydrogen atoms from molecules in its immediate environment, resulting in propagation of radical formation through oxidation of neighboring biomolecules. In adipocytes, one common substrate for radical attack is the fatty acyl groups of membrane phospholipid or triacylglycerol. It is this mechanism that links hydroxyl radical formation to the production of lipid

aldehydes and therefore protein carbonylation (**Figure 1**). Once oxidized, such lipids undergo bond rearrangement that can capture further radicals allowing for chain propagation. Secondary oxidation products of fatty acids followed by Hock cleavage can lead to a number of aldehydic products, including malondialdehyde (MDA), straight chain aldehydes and α,β-unsaturated aldehydes such as 4-HNE, 4-ONE, acrolein and 4-HHE (**Figure 2**).

The formation of specific α,β-unsaturated aldehyde species is dependent on the fatty acid composition of membrane phospholipids or triacylglycerol. The length of the fatty acid can play a role, but more importantly in determining the species of aldehyde produced is the degree and location of unsaturation of the fatty acyl unit. As such, 4-HNE and 4-ONE can be formed from n-6 poly-unsaturated fatty acids (PUFAs) such as arachidonic acid (AA) (20:4; n-6) or linoleic acid (18:2; n-6) [20]. This is in contrast 4-HHE, which can be formed from n-3 PUFAs such as docosahexaenoic acid (DHA) (22:6; n-3) and α-linolenic acid (18:3; n-3) (**Figure 2**)[20]. Adipose triacylglycerol is rich in polyunsaturated fatty acids and is therefore a likely site for aldehyde synthesis. Tissues with high levels of DHA and other n-3 PUFAs, like in the brain, can be expected to produce increased levels of 4-HHE compared to 4-HNE/4-ONE[21-24]. Both subcutaneous as well as visceral adipose depots exhibit high levels of n-6 PUFAs and thus can be predicted to produce more 4-HNE/4-ONE[25-27]. This is exemplified by the observation that in murine

liver, levels of 4-HHE are around ~1500 ng/g tissue and 4-HNE levels are adipose tissue free HNE levels are ~100ng/g and free HHE is undetectable[28].

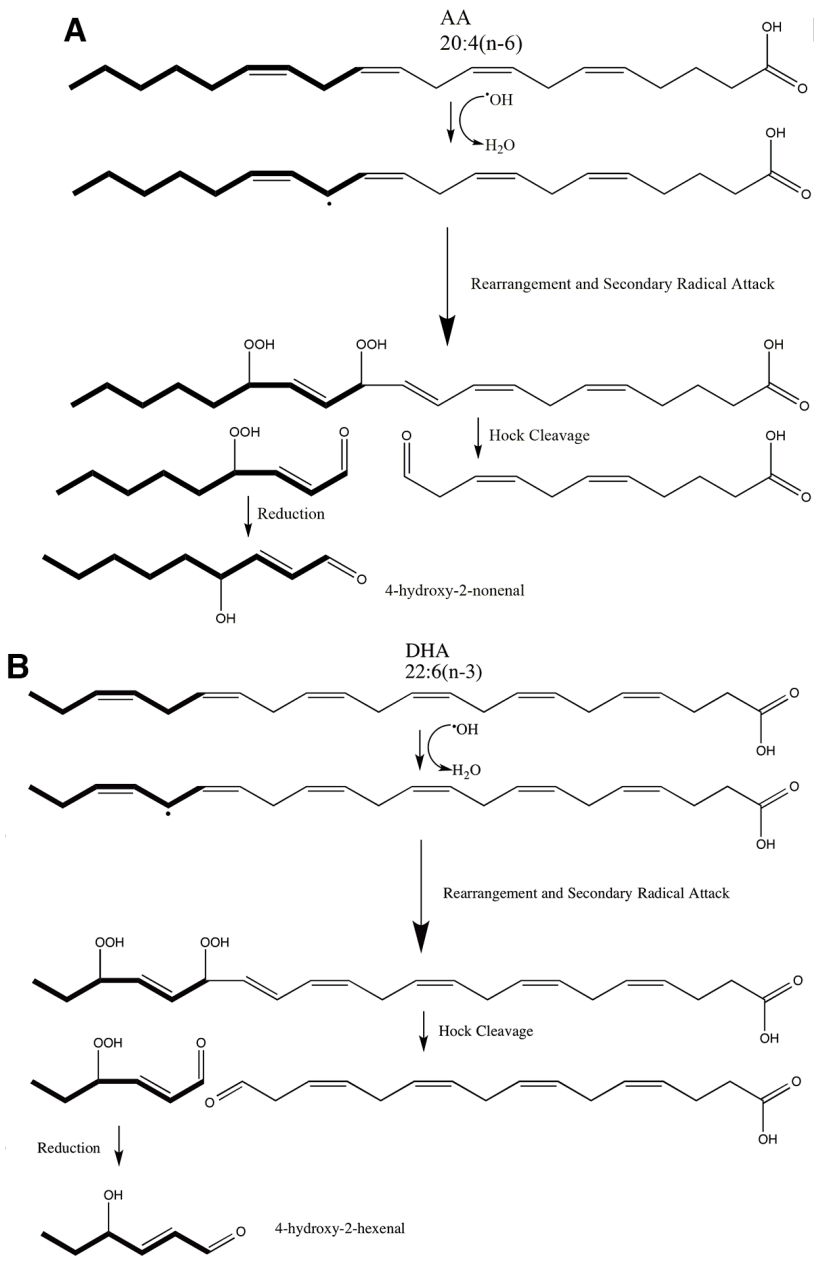

Figure 2. Mechanism of formation of reactive α,β-unsaturated aldehydes from PUFA. Formation mechanism of A) 4-HNE from arachidonic acid (AA) and B) 4-HHE from docosahexaenoic acid (DHA).

Metabolism of Reactive Lipid Aldehydes

In addition to the multiple enzymes expressed by the adipocyte that metabolize and detoxify ROS ($^{\bullet}O_2^-$ and H_2O_2) before they can cause oxidative damage to biomolecules, the cell is also equipped with enzymes that can reduce or mitigate damage to lipids and proteins after it takes place. In particular, the enzymes responsible for the detoxification of reactive lipid aldehydes are of central importance in the adipocyte because this cell type houses large amounts of lipid and thus is particularly susceptible to oxidative damage to lipids under conditions of oxidative stress. Detoxification is achieved via several antioxidant pathways that either enzymatically decrease the reactivity of the lipid (phase I metabolism) or conjugate the lipid to glutathione, allowing for further modification and subsequent export from the cell (phase II metabolism). Here we will consider the specific pathways that are involved in 4-HNE metabolism, as this is the most abundant lipid aldehyde in the adipocyte.

During phase I metabolism, several key enzymes catalyze oxidation and reduction reactions that primarily serve to reduce the reactivity around carbon 3 of the lipid. These reactions are appropriately heralded as detoxification reactions because they yield lipid products that are orders of magnitude less reactive towards proteins, nucleic acids, and lipids. In general, phase I metabolism of reactive lipid aldehydes reduces the susceptibility of the lipid to

Michael addition, therefore protecting the cell against oxidative damage by protein carbonylation[29]. In adipose tissue, aldehyde dehydrogenase (ALDH), aldo-keto reductase (AKR), and alkenal/one oxidoreductase (AO) are the primary enzymes that are responsible for phase I metabolism of 4-HNE (**Figure 1**)[29].

In contrast to phase I metabolism which decreases the reactivity of the lipid, phase II metabolism prevents any possibility for the lipid to undergo Michael addition by conjugating glutathione to the lipid at the C3 carbon[30]. This reaction is primarily carried out by glutathione S-transferases (GSTs) subtype A3 or A4. GSTA4 has a higher affinity for 9 carbon aldehydes than for 6 carbon lipids and has a much greater catalytic efficacy than does GSTA3, making it the primary glutathione S-transferase involved in 4-HNE or 4-ONE dependent protein carbonylation[31]. Glutathionylated lipid metabolites can be further metabolized by phase I enzymes ALDHs and AKRs and are eventually exported from the cell by the Ral-binding GTPase activating protein RLIP76 or multidrug resistance protein 1[32-34].

Oxidative Stress in Obese Adipose Tissue

Research over the last decade has demonstrated that a defining feature in the development of metabolic disease in the obese state is elevated oxidative stress in the adipose tissue. This observation has generated great interest in three central themes: identification of the site/source of ROS production in obese

adipose tissue, uncovering the causes of increased oxidative stress in the disease state, and elucidation of the pathways/mechanisms that connect oxidative stress to metabolic dysfunction and insulin resistance.

At the cellular level there are several sites within the adipocyte that produce high levels of ROS under both physiological and pathological conditions. For example, studies in KKAy mice, a genetic model of hyperphagy, revealed that elevated levels of hydrogen peroxide within adipose tissue is associated with obesity.[35] White adipose tissue from KKAy mice exhibits increased transcript levels of multiple NADPH oxidase subunits including $gp91^{phox}$, the cytosolic component $p47^{phox}$, and $p67^{phox,}$ with no change in transcript levels in liver or skeletal muscle[35]. Consistent with this observation, Pu.1, a transcription factor that has been shown to be responsible for increasing transcription of NADPH oxidase subunits is up-regulated[35].

An additional source of ROS in adipose tissue is xanthine oxidoreductase (XOR), which catalyzes oxidation of xanthine/hypoxanthine to produce uric acid and forms superoxide anion as a byproduct[36]. XOR mRNA expression and enzymatic activity are increased in adipose depots from *ob/ob* mice compared to lean controls, indicating that XOR may be a major cytoplasmic source of ROS in obese adipose tissue[37,38]. Interestingly, targeted deletion of XOR or silencing of its mRNA reduce ROS synthesis, but also attenuate adipogenesis, suggesting a mechanistic link between oxidative stress and preadipocyte differentiation[37]. Indeed, XOR mRNA is upregulated early in the differentiation program of 3T3-L1

cells, concomitant with that of peroxisome proliferator activator γ (PPARγ) and prior to the classical marker of fat cells, fatty acid binding protein 4 (FABP4). These data suggest that XOR-derived ROS may function to activate signaling pathways required for adipogenesis.

Mitochondrial respiration is another a major source of ROS under diseased conditions. Importantly, mitochondrial antioxidants Gsta4, Prdx3, Gpx4 and Aldh2 are all down regulated within visceral adipose tissue of both high fat fed C57Bl/6J mice as well as *ob/ob* mice[28]. Additionally, expression at the transcript level of Sod2 is significantly elevated in visceral adipose tissue of *ob/ob* mice while its cytoplasmic isoform remains unchanged[28]. The increased expression of Sod2 coupled to decreased expression of Prdx3, GPx4 and Gsta4 suggests that enzymatic production of H_2O_2 and chemical synthesis of hydroxyl radicals may drive the oxidative stress phenotype associated with obesity.

Extending this analysis, Curtis *et al.* have shown that Gsta4 is also down regulated in visceral adipose tissue of obese, insulin resistant humans, but not obese insulin sensitive individuals, suggesting that the decreased expression is linked to metabolic disease rather than obesity, per se. The molecular mechanisms that lead to the decreased expression of Gsta4, Prdx3, Gpx4 and Aldh2 are complex and are likely due to inflammatory cytokines. Indeed, treatment of 3T3-L1 adipocytes with either TNF-α, IL-1β, IL-6 or IFNγ leads to

decreased expression of the antioxidant genes, implying that immune cell factors drive increased oxidative stress and mitochondrial ROS synthesis in adipocytes.

While there are many sites of ROS production in the adipocyte that are relatively well characterized, less is known about the upstream signaling events that initiate oxidative stress. Substantial evidence from obesity models in rodents as well as human studies support a mechanistic link between inflammation and oxidative stress, and much recent work has focused on characterizing the pathways and signaling events that support this linkage[6,39-43].

Adipose tissue is composed of multiple cellular subtypes including adipocytes, macrophages, pre-adipocytes and endothelial cells. It has long been appreciated that adipose tissue under obese conditions is characterized by a state of chronic, low grade inflammation, and during the transition from lean to obese the population of pro-inflammatory immune cells increases, occupying up to 40% of the adipose tissue itself[44]. Additionally, pro-inflammatory cells communicate in a paracrine fashion with the adipocyte through secretion of cytokines like TNF-α, IFNγ, IL 1β and IL-6[44]. Increased concentrations of these markers in adipose tissue positively correlates with insulin resistance in humans and rodents[45].

Interestingly, although obesity and metabolic syndrome are tightly linked, there remains a subset of obese individuals who maintain insulin sensitivity[46,47]. These

metabolically healthy, but obese individuals confirm that obesity and metabolic disease can be uncoupled[48]. Indeed, there are many mouse models that de-couple obesity from insulin resistance[49-51]. These models have been crucial tools for understanding metabolic disease. Importantly, evidence from these models has indicated that, in general, insulin sensitivity is maintained under obese conditions when the adipose tissue does not transition to a proinflammatory state. Conversely, insulin resistance is positively correlated with inflammation, particularly within visceral adipose depots[52,53]. As such, it has been suggested that the presence or absence of pro-inflammatory cells within specific adipose tissue beds is a good indicator of whole body insulin sensitivity and metabolic health.

Anatomically, adipose tissue is typically deposited either intra-abdominally or peripherally. Intra-abdominal, or visceral adipose tissue is composed of adipose depots that surround organs within the abdominal cavity. Conversely, subcutaneous adipose tissue is categorized as adipose tissue accumulating directly beneath the skin. Previously, increases specifically in intra-abdominal obesity have been correlated with decreased insulin sensitivity, increased circulating triglycerides and concomitant decreases in high-density lipoprotein levels[54,55]. Consistent with this observation, in humans after adjusting for body mass index, individuals with increased visceral adipose tissue mass also had a greater level of insulin resistance, whereas individuals with an increase only in

subcutaneous adipose tissue mass showed a decreased risk for insulin resistance[54]. Generally, it is the pro-inflammatory phenotype is specific to the visceral depots under obese conditions.

In order to evaluate molecular mechanisms that may contribute to the differences observed in visceral and subcutaneous adipose depots, Long et al analyzed transcriptional antioxidant expression within each depot from both ob/ob mice as well as high-fat fed mice. Overall Prdx3, Gpx4 and Gpx3 expression did not change significantly in subcutaneous tissue in either high fat fed mice or ob/ob mice, whereas the same antioxidant profile was decreased in the visceral adipose tissue depot[28]. Additionally, unlike the visceral adipose tissue from high fat fed C57Bl/6J mice, the subcutaneous adipose tissue showed a significant decrease in free aldehyde levels[28]. Analysis of protein adducts modified by 4-HNE and 4-ONE revealed a significant decrease in protein carbonylation in the subcutaneous and a significant increase in the visceral depots of high-fat fed mice compared to lean controls[28]. In the KKay mouse model, hydrogen peroxide is elevated selectively in the visceral adipose tissue with no change in oxidative stress in liver, skeletal muscle or aorta at seven weeks of age[35]. These data indicate that it is primarily the inflamed adipose depots (visceral) that exhibit oxidative stress and protein carbonylation. This is consistent with a model in which adipose inflammation, oxidative stress, and protein carbonylation are tightly linked in the obese state.

Protein carbonylation in the adipocyte

The generation of reactive lipid aldehydes in adipose tissue is intimately linked to oxidative stress due to the carbonylation of lysine, cysteine, and histidine residues. Carbonylation is the chemical, non-enzymatic nucleophilic addition of the aldehyde to the side chain of lysine, histidine, or cysteine residues at the lipid C3 carbon, producing a covalent lipid adduct on proteins. Following Michael addition, intramolecular rearrangement can occur to generate the more stable hemi-acetal[56-58]. Schiff base formation via the primary amine of lysine residues can also occur, resulting in dehydration of the aldehyde and loss of the free carbonyl. These events are technically not protein carbonylation since the definition has historically been operational through carbonyl-reactive probes, but is often considered in the same class of modifications due to the addition of the lipid aldehyde to lysine residues. Michael adducts are generally more stable and believed to account for the majority of protein-lipid adduction events[59,60].

There are several properties of carbonylation that distinguish it from other well-known types of protein modifications. Most importantly, carbonylation occurs via a non-enzymatic mechanism. Furthermore, there are currently no known enzymes that can remove the modification. Thus, unlike phosphorylation, which is regulated by kinases and phosphatases, or acetylation that is controlled by acetyl transferases and deacetylases, carbonylation is subject to a much less

stringent regulatory cascade. Despite this quality, it is clear that *specific* proteins are highly susceptible to modification, though the regulatory mechanisms that contribute to the specificity of these events are not well understood.

Although increases in ROS can initiate a wide variety of effects throughout the cell, protein carbonylation has garnered much attention as a primary outcome of oxidative stress in obese adipose tissue. Two key points illustrate this logical framework: first, the adipocyte contains a large lipid droplet, which is believed to be a rich potential source for aldehyde synthesis. Second, as mentioned previously, many of the mitochondrial antioxidants involved in reducing lipid peroxides (Gpx4) and detoxifying lipid peroxidation products (Aldh2 and Gsta4) are transcriptionally down regulated in obese, visceral adipose tissue. This expression pattern of antioxidants effectively channels ROS towards lipid peroxidation, resulting in elevated reactive lipid aldehyde pools (4-HNE, 4-ONE, and 4-HHE) within the adipocyte (**Figure 3**). Consistent with this, Long *et al.* measured significantly increased free levels of 4-HNE and 4-ONE in visceral adipose depots of high fat fed and *ob/ob* mice compared to lean controls[61].

Importantly, multiple studies have reported increased protein carbonylation by reactive lipid aldehydes in adipose tissue. In wild-type mice fed a high fat diet protein carbonylation is significantly increased compared to lean controls in visceral adipose depots[6,61]. In humans, adipose tissue protein carbonylation is

positively correlated to body mass index and obese humans exhibit a significant increase in protein carbonylation in whole cell extract from subcutaneous fat depots compared to lean controls[54]. In cultured adipocytes, treatment with the inflammatory cytokine TNF-α or knockdown of antioxidant GSTA4 results in elevated protein carbonylation[11,62].

Together, the combined observations of decreased antioxidant capacity, specifically those that detoxify lipid peroxides and elevate hydrogen peroxide support a model in which the ROS produced in obese adipose tissue is channeled towards the production of reactive lipid aldehydes such as 4-HNE, 4-ONE, and 4-HHE (**Figure 3**). The observed increases in protein carbonylation in adipose cell lysates support the hypothesis that protein carbonylation is a mechanism by which elevated oxidative stress initiates metabolic dysfunction, particularly in the mitochondrion.

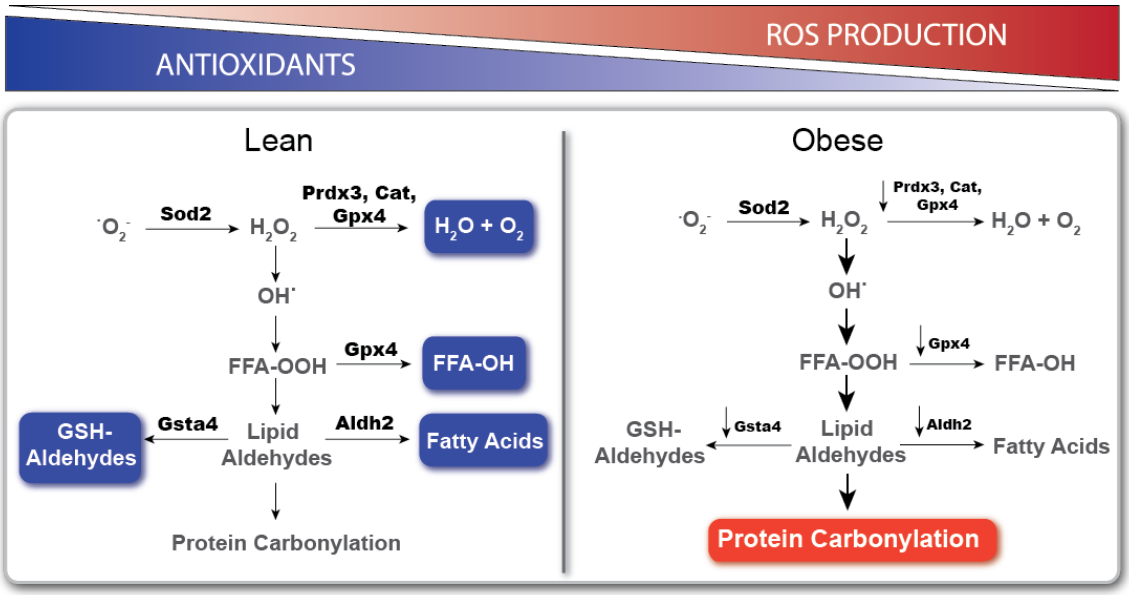

Figure 3. Oxidative stress and antioxidant expression in obese adipose tissue.

Expression of major antioxidant enzymes is downregulated in the transition from the lean to obese state. As a result, ROS is channeled towards the formation of reactive lipid aldehydes and protein carbonylation.

Additional outcomes of oxidative stress

While protein carbonylation is the focus of this chapter, it is important to acknowledge other types of protein modifications that can occur in response to increased oxidative stress. Primarily, alterations in the redox status of proteins by ROS plays an important role both physiologically as well as under diseased states[41,63-65]. Specifically, hydrogen peroxide is thought to play a large role in altering the redox state of proteins. Even at low levels, H_2O_2 can oxidize a variety of targets within the cell, resulting in altered protein function and signaling

pathways. Hydrogen peroxide is capable of oxidizing sulfur atoms of either cysteine or methionine containing proteins (**Figure 1**). Although methionine oxidation is known to occur, its physiological effects on protein function has been limited to only a few well-characterized systems.

It is estimated that approximately 10% of all cysteine residues within the proteome are redox sensitive.[41] Additionally, the sulfur atom, found on cysteine residues, can exist as a thiolate anion ($-S^-$), a free sulfhydryl (-SH), sulfenic acid (-SOH), sufinic acid ($-SO_2H$), sulfonic acid (SO_3H) and as a disulfide (-S-S)[41]. For a given cysteine residue, each oxidation state can have a profound effect on protein conformation, intermolecular interactions, intrinsic activity and degradation[66]. Although hydrogen peroxide is capable of oxidizing free sulfhydryls of cysteine residues, this reaction is unfavorable under physiological conditions. Conversely, hydrogen peroxide is much more reactive with the thiolate anion. Under physiological conditions the pKa of solvent exposed cysteine residues is about 8.3 and therefore, most cysteine residues exist in the protonated form[65,66]. Interestingly, because not all proteins contain cysteine residues in the thiolate form, this offers a level of targeted specificity for oxidation by hydrogen peroxide[41,66]. Unlike other oxidation states, sulfenic acid can be reduced by the enzyme thioredoxin consuming reduced glutathione[65,67]. Although the effects of ROS are primarily discussed under diseased states, it is important

to note that redox state switching is a process that occurs both physiologically and pathologically.

Detection of Protein Carbonylation

Protein carbonylation has taken the spotlight in the field of oxidative stress as a likely mechanism by which oxidative stress initiates metabolic dysfunction and disease. As such, there is an enthusiasm in the field to I) identify proteins that are targets of carbonylation and II) characterize how carbonylation of target proteins changes in response to oxidative stress. Here, we will briefly discuss techniques that have been used successfully to assess carbonylation in adipose tissue or cultured adipocytes. The reader is referred to excellent chapters in this volume that focus exclusively on carbonylation detection methodologies.

Due to the lack of quantifiable properties (UV, spectrophotometric fluorescence or absorbance) of peptides with free carbonyl groups, the detection of carbonylated proteins has largely relied on the use of chemical probes that react with free carbonyls[68,69]. Carbonyl reactive probes have been successfully used for profiling carbonylation patterns and identification of proteins that are susceptible to carbonylation in adipose tissue. Due to the high content of lipid in fat tissue, adipocytes pose a unique challenge to carbonylation research. However, several systems have been successfully employed to assess carbonylated proteins.

2,4-Dinitrophenylhydrazine (DNPH) and biotin-hydrazide (BH), as used by Regnier and colleagues, are the two most widely used carbonyl-reactive probes. These two reagents share in common a hydrazine-like group that undergoes a condensation reaction with free carbonyls. This effectively labels carbonylated proteins and allows for relatively straightforward detection and analysis of labeled proteins using biochemical methods specific for the probe (**Figure 4**). It was DNPH-derivitization of carbonyls that was first used to show that protein carbonylation does not occur equally across the proteome, but rather that specific proteins are subject to oxidative damage by carbonylation under conditions of oxidative stress, an observation that was fundamental for our understanding of the oxidative stress response[70]. In addition, anti-DNPH antibodies used in concert with fluorescent secondary antibodies can be used to assess protein carbonylation by western blot, a method that has been widely employed to study protein carbonylation profiles in response to oxidative stress[71].

The biotin hydrazide probe, like DNPH, forms a hydrazone bond with carbonylated substrates. This method capitalizes on the strong affinity between biotin and avidin (or streptavidin) as it enables detection, capture, and analysis of biotinylated proteins using well-established avidin-based reagents. Beyond 1D western blotting, biotin hydrazide has been used successfully in 2D profiling of carbonylated proteins, quantitative assessment of protein carbonyl content, and

importantly, affinity capture of carbonylated proteins[6,11,62,72]. This method has also been modified to be compatible with mass spectrometry based analysis techniques and has been widely utilized in adipose biology.

Though hydrazine-based probes are by far the most popular reagents used to derivatize protein carbonyls, it worth noting that the excitement in the field for identifying proteins affected by carbonylation has led to the development of new probes designed specifically for mass spectrometry-based approaches. One such probe, AminoxyTMT, contains a carbonyl reactive amine-oxy moiety that reacts specifically with free carbonyls to form an oxime bond and has been used by Griffin and colleagues to detect and analyze sites of protein carbonylation. The conjugation product is slightly more stable and exhibits increased specificity for carbonyls compared to the hydrazine-containing methods. Furthermore, its compatibility with mass spectrometry techniques renders it an attractive alternative to DNPH and BH.

In adipose tissue, many groups have shown that lipid peroxidation products are produced at high levels under conditions of oxidative stress[61,73]. It has been hypothesized that these products constitute the majority of carbonylation events that occur in adipose in response to oxidative challenge. To this end, there are commercially available antibodies directed against common reactive lipid aldehyde adducts including 4-ONE, 4-HNE, MDA, and acrolein. These

antibodies are now widely used to perform gel-based analyses of modified proteins.

Methods for detection of carbonylated peptides

Reagent	*Structure*	*Product*	*MS/MS Compatible*
DNPH	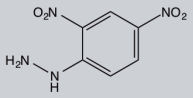	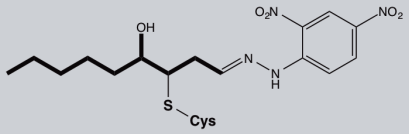	Peptide ID
Biotin-Hydrazide	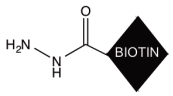	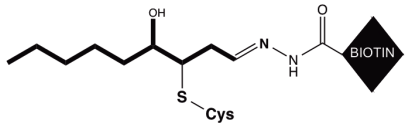	Peptide ID
Aminoxy-TMT	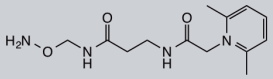	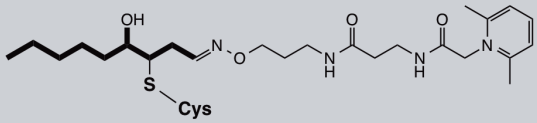	Peptide & Residue ID

Figure 4. Methods for detection of carbonylated proteins

While the number of carbonylation studies is steadily growing, there have been only five studies specifically aimed at identifying targets in adipose tissue or adipocytes. Overall, the number of proteins identified as carbonylated in models of obesity or obese patients is over 400. There are, however, many other proteins have been identified as carbonylated in adipose, but not in the context of a proteomic study. **Figure 5** summarizes five proteomic studies.

Despite the large number of known protein targets, few direct sites of modification have been identified, as BH has been the most commonly used reagent for untargeted approaches to carbonylation proteomics. Newer reagents, such as AminoxyTMT, may increase the ability to identify the specific sites of

modification within adipose tissue. The site-specificity may allow for more mechanistic studies to be done, thus providing direct evidence of how carbonylation effects metabolism and help explain the correlations observed with insulin resistance and oxidative stress.

Proteomic studies of carbonylation targets in adipose tissue

Study	*Year*	*Tissue*	*Number of Targets Identified*	*Derivitization Agent Used*	*Key Proteins Identified*
Grimsrud *et al.*	2007	Mouse Epididymal Adipose Tissue from High Fat Diet	35	Biotin-Hydrazide	AFABP
Singh *et al.*	2007	Human Liposarcoma Cells (SW872)	8	DNPH	AFABP, ALDH
Curtis et al.	2010	Gsta4 Knockdown 3T3-L1 Adipocyte Cell Line	1	Biotin-Hydrazide	XDH
Frohnert *et al.*	2011	Human Subcutaneous Adipose Tissue from Lean and Obese Patients	2	Biotin-Hydrazide	AFABP, EFABP
Curtis *et al.*	2012	Gsta4 Knockdown or Overexpressed 3T3-L1 Adipocyte Cell Lines	370	Biotin-Hydrazide	SLC25A3, NDUFA2, NDUFA3, TCA Cycle Enzymes, BCAA Metabolism Enzymes, OxPhos Enzymes

Table 1. Proteomic studies of carbonylated targets in adipose tissue

Outcomes of Protein Carbonylation

Since its first report extensive studies have been carried out to identify the mechanisms that generate protein carbonyls and develop methods to measure global carbonylation levels in biological systems. This work set the foundation for second-generation studies focused on using proteomic tools to identify specific carbonylated proteins and understanding how these events affect cellular metabolism. Taken together, these studies have yielded three central points:

- ***Hundreds of proteins are modified by reactive lipid aldehydes in metabolically active cells* such as adipocytes, neurons, and muscle cells**. Carbonylation targets include proteins from many distinct locations including the mitochondria, nucleus, ER, and cytoplasm.
- ***Protein carbonylation is a regulatory mechanism.*** It is clear that *specific* proteins become carbonylated, especially under conditions of high oxidative stress. This is an important point for it supports a role for carbonylation as a redox-regulated signaling mechanism rather than simply an endpoint of oxidative damage.
- ***Protein carbonylation is dynamic.*** Increased oxidative stress results in the transition from physiological levels of protein carbonylation to pathological levels. This switch is intimately tied to metabolic dysfunction and disease.

Most critically, the emphasis is now aimed at determining how carbonylation affects individual protein function and, more broadly, how carbonylation shapes cellular processes on a systems level. Here, we will focus on the major findings in adipose tissue, though it is prudent to note that many of these findings are relevant to other cell types and disease states as well.

Modification of proteins by 4-HNE and altered function

Protein carbonylation is often described as oxidative damage with concomitant loss of function. Since modification by 4-HNE is believed to be irreversible, a leading hypothesis is that carbonylation generally results in permanent disruption of proper protein function, targeting it for degradation. For example, Uchida *et al.* demonstrated that *in vitro* modification of glyceraldehyde-3-phosphate

dehydrogenase (GAPDH) by 4-HNE resulted in decreased enzymatic activity in a concentration-dependent manner[74]. Subsequently, Grimsrud *et al*[6] reported that GAPDH is carbonylated in adipose tissue from high fat fed mice[6]. Although it had been appreciated for many years that GAPDH activity was inhibited by oxidative stress, the mechanism underlying this inhibition was unknown. As such, this was a key study because it not only proposed a mechanism for oxidative stress dependent regulation of GAPDH function, but it was one of the first studies to directly test the effects of carbonylation on protein function. What is not known within the context of cellular metabolism and obesity is if the fraction of GAPDH that is carbonylated is sufficient to restrict carbon flow through glycolysis. If so, then oxidative modification of GAPDH may be a protective mechanism to attenuate glycolysis and potentiate the pentose pathway producing additional NADPH that could be utilized for enhanced glutathione synthesis under conditions of increased oxidative stress.

Following these studies, many other groups have shown that modification of proteins with 4- HNE can inactivate enzymatic function. One of the most well studied targets of 4-HNE modifications is ALDH2. ALDH2 is a mitochondrial enzyme that catalyzes the oxidation of aldehydes to carboxylic acids, and is most well known for its role in alcohol metabolism[75]. ALDH2 is also a principal antioxidant that detoxifies lipid peroxidation products such as 4-HNE and 4-ONE. Notably, decreased ALDH2 activity has been linked to many disease states

including certain cancers, neurodegenerative disease, and type II diabetes, a topic that was recently reviewed by Chen *et al*. (2014)[75]. In 1991, Mitchel et al. showed that 4-HNE can be both a substrate and inactivate ALDH2[76]. This result has since been observed in several different cell types and tissues[77-79]. These data are consistent with a feed-forward mechanism in which loss of ALDH2 activity by 4-HNE and/or 4-ONE exacerbates the oxidative environment by decreasing the ability of the cell to detoxify the lipids.

Interestingly, during the first mass-spectrometry based proteomic analysis of carbonylated proteins in adipose tissue, many antioxidant enzymes were identified as carbonylation targets. In this study, soluble proteins from epididymal adipose tissue from mice fed a high fat diet were analyzed using BH derivitization followed by LC/MS/MS[6]. Using this approach, Grimsrud *et al.* identified over 35 proteins that are carbonylated in obese adipose tissue. Notably, this list included not only several members of the aldehyde dehydrogenase family, but also peroxiredoxin 1 (Prdx1), glutathione peroxidase 1 (Gpx1), and glutathione S-transferase M1 (Gstm1)[6]. Although it remains unclear how carbonylation may specifically impact the function of each of these enzymes, one hypothesis is that inhibition of antioxidant function by 4-HNE modification may underlie the oxidative stress that is linked to high fat feeding and obesity-linked metabolic disease.

In addition to the antioxidants identified by Grimsrud and colleagues, KEGG pathway analysis of the targets revealed five other pathways enriched for carbonylation in obese adipose tissue: carbohydrate/lipid metabolism, signal transduction, nucleic acid metabolism, protein synthesis/degradation and structural/motor proteins. One of the most notable proteins in this list is fatty acid binding protein 4 (FABP4, aP2). FABP4 is a cytoplasmic fatty acid binding protein and is of particular interest because in contrast to many of the identified targets, FABP4 is an adipose-specific protein that facilitates lipolysis and is known to play a critical role in obesity induced insulin resistance. Specifically, whole body knockout of Fapb4 results in a general metabolic improvement and prevention of metabolic disease[80]. A caveat of this analysis is that adipose tissue contains not only adipocytes, but also immune cells, endothelial cells and pre-adipocyte stem cells and therefore the cell type in which Fabp4 is carbonylated is not known. Fabp4 is expressed in not only adipocytes, but also macrophages and dendritic cells. Following this initial observation, carbonylation of Fabp4 as well as its family member, endothelial fatty acid binding protein (Fabp5), have been confirmed in two other studies[54,81]. While the specific mechanisms that connect Fabp4 to the progression of metabolic disease remain complex, it is clear that loss of function for this protein has dramatic effects on adipose metabolism. *In vitro* studies of 4-HNE modified Fabp4 revealed that carbonylation at Cys117 attenuated the lipid-binding capacity of the protein, consistent with a model in which carbonylation inactivates the protein leading to

increased unbound free fatty acids [6]. Interestingly, Xu et al. reported that increased free unbound fatty acids in macrophages leads to increased expression of Ucp2 and attenuation of inflammatory NF-κB signaling [49]. It is not known if sufficient molar amounts of Fabp4 is carbonylated in macrophage cells to cause an increase Ucp2 expression but it is tempting to speculate that oxidative modification of Fabp4 may be a regulatory mechanism to maintain metabolic homeostasis.

Another protein of interest in adipose tissue is xanthine oxidoreductase (XOR). XOR is translated from a single transcript, but exists as two unique and interchangeable forms; xanthine dehydrogenase (XDH) and xanthine oxidase (XO). Although both enzymatic forms convert hypoxanthine to xanthine and xanthine to uric acid, XDH reduces NAD^+ to NADH while XO reduces molecular oxygen, producing superoxide anion [82]. XO is known to be a critical source of ROS in many tissues under inflammatory and hypoxic conditions [82,83]. Recently, XOR was identified as a target of protein carbonylation in cultured adipocytes [62]. In this study, protein carbonylation of XOR was significantly increased in Gsta4 knockdown 3T3-L1 adipocytes compared to control cells, indicating that the enzyme is preferentially carbonylated under conditions of oxidative stress in adipocytes [62]. Interestingly, oxidation of key cysteine residues in XDH is known to result in the conversion of the enzyme to XO, the superoxide-producing form [83,84]. As such, although the specific sites of carbonylation have not yet been

identified, a reasonable hypothesis is that carbonylation of XDH in obese adipose tissue is a mechanism that converts XDH to XO, thereby elevating ROS production in a feed-forward loop. Consistent with this, silencing of XDH/XO in 3T3-L1 cells results in markedly decreased ROS levels, implying that XO is a major source of cytoplasmic oxidative stress.

Carbonylation in cell signaling

Protein carbonylation is not only known to inactivate the function of individual proteins, but is now emerging as a critical regulatory mechanism in cellular signaling. Two examples in the adipocyte include the oxidative stress response and programmed cell death/apoptosis.

In the adipocyte, reactive lipid aldehydes are present at low levels under basal conditions. When the cell experiences an oxidative challenge, ROS levels increase and 4-HNE levels rise. One important outcome of this effect is the initiation of an oxidative stress response via the nuclear factor (erythroid-derived-2)-like 2 (NRF2)-Kelch-like ECH-associated protein 1 (KEAP1) pathway. Under normal conditions, KEAP1 binds to NRF2 to sequester it in the cytoplasm [85]. However, when 4-HNE levels rise in response to oxidative stress, KEAP1 becomes carbonylated at two key cysteine residues (Cys273 and Cys288), leading to the release of NRF2 and proteasomal degradation of KEAP1 [86,87]. NRF2 then translocates to the nucleus where it initiates transcription of many

crucial antioxidant genes through the interaction with antioxidant response elements (AREs), thereby initiating a transcriptional program that allows for the cell to recover from the oxidative challenge. This, in turn, ablates the carbonylation of KEAP1, allowing it to once again bind to NRF2, effectively turning the pathway off. The elucidation of this pathway was important not only for our understanding of the antioxidant response, but also because it is a key example of a situation in which physiological levels of protein carbonylation act as an *activating* signal in a highly regulated pathway.

The previous example is known to occur under physiological oxidative challenge to the cell. However, when the oxidative challenge outweighs the antioxidant capacity, 4-HNE and other lipid peroxidation products rise to a pathological level, and are known to be involved in the initiation of programmed cell death via both intrinsic and extrinsic pathways. Specifically, it has been shown that thioredoxin (TRX) contains two cysteine residues (Cys32 and Cys35) that are sensitive to carbonylation under conditions of oxidative stress [88]. Modification at these two residues leads to the release of TRX binding partner apoptosis signal-regulating kinase 1 (ASK1). ASK1 is subsequently activated by autophosphorylation and initiates a pro-apoptotic signaling cascade through the activation of key signaling kinase c-Jun N-terminal kinase (JNK) [89]. Interestingly, other studies have attributed JNK activation to transcriptional increases in p53 expression due to

high levels of 4-HNE, though the mechanism by which 4-HNE elevates p53 expression is unclear [90].

Carbonylation and mitochondrial dysfunction

Mitochondrial dysfunction has long been appreciated to be a hallmark of metabolic disease. In adipose tissue, transition from the lean to obese state is coupled with decreased respiration and impaired glucose and lipid homeostasis [62]. Since the mitochondrion is a major source of ROS in adipocytes, and many proteins become carbonylated under conditions of oxidative stress, one hypothesis is that carbonylation is a molecular link between oxidative stress and mitochondrial dysfunction. To test this hypothesis, Curtis *et al.* generated Gsta4 knockdown and Gsta4 overexpressing 3T3-L1 adipocytes [11]. Previously, it was shown that Gsta4 is selectively down-regulated in adipose tissue of obese mice and humans, and knockdown in 3T3-L1 cells leads to increased ROS, elevated protein carbonylation, and compromised mitochondrial respiration [62]. Consistent with these data, Curtis and colleagues observed decreased Complex I activity, impaired mitochondrial respiration, increased levels of superoxide anion, and decreased membrane potential in Gsta4 knockdown adipocytes compared to controls [62].

To identify specific carbonylation targets that contributed to this phenotype, Curtis *et al.* undertook a large-scale mass-spectrometry based proteomic

profiling of mitochondrial extracts from each cell line. In this case, a BH labeling scheme was utilized coupled with iTRAQ, an isobaric tagging method for multiplexing mass spectrometry studies. This method allowed for quantitative comparison of carbonylation of specific targets between Gsta4 knockdown and overexpressing cell lines. Using this methodology, over 370 mitochondrial-specific carbonylation targets were identified. A KEGG analysis of the identified carbonylation targets revealed the TCA cycle, oxidative phosphorylation and branched chain amino acid (BCAA) metabolism pathways as the top three pathways enriched for carbonylation (**Figure 6**).

The observation of enriched carbonylation of the BCAA metabolism pathway is particularly interesting for this pathway has recently been linked to obesity, type II diabetes and mitochondrial dysfunction in white adipose tissue [91-93]. Furthermore, work by Herman *et al* have shown that adipocytes play a pivotal role in BCAA metabolism and readily metabolize BCAAs to lipogenic precursors acetyl-CoA and succinyl-CoA [91,94]. Recent work from the Bernlohr and Lynch labs have shown that inflammation and obesity affect the ability of visceral white adipose tissue to transport and metabolize BCAAs fully [95-97]. These findings link carbonylation, adipose tissue mitochondrial dysfunction and BCAA metabolism.

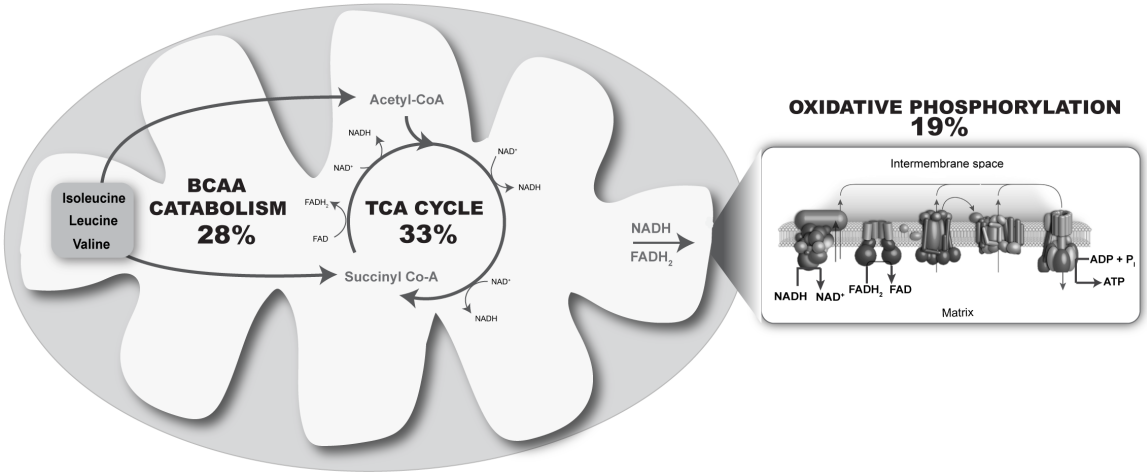

Figure 5. KEGG analysis of mitochondrial protein carbonylation in adipocytes. Schematic representation of key mitochondrial pathways that contain carbonylated proteins. The number represents the fraction of pathway proteins, based on KEGG analysis, that are known to be carbonylated. Data from Curtis *et al*., ref 11.

Another key finding in the Curtis study was the identification of many proteins in the electron transport chain (ETC) that were enriched for protein carbonylation in the Gsta4 knockdown cells. Two noteworthy targets include NADH dehydrogenase (ubiquinone) 1α subunit 2 (Ndufa2) and solute carrier family 25 member 3 (Slc25a3). Ndufa2 is a subunit of Complex I of the electron transport chain, which catalyzes the transfer of electrons from NADH to ubiquinone. Slc25a3, which is more commonly referred to as the mitochondrial phosphate carrier (PiC), is a critical part of Complex V of the electron transport chain. PiC

functions to transport inorganic phosphate from the inner mitochondrial space to the matrix: a step that is required for ATP production by oxidative phosphorylation. The transport activity of the PiC is known to be sensitive to cysteine alkylating reagents suggesting that carbonylation may attenuate phosphate influx into the mitochondrion [98]. Since carbonylation of proteins often disrupts proper function, and electron leak from the ETC is a major source of ROS, one hypothesis is that carbonylation of critical proteins involved in oxidative phosphorylation plays a causative role in the development of mitochondrial dysfunction and impaired respiration in adipocytes.

Human studies of adipose carbonylation

Although the number of carbonylation studies in murine-derived cell lines and tissue are by far the most pervasive, there have been several studies aimed at profiling carbonylation in human-derived cell lines and primary tissue biopsies. In one such study, Singh *et al.* investigated carbonylation in the human liposarcoma cell line SW872 [81]. Previously, the authors had observed that treatment of cells with glycated albumin led to the accumulation of oxidatively modified proteins. To identify modified proteins, SW872 lysates were harvested after treatment with or without glycated bovine serum albumin (BSA) and were subjected to DNPH derivitization. These lysates were then separated by 2D gel electrophoresis and differentially regulated proteins were recovered and subjected to MS/MS identification. The eight proteins identified were Annexin A2, β-actin, FABP4,

ATP synthase, Annexin V, Aldehyde dehydrogenase, Mitochondrial aldehyde dehydrogenase 2 precursor and Annexin VI isoform 1. Notably, there was a 6-fold increase in Annexin A2 carbonylation and a 4-fold increase in β-actin carbonylation in the glycated-BSA treatment compared to controls. The authors concluded that there is a relationship between advanced glycated end products (AGEs) and metabolic syndrome. This relationship may the result of increased carbonylation of β-actin and Annexin A2, which can interrupt actin dynamics and proper cellular function [81].

In 2011, Frohnert *et al.* undertook a study to investigate the relationship between human obesity and carbonylation levels. In this study, omental adipose tissue was obtained from lean and obese patients, biotin-hydrazide derivitized, and proteins were separated by 2D-SDS-PAGE. This was the first study to use human samples to examine carbonylation levels within the context of the lean-to-obese transition. This study demonstrated a positive correlation between carbonylation levels within visceral adipose tissue, serum free fatty acids (FFA), and body mass index thereby verifying much of what had previously been observed in murine obesity models. In addition, a negative correlation was observed between protein carbonylation and insulin sensitivity [54]. Finally, in agreement with previous proteomic studies, FABP4 and FABP5 were identified as targets of carbonylation in the human omental adipose depots. Although the proteomic methods used to identify carbonylation targets was a limiting factor in

this study, these findings were paramount in the context of diabetes as it was the first study to directly correlate carbonylation and insulin resistance in a human population.

More recently, several human studies have focused on the metabolic effects following Roux-en-Y gastric bypass (RYGB) surgery. RYGB is a widely used surgical method for treatment of obesity and associated metabolic disease. Shortly after RYGB, patients exhibit drastically improved glycemia and improved metabolic phenotype prior to significant weight loss. In order to assess changes that occur in white adipose tissue during this shift, subcutaneous adipose biopsies were obtained prior to, and 7-8 days following, gastric bypass surgery. Interestingly, there was a significant decrease in protein carbonylation following surgery [99]. This effect was concomitant with decreased homeostatic model assessment of insulin resistance and increased expression of mitochondrial biogenesis markers. While the mechanisms that lead to post-operative metabolic improvements remain complex, this study suggests that decreases in carbonylation directly following surgery may play an important regulatory role.

Concluding Remarks

Although the number of carbonylation studies is rapidly growing, there remain many open questions in the field. Namely, of the hundreds of proteins that have been identified as targets of 4-HNE modification, only a handful have been

subject to thorough investigation to elucidate specific sites modified and determine how, specifically, carbonylation affects protein function *in vivo*. As such, studies aimed at how carbonylation affects protein structure and function will be important in moving forward. In addition, many of the proteomic studies in adipose and other tissues have focused on mitochondrial targets of 4-HNE modification. Relatively few have considered the effect of carbonylation on proteins in other subcellular localizations and even fewer on the signaling roles of other types of lipid adducts, such as 4-HHE. While the mitochondrion is known to be the primary producer of ROS in adipose, and therefore has been the focal point of oxidative stress studies, molecules like 4-HNE and 4-HHE are readily diffusible and it is clear that many proteins in the cytoplasm, ER, and nucleus are modified by lipid peroxidation products. Moreover, lipid aldehydes can diffuse across cellular membranes suggesting that protein carbonylation may link activities in adjacent cells. Finally, it is not well understood what happens to proteins once they become carbonylated. While several studies suggest that carbonylated proteins are degraded by the proteasome, the details of such mechanisms remain unclear. Moreover, there are no known enzymes that can hydrolyze Michael adducts from proteins.

Despite these many open questions, protein carbonylation has emerged as an important effector of oxidative stress and cellular metabolism. Recent work has demonstrated that hundreds of distinct proteins are carbonylated within adipose

tissue and that these events initiate a wide variety of signaling cascades across the cell. A better understanding of these processes holds great promise for future work aimed at elucidating the role of oxidative stress in the etiology of obesity and metabolic disease.

Acknowledgements and Abbreviations

Acknowledgements

We would like to thank the members of the Bernlohr laboratory for helpful discussions during the preparation of this chapter. Supported by NIH DK084669 to DAB

Abbreviations

Tumor necrosis factor alpha (TNF-α), Interleukin 1 beta (IL-1β), Interleukin 6 (IL-6), Interferon gamma (IFNγ), Endoplasmic reticulum (ER), 4-hydroxy trans-2,3-nonenal (4-HNE), 4-oxo trans-2,3-nonenal (4-ONE), Reactive oxygen species (ROS), Superoxide dismutase (SOD), Malondialdehyde (MDA), 4-hydroxy 2,3-hexenal (4-HHE), Poly unsaturated fatty acids (PUFAs), Arachadonic acid (AA), Docosahexaenoic acid (DHA), Peroxiredoxin (PRDX), Glutathione peroxidase (GPX), Lipid hydroperoxide (LOOH), Aldo-keto reductase (AKR), Aldehyde dehydrogenase (ALDH), Aldehyde oxidase (AO), Glutathione-S-transferase (GST) and Glutathione (GSH), Xanthine oxidoreductase (XOR), Fatty acid binding protein (FABP), Thiobarbituirc acid reactive substance (TBARS), Aminooxyacetic acid (AOAA), 2,4-Dinitrophenylhydrazine (DNPH), Glyceraldehyde-3-phosphate dehydrogenase (GAPDH), Xanthine dehydrogenase (XDH), Xanthine oxidase (XO), Nuclear factor erythroid-derived-2-like-2 (NRF2), Kelch-like ECH-associated protein 1 (KEAP1), Antioxidant response elements (AREs), Thioredoxin (TRX), Apoptosis signal-regulating kinase 1 (ASK1), c-Jun N-terminal kinase (JNK), Branched chain amino acid

(BCAA), NADH dehydrogenase (ubiquinone) 1α subunit 2 (NDUFA2), solute carrier family 25 member 3 (Slc23a3), Advanced glycated end products (AGEs), Roux-en-Y gastric bypass (RYGB), Bovine serum albumin (BSA).

CHAPTER TWO

Redox regulation of DNA binding proteins and the role of adipose nuclear protein carbonylation

Amy K. Hauck, Wendy S. Hahn, Tong Zhou, Yue Chen, and David A. Bernlohr[1]

[1]Department of Biochemistry, Molecular Biology, and Biophysics, University of Minnesota, Minneapolis, MN 55455

This chapter contains an original research article in preparation to be published.

Wendy Hahn performed EMSA experiments in Figure 5, Amy Hauck, Tong Zhou and Yue Chen performed LC-MS/MS experiments and Amy Hauck performed all other experiments, analysis, and preparation of the manuscript

Summary

Oxidative stress plays a causal role in metabolic dysfunction in adipocytes, but the mechanisms that contribute to this process remain controversial. In the obese state, oxidative stress enables lipid peroxidation and subsequent protein carbonylation by diffusible lipid electrophiles. Here, we show the specific accumulation of carbonylated proteins in the nucleus of adipocytes in the obese state. We developed a novel methodology in order to perform site-specific proteomic analysis of lipid carbonylation targets of 4-hydroxy-nonenal (4-HNE) and 4-hydroxy-hexenal (4-HHE). Using this method, we identified over 100 novel nuclear carbonylation target proteins. Interestingly, 4-HNE and 4-HHE display distinct target patterns despite their chemical similarity. Analysis of primary and secondary motifs surrounding the sites of modification revealed that that zinc-coordinating cysteines within zinc fingers are a hotspot for protein carbonylation. Analysis of one such target, the transcriptional regulator Estrogen Related Receptor Gamma (ERRγ), indicates that carbonylation of the identified cysteine results in a dramatic loss in DNA binding activity. Together these data demonstrate a novel pattern for protein carbonylation whereby the modifications accumulate in the nucleus, potentially driving redox-regulated transcriptional outcomes through altered function of DNA binding proteins.

Introduction

Protein carbonylation refers to the post-translational modification (PTM) of the side chains of lysine, cysteine, and histidine residues by reactive lipid aldehydes such as 4-hydroxy-*trans* 2,3 nonenal or 4-hydroxy-*trans* 2,3 hexenal. [1,100]. Such lipids are formed in response to oxidative stress and accumulate when reactive oxygen species (ROS) are elevated or the cellular antioxidant capacity is depleted [61,101]. As such, protein carbonylation is largely recognized as a marker of pathological ROS production in a variety of cell types and tissues. Much work has focused on identifying protein targets of carbonylation with the goal of making specific mechanistic connections between oxidative stress and the subsequent development of metabolic disease.

Previous work from our lab and others has demonstrated a striking decrease in the expression of major antioxidants in epididymal adipose depots from murine models of obesity as well as in cultured adipocytes in response to inflammatory stimuli [61,62,102,103]. This decrease in antioxidant capacity is coincident with elevated ROS and increased levels of select reactive lipid aldehydes within the tissue [61,102]. This leads to a significant increase in protein carbonylation of many different proteins within the adipocyte [6,11,104]. Of the antioxidant enzymes, the down regulation of glutathione-S-transferase A4 (Gsta4) in response to tumor necrosis factor α is particularly noteworthy. This enzyme is a major route for detoxification of reactive lipid aldehydes and depletion of Gsta4 in vivo leads to

elevated protein carbonylation, oxidative stress, mitochondrial dysfunction, and impaired insulin signaling [11,62]. Consistent with glutathionylation of reactive aldehydes being linked to insulin action but not obesity per se, human GSTA4 is down regulated in the obese, insulin resistant but not the obese insulin sensitive state [62]. Moreover, in worm models of glutathione S-transferase deficiency (C.elegans *gst10*), lifespan was attenuated and following rescue with murine Gsta4, lifespan was potentiated[105] suggesting that protein carbonylation plays a fundamental role in longevity. Together these observations strengthen the hypothesis that oxidative stress and subsequent protein carbonylation play a causal role in metabolic disease.

Several large proteomic studies in a variety of disease models have aimed to identify carbonylated proteins and to characterize the effect of protein carbonylation on function [11,106,107]. Although these studies were successful in that they identified many protein targets, and, in a few cases, demonstrated direct impact on protein function, several shortcomings still remain. Firstly, most of the proteomic studies to date lack site-specific information, making functional studies challenging and time-consuming. Secondly, of the proteins identified so far, very few have been shown to play a major role in the metabolic deficiencies observed in obesity (or other disease) models. Thirdly, the workflow for several proteomic analyses have relied on exogenous addition of reactive aldehydes to cells rather than defining endogenously modified proteins. Finally, much of the

previous work for protein carbonylation had been directed at mitochondrial targets, as this is a major ROS-producing organelle.

In this study, we present the novel finding that protein carbonylation endogenously accumulates in the nucleus of adipose tissue and modifies critical metabolic transcriptional regulators in the obese state. Furthermore, we have generated a method by which to identify these proteins and obtain site-specific and lipid-specific information. Importantly, this not only allows for more facile study of carbonylated targets but also allows for more broad analysis of carbonylation patterns and motifs.

Materials and Methods

Animal protocol

Wild-type C57Bl/6J mice were weaned at 3 weeks of age and then fed either a high fat diet (20% protein, 35.5% fat, 36.3% carbohydrate; BioServ F3282) or a chow diet for 12 weeks. Animals were sacrificed by cervical dislocation and epididymal and inguinal white adipose depots were removed for analysis. Experiments were carried out were approved by the University of Minnesota Institutional Animal Care and Use Committee.

Cell Culture

3T3-L1 fibroblasts were grown to confluence and differentiated as previously described[108] using the standard differentiation cocktail consisting of dexamethasone, methylisobutylxanthine, and insulin. On day 7 of differentiation, cells were treated with 10 uM erastin (Cayman Chemical 177754) or vehicle (DMSO) in DMEM +5% Fetal Bovien Serum (FBS) for 24 hours before harvesting or for use for microscopy experiments. For ERRγ inhibitor experiments, day 8 cells were treated with 10 uM GSK5182 (Aobios AOB1629) or vehicle (DMSO) for 6 or 20 hours.

Nuclear lysate preparation

Fresh tissue was minced on ice in hypotonic lysis buffer (10 mM Tris-Cl pH 8.0, 1 mM KCl, 1.5 mM MgCl2, 1mM DTT) with protease and phosphatase inhibitors. Tissue was homogenized with a glass-Teflon system using an electric homogenizer (8 strokes, 1600 rpm). Samples were spun at 1000 rpm at 4°C for 10 minutes and the fat cake was discarded. Then, samples were briefly vortexed and spun at 3700 rpm at 4°C for 10 minutes to collect nuclei. For several experiments, the post nuclear extract was stored for western blotting analysis. Nuclei were washed 3X before use in subsequent analysis. Nuclei were resuspend in reduction buffer (15mM $NaBH_4$ in PBS) in incubated for 30 min. Samples were dialyzed overnight into PBS, sonicated, and spun (16000 rpm at 4°C for 10 min) to remove nuclear debris. Samples were quantitated with the

bicinchoninic acid protein quantitation assay (Sigma Aldrich) prior to downstream applications. For western blotting, samples NP-40 and SDS were added to a final concentration of 1% and .1% respectively to samples. For mass spectrometry experiments, histone proteins were separated from other nuclear proteins by acid extraction prior to analysis.

Glutathione content assay

This was performed using the GSH/GSSG Ratio Detection Kit (Abcam 65393) according to manufacturer's instruction.

Western blotting analysis

Samples were prepared for western blot by mixing normalized samples with 4X loading buffer. Samples were resolved by SDS-PAGE, wet transferred to PVDF membrane, blocked for 1 hour with blocking buffer (LI-COR 927-4000) and incubated with primary antibodies overnight at 1:1000 dilutions in TBS-T + 5% BSA. Membranes were then washed 3X in TBS-T and incubated for 1 hour with fluorescently labeled secondary antibodies (LI-COR) and imaged using the LI-COR Odyssey Imager. Antibodies used include 4-HNE (Millipore, 393207), 4-HHE (non-commercial), β-Actin (Sigma-Aldrich A5441), Histone H3 (abcam 10799), Histone H4 (Cell Signaling 2935S). ERRγ (abcam ab128930), ERRα (Thermo Fisher, H5844).

Immunofluorescence and microscopy

3T3-L1 fibroblasts were grown on coverslips (#1.5 coverslips, EMS72224-01) in 6-well plates. Cells were differentiated according to normal protocol and treated with erastin or DMSO for 24 hours on day 7. On day 8, cells were fixed with 4% paraformaldehyde (EMS15714). Cells were blocked and permeabilized with blocking buffer (PBS, .1%Triton X-100, .2% gelatin, 1% BSA). Cells were incubated with primary antibody (α-4-HNE, abcam 46545) overnight and washed with PBS + .1%TX-100. Cells were then incubated with secondary antibody at a 1:1000 dilution (Donkey anti-rabbit IgG Alexa Fluor 488, abcam 150073) and 500 nM DAPI for 30 minutes. Following washing, cells were mounted on slides with mounting solution (Invitrogen P10144) and stored at 4° until imaging. Slides were imaged at the University of Minnesota Imaging Centers using the Olympus FV1000 Bx2 upright confocal microscope at 60X with an oil immersion lens.

Immunoprecipitation of carbonylated proteins

For IP of proteins, 70-100 µg of reduced nuclear extract (in PBS) was diluted to 500 ul with a PBS+ 1% NP40 and then was pre-cleared with protein A/G agarose resin (Sant Cruz sc-2004). 4-HNE primary antibody (Millipore 393207) was cross-linked to protein A/G agarose resin using DMP imidoester crosslinking reagent (Thermo Scientific) according to manufacturer's instructions. Cross-linked antibody/resin was incubated with nuclear lysates overnight. The next day, resin was washed 3X with RIPA buffer and proteins were eluted by boiling in 4X DNS.

Samples were resolved by SDS-PAGE, stained with Imperial Protein Stain (Thermo Scientific) prior to in gel digestion.

In gel digestion

SDS-PAGE gel bands were first washed by 50% EtOH in water for overnight and then washed by water for an hour. Each gel band was cut into small pieces and then dehydrated by acetonitrile. Proteins were reduced and alkylated at room temperature in dark by TCEP (15 mM) and iodoacetimide (45 mM) in PBS. Then the gel pieces were washed sequentially by 50 mM ammonia bicarbonate, 100% acetonitrile, and dried completely by SpeedVac (ThermoFisher). Trypsin stock solution (Promega) was reconstituted in 50 mM ammonia bicarbonate buffer to 10 ng/μl and applied to digest proteins in-gel for overnight at 37 °C. Peptides were extracted sequentially by Extraction Buffer (5% trifluoroacetic acid and 50% acetonitrile in water, v/v) and 100% acetonitrile. The pooled peptide extracts were dried in SpeedVac and then desalted by C18 Stagetip as previously described.[109]

In solution protein digestion and immunoprecipitation of peptides

Proteins were resuspended in the urea lysis buffer (9M urea in PBS [pH 7.2] with HALT protease inhibitor cocktail (Thermofisher)). Proteins were subjected to reduction and alkylation at room temperature in dark by TCEP (10 mM) and iodoacetamide (30 mM) in PBS. Excessive amount of iodoacetamide were

quenched by Cys (30 mM). After six fold dilution with PBS, proteins were digested by sequencing-grade trypsin (1:50 enzyme to substrate ratio, w/w) (Promega) at room temperature for overnight, followed by a second tryptic digestion (1:100 enzyme to substrate ratio, w/w) for 3 hours. Peptides were desalted with Sep-pack C18 cartridge (Waters) following the manufacturer's instructions. Following digestion, samples were incubated with 4-HNE-agarose cross-linked resin overnight and eluted with .1% TFA.

LC-MS/MS

Peptides were reconstituted in HPLC buffer A (0.1% formic acid in water, v/v) and injected into a Proxeon Easy nLC 1000 HPLC system (ThermoFisher) by autosampler. Peptides were separated by C18 column packed in-house (15 cm × 75 μm, ReproSil-Pur Basic C18, 2.5 μm, Dr. Maisch GmbH) with a linear gradient of 5%-35% HPLC buffer B (0.1% formic acid in acetonitrile, v/v) at a flow rate of 200 nl/min. Eluted peptides were directly electrosprayed into the Fusion Orbitrap mass spectrometry (ThermoFisher). The instrument was operated in a data-dependent mode with full mass spectra were acquired with a resolution of 120,000 FWHM at 200 m/z and MS/MS spectra were acquired using collision-induced dissociation (CID) with 35% collision energy for detection in the ion trap.

MS data processing

Raw MS data were processed by MaxQuant software (v 1.5.3.12) for protein identification.[110] Variable modifications include carbamidomethylation on cysteine and lysine, methionine oxidation, protein N-terminal acetylation, HNE and reduced HNE on cysteine, histidine and lysine, as well as HHE and reduced HHE on cysteine, histidine and lysine. Trypsin was selected as the proteolytic enzyme and a maximum of two missing cleavages were allowed. The precursor ion mass tolerance was set to +/-4.5 ppm and the fragment ion mass tolerance was set to +/-0.6 Da. MS data were searched against the Uniprot mouse database (released on 2013/09/27 and containing 43310 sequences). Peptides were filtered with a 1% False Discovery Rate (FDR) at the peptide, protein and modification site levels. A minimum Andromeda score of 40 was required for the identification of modified peptides.

Bioinformatic Analysis

Pathway and functional annotation enrichment was performed using DAVID bioinformatics resources[111,112]. All statistics reported are Benjamini-Hochberg corrected P-values. Molecular function categorization was performed using PANTHER[113]. Statistical analysis of enriched motifs was performed using motif-x [114,115]. Network analysis was performed using Ingenuity Pathway Analysis (https://www.qiagenbioinformatics.com/products/ingenuitypathway-analysis)

Cloning and expression of GST-ERR2

We obtained the ERR2-DBD in pET24a vector as a kind gift from Peter Wright. We subcloned the original construct into pGEX2T in order to tag with GST using the following primers: ERR2 pGEX Fwd ; CACCGGATCCGCTATCCCGAAGCGCCTGTG, ERR2 pGEX Rev ; CGATGAATTCTTAAGAGTTTTCGC ATCCA. We then expressed in BL21 LysS E. Coli. GST-tagged protein was purified using GSH-column chromatography, eluted with Elution buffer (50mM Tris, PH 8.0, 100 uM ZnCl2, 10 mM GSH).

In vitro modification with 4-HHE

Purified protein was dialyzed into Adduction Buffer (100 mM potassium phosphate pH 7.4, 150 mM NaCl). Samples were treated for 1-48 hours with .5 mM 4-HHE (Cayman Chemical 32060). Reaction was quenched with 5 mM DTT. Modification was verified by western blotting.

q-RT-PCR

Cells were washed in PBS and RNA was isolated using TRIzol reagent (Invitrogen) according to the manufacturer's instructions. Real-time amplification was performed using a Bio-Rad iCycler thermocycler with iQ SYBR Green Supermix. Gene expression assays were performed for Atp2a2, Cpt2, Ndufs2, Pdk4, and Txn2. Primer pairs are listed in Table 1. Relative gene expression was calculated using transcription factor 2E (TFIIE) as an endogenous control.

Electromobility Shift Assay (EMSA)

10 ul of purified protein was combine with 2 ul 10X binding buffer (100 mM Tris pH 7.5, 500 mM KCl, 10mMDTT), 1 ug Poly dI dC, 2 ul 25 mM DTT, 2.5% Tween-20, 1 ul DNA probe, and water to final volume of 20 ul. Reactions were incubated for 20-30 minutes in the dark. 10 loading dye was added to each reaction and Electrophoresis was carried out using 5% TBE Criterion Precast Gels (#3450048) in TBE running buffer. Gels were imaged using the LI-COR Odyssey Imager. The following IR700 probes were used: forward, /5IRD700/TCGAGCATTGATCAAGGTCAGTGATGC. Reverse (/5IRD700/TCGAGCATCACTGACCTTGATCAATGC.

Biotin-hydrazide derivitization and immunoprecipitation

Nuclear extracts (from 1 mg starting tissue) were diluted to 1 mL with biotin hydrazide coupling buffer (100 mM sodium acetate, pH 5.5, 20 mM NaCl, 0.1 mM EDTA, 2% SDS, protease inhibitors). Biotin hrydrazide (Pierce 21339) was added to a final concentration of .5 mM and reactions were incubated for 2 hours. Samples were dialyzed into PBS. Samples were incubated overnight with streptavidin-conjugated agarose (Thermo Scientific 20357). Samples were spun to collect resin. Resin was washed 3X with PBS + .01% SDS, resuspended in 2X DNS and boiled to elute proteins. The supernatant was retained and pooled with

the washes to assess the non-carbonylated fraction. The entire IP fraction and supernatant were loaded into each well to compare ERRγ/α content.

Statistical Analyses. All statistical analyses were done using unpaired two-tailed student's t-tests with significance level set at $p<0.05$.

Primer	Accession	Forward	Reverse
TfIIe	NM_026584	CAAGGCTTTAGGGGACCAGATAC	CATCCATTGACTCCACAGTGACAC
Atp2a2	NM_001110140	CTG TGG AGA CCC TTG GTT GT	CAG AGC ACA GAT GGT GGC TA
Cpt2	NM_009949	TGATGGCTGAGTGCTCCAAAT	AACAGCATACGCAATGCCAA
Ndufs2	NM_153064	GAT CCG AGT GCT CTT TGG AG	ATG TCA TCC AGA AGC CCA AG
Pdk4	NM_013743	TCACACCTTCACCACATGCT	CGCCTCCTCGGTCAGAAATC
Txn2	NM_019913	AGAGAAGATGGTCGCCAAGC	CTCTCTGCTCGTCAGCCAAT

Table 1. q-RT-PCR primer pairs

Results

Carbonylated proteins accumulate in the adipocyte nucleus

To assess protein carbonylation in adipose tissue we compared 4-HNE adducts formed in epididymal (eWAT) and inguinal (iWAT) depots of C57Bl/6J mice using an antibody directed towards 4-HNE Michael adducts. Michael adducts represent >90% of all carbonylation events [59,116,117] and are largely formed via alkylation of cysteine, lysine and histidine side chains. In agreement with previous work [61], whole cell extracts of white adipose tissue from both chow-fed and high-fat fed mice exhibit extensive 4-HNE modification of proteins (Figure 1A). Previous studies have focused on mitochondrial targets of 4-HNE modification due to the relatively high local production of reactive oxygen species (ROS) [11,62,118]. Interestingly, while previous studies have delimited clear differences in ROS accumulation in the mitochondria from lean and obese

animals as well as differences in the carbonylation status of individual proteins, whole mitochondrial extracts of eWAT from lean and obese animals did not exhibit a significant global difference (Figure S1A) and as such, we evaluated 4-HNE-protein adducts formed in other subcellular localizations. Unexpectedly, we identified a striking accumulation of 4-HNE modified proteins in nuclear extracts of HFD-fed mice compared to chow-fed animals (Figure 1B). Furthermore, increased nuclear protein carbonylation was specific to the eWAT depot as levels of carbonylated proteins in samples from iWAT between chow and HFD-fed animals were largely unchanged (Figure 1B).

To evaluate the biology of nuclearly carbonylated proteins, we utilized the cultured 3T3-L1 adipocyte cell system [108]. Differentiated 3T3-L1 cells exhibit reduced glutathione levels and robust protein carbonylation under conditions of oxidative stress [119,120]. To reduce cellular glutathione levels and achieve a pro-oxidative environment in 3T3-L1 adipocytes, cells were treated with erastin. Erastin is an inhibitor of the cysteine/glutamate antiporter (system X_c^-), and treatment (10 μM) results in the depletion of glutathione pools (Figure 1C) [121] without cytotoxicity or altered cell morphology (Figure 1C, Figure S1B). Glutathione is critical for maintenance of redox homeostasis and its depletion represents a global cellular oxidative stress phenotype. In particular, the major mechanism by which reactive lipid aldehydes such as 4-HNE and 4-HHE are detoxified is through glutathionylation by glutathione-*S*-transferase A4 [62,122]. Previous work from our lab and others has shown that glutathione *S*-transferase

A4 mRNA and protein are down regulated in the eWAT of obese, insulin resistant C57Bl/6J mice [61] and in iWAT in obese, insulin resistant humans [54]. As such, erastin treatment of 3T3-L1 adipocytes phenocopies glutathione depletion in vivo. Confocal immunofluorescence microscopy of erastin-treated cells showed a clear co-localization of 4-HNE modified proteins with the DAPI-labeled region suggesting that carbonylated proteins accumulate in the nucleus of 3T3-L1 adipocytes (Figure 1D). Interestingly, the 4-HNE adducts appeared as distinct puncta, but did not overlap with the DAPI staining, suggesting there may be specific intra-nuclear sites that are preferentially modified.

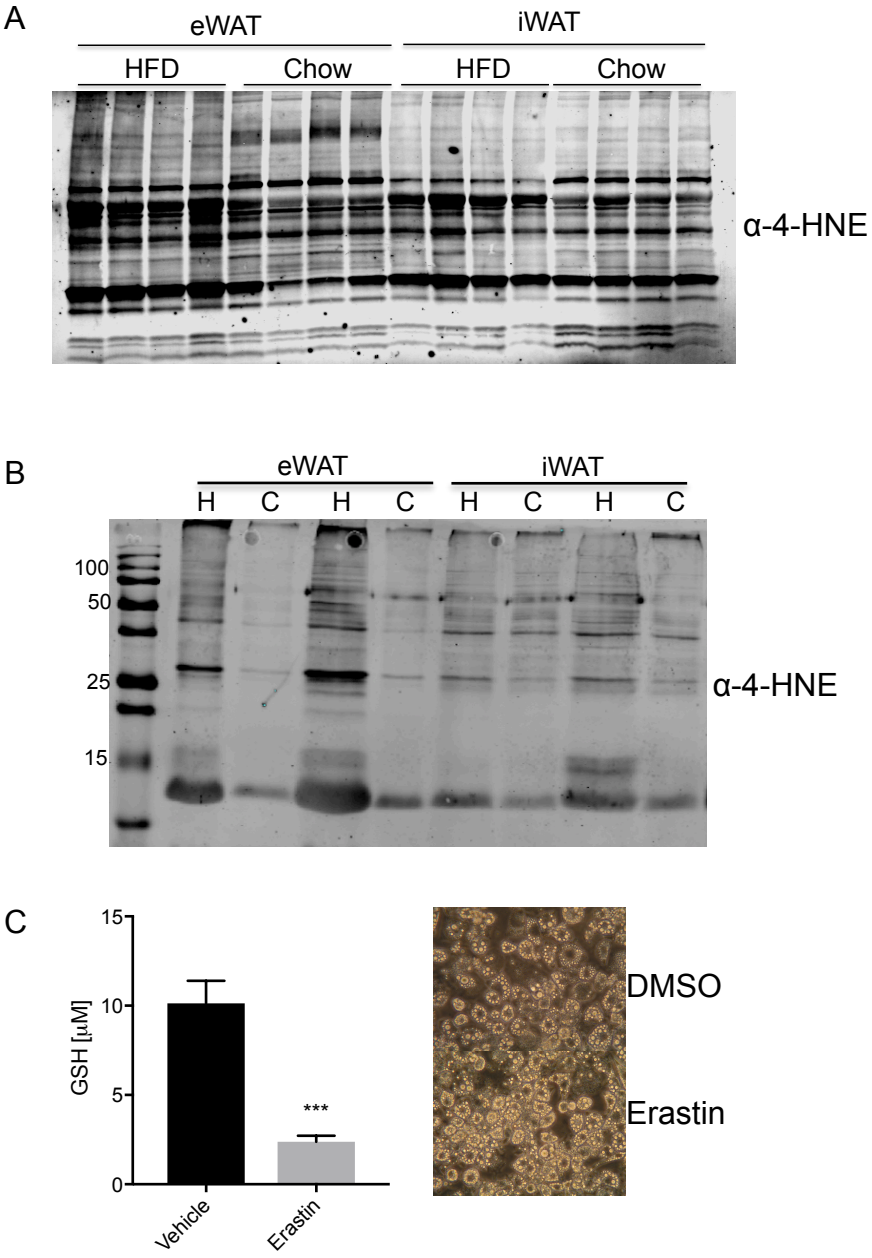
A
eWAT
iWAT
HFD
Chow
HFD
Chow
α-4-HNE
B
eWAT
iWAT
H
C
H
C
H
C
H
C
100
50
25
15
α-4-HNE
C
15
10
5
0
GSH [μM]
***
Vehicle
Erastin
DMSO
Erastin

D

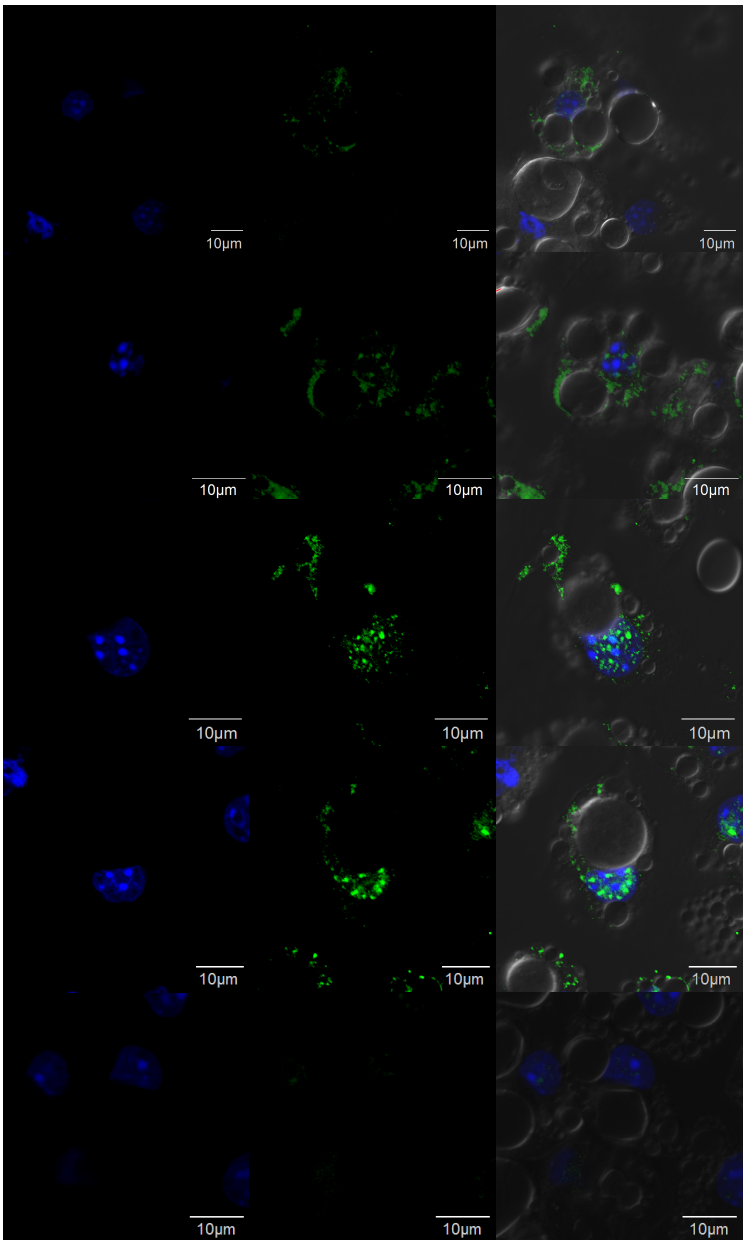
DAPI
4-HNE
MERGE
Control_1
Control_2
Erastin_1
Erastin_2
2° Only Control
10µm

Figure 1. Protein carbonylation accumulates in the nucleus of adipocytes in vivo

(A) Western blot of 4-HNE protein adducts of whole cell lysates from epididymal (eWAT) and inguinal (iWAT) adipose depots from 15-week only mice fed a chow or high fat diet (HFD) for 12 weeks.

(B) Western blot of 4-HNE protein adducts from nuclear lysates from chow- (C) and high-fat (HFD) fed mice.

(C) (Left) Glutathione (GSH) levels in day 8 3T3-L1 adipocytes treated for 24 hour with 10 μM erastin or vehicle (DMSO). (Right) Light microscope image (60X magnification) of control and erastin treated cells.

(D) DAPI and Alexa Fluor 488 fluorescence (60X) in control and erastin-treated cells. 2° only was incubated with Alexa Fluor 488 antibody but no primary antibody (α-4-HNE). Merge is the DAPI and AF488 combined with the transmitted light image.

Site-specific proteomic analysis of nuclear carbonylation

Several published studies of protein carbonylation have utilized mass-spectrometry based methods and have led to the identification of numerous targets of protein carbonylation [11,123-125]. However, the majority of these studies lacked the ability to identify the sites of modification in a high throughput manner. Furthermore, the hydrazide- or DNPH-based derivitization method most commonly utilized is not specific for lipophilic carbonyl adducts and will recognize any free carbonyl, thereby making it difficult to verify what type of modification a given protein harbors. Together, these shortcomings have made functional studies of protein carbonylation challenging. Therefore we developed a label-free method by which to identify site-specific Michael adducts on nuclear proteins

(Figure 2A). This method relies on affinity purification with an antibody directed against 4-HNE Michael adducts. Importantly, this antibody is specific for the 9-carbon 4-HNE adduct and does not bind to the 6-carbon 4-HHE adducts (Figure S1C), allowing for enrichment of proteins and peptides carrying specific linkages.

To identify carbonylated proteins that accumulate in the nucleus, we isolated nuclei from eWAT depots from obese C57Bl/6J mice. We analyzed un-enriched samples and samples enriched for adducts at both the protein and the peptide level before proteomic analysis to identify peptides carrying 4-HNE adducts (Figure 2A). Shown in Figure 2A are the linear structures of the Michael adduct formed between 4-HNE and target amino acids. It should be noted that linear lipid aldehydes adducted onto proteins typically cyclize to form the more stable hemiacetal (reference here?). However, in the workflow, we reduced all adducts with sodium borohydride to allow for efficient immunoaffinity capture. Through this workflow we identified 65 proteins and 95 sites of 4-HNE modification (Figure 2B). 4-HHE is reactive lipid that is closely related to 4-HNE and has been studied at length for its role in oxidative stress-related outcomes [24,126-128]. As such, we also searched for 4-HHE modifications and identified 134 sites on 57 distinct proteins (Figure 2B). Since the antibody we used for enrichment is specific for the 9-carbon adduct this suggests that nuclearly carbonylated proteins may be organized in a complex or physically associate with each other. Interestingly, we did not identify any overlapping proteins or sites for both 4-HNE and 4-HHE modification, suggesting that despite their chemical similarly, these

lipids display distinct molecular protein targets. Analysis of the sites of modifications revealed a roughly equal distribution between lysine, histidine, and cysteine modifications, suggesting that neither 4-HNE nor 4-HHE exhibit a side chain preference (Figure 2C). It should be noted that in this workflow analysis, histones were excluded. We have found that histones are a major nuclear carbonylation target and specifics as to their sites, specificity and biological impact will be reported separately.

Molecular Function Analysis (PANTHER) of all sites identified revealed that roughly one-third of proteins identified exhibit enzymatic activity (Figure 2D upper). The remaining proteins cluster into a variety of categories including a large number of nucleic acid binding proteins (Figure 2D, lower). To further assess the physiological significance of carbonylation in the nucleus, we performed pathway Gene Ontology (GO) analysis of the combined (4-HNE and 4-HHE) protein dataset. Interestingly, there was no significant enrichment for biological processes or KEGG pathways (Figure 2D, upper panel & Supplementary Table 2). In molecular function enrichment analysis, we found that carbonylation substrates were highly enriched for metal binding proteins (adj $P= 1.2x10^{-7}$), nucleic acid binding proteins (adj $P= 9.7x10^{-5}$), and zinc ion binding proteins (adj P=0.005). In addition, keyword enrichment analysis and sequence feature analysis revealed that zinc finger-containing proteins were the most highly enriched class of proteins (adj $P=2.6x10^{-12}$) (Figure 2D, lower panel & Supplementary Table 2).

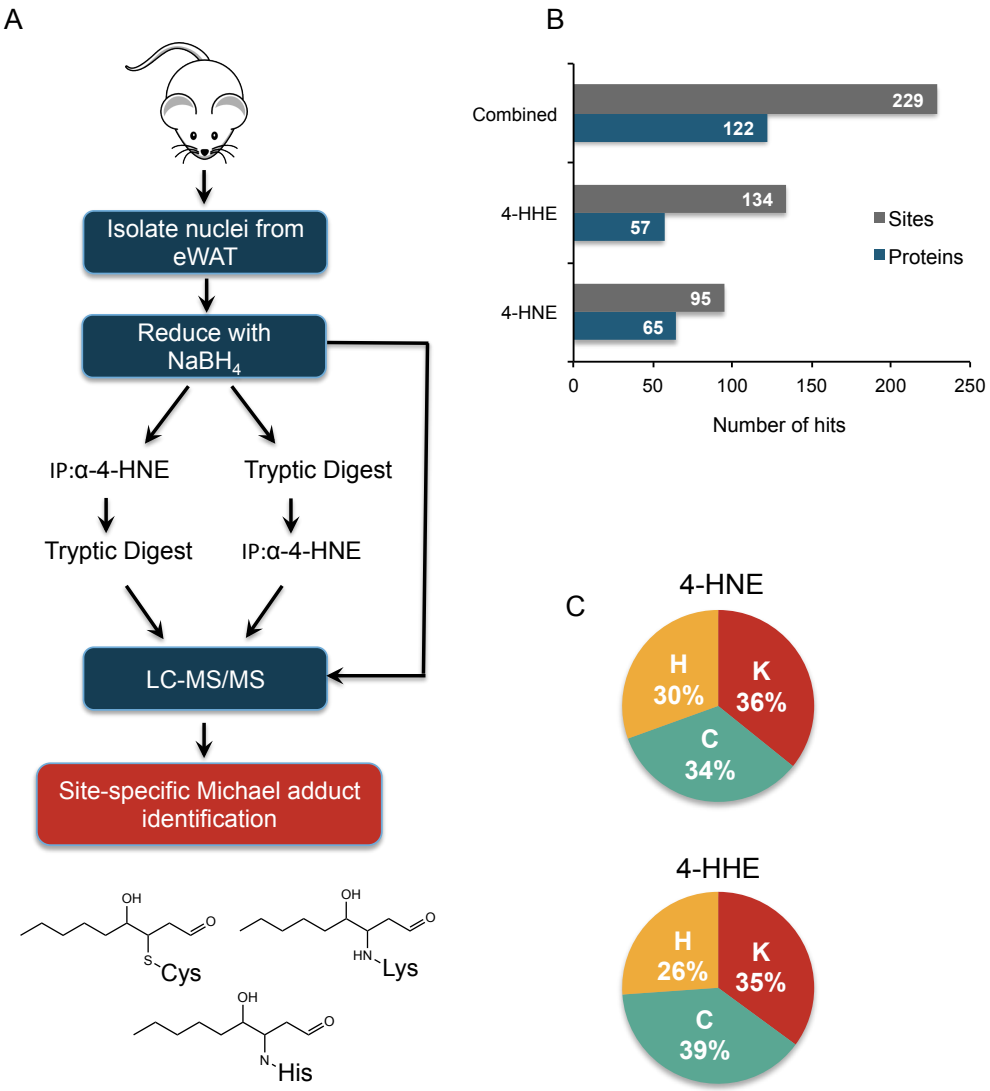
A
Isolate nuclei from eWAT
Reduce with NaBH4
IP:α-4-HNE
Tryptic Digest
Tryptic Digest
IP:α-4-HNE
LC-MS/MS
Site-specific Michael adduct identification
OH
O
S
Cys
OH
HN
Lys
OH
N
His
B
Combined
229
122
4-HHE
134
57
4-HHE
95
65
Sites
Proteins
0
50
100
150
200
250
Number of hits
C
4-HNE
H 30%
K 36%
C 34%
4-HHE
H 26%
K 35%
C 39%

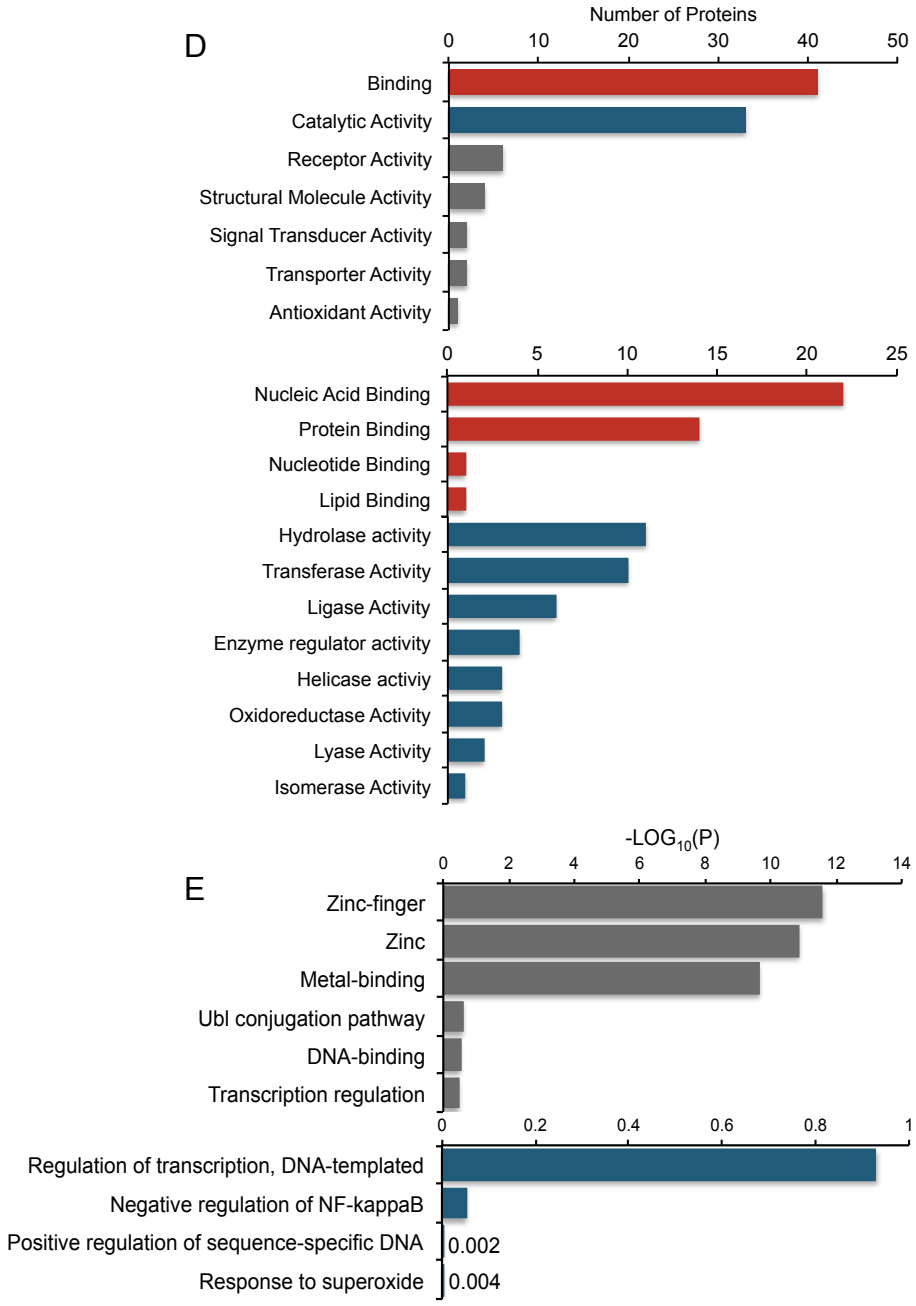
D
Number of Proteins
0
10
20
30
40
50
Binding
Catalytic Activity
Receptor Activity
Structural Molecule Activity
Signal Transducer Activity
Transporter Activity
Antioxidant Activity
0
5
10
15
20
25
Nucleic Acid Binding
Protein Binding
Nucleotide Binding
Lipid Binding
Hydrolase activity
Transferase Activity
Ligase Activity
Enzyme regulator activity
Helicase activiy
Oxidoreductase Activity
Lyase Activity
Isomerase Activity
E
-LOG10(P)
0
2
4
6
8
10
12
14
Zinc-finger
Zinc
Metal-binding
Ubl conjugation pathway
DNA-binding
Transcription regulation
0
0.2
0.4
0.6
0.8
1
Regulation of transcription, DNA-templated
Negative regulation of NF-kappaB
Positive regulation of sequence-specific DNA
Response to superoxide
0.002
0.004

Figure 2: Site-specific proteomic analysis of 4-HNE and 4-HHE Michael adducts

(A) Workflow diagram for proteomic analysis. eWAT depots were collected from mice fed a HFD. Following nuclear isolation, 4-HNE modifications were enriched by immunoaffinity purification at both the protein and peptide levels prior to LC-MS/MS analysis.

(B) Quantitation of the number of 4-HNE and 4-HHE modified sites and proteins identified.

(C) Distribution of 4-HNE and 4-HHE sites on Histidine (H), Lysine (K), and Cysteine (C) residues. Represented as percent of total 4-HNE (upper) and total 4-HHE (lower) hits.

(D) Number of proteins identified for molecular function categorization from PANTHER (upper). Red bars are subcategories of binding and blue bars are subcategories of catalytic activity (lower).

(E) Gene Ontology Analysis of the nuclear carbonylome with statistical enrichment for keywords (upper) and molecular function (lower) (BH adjusted Pvalue).

Sequence preference analysis for carbonylation sites

Using our dataset containing over 100 carbonylated proteins we evaluated the amino acid sequence flanking each carbonylation site in order to determine if there are sequence motifs that are enriched at 4-HNE or 4-HHE sites. Firstly, we calculated the occurrence of each amino acid surrounding the modification from the -7 to +7 positions (Figures 3A, 3B and 3C). This analysis revealed a strong preference for cysteine at the +3 position and a cysteine or proline at the -3 position for both 4-HNE and 4-HHE cysteine modifications (Figure 3A).

While the 4-HNE and 4-HHE cysteine modifications displayed clear similarities in their flaking sequences, the lysine and histidine modifications did not. 4-HNE lysine modifications showed a strong preference for polar charged residues in the -2,-1,+1, and +2 positions (Figure 3B). In contrast, the 4-HHE lysine adduct was more commonly surrounded by hydrophobic residues on both sides (Figure 3B). 4-HNE histidine adducts were flanked by polar uncharged residues on the N-terminus while the 4-HHE modification was surrounded primarily by hydrophobic residues on both sides (Figure 3C). Overall, lysine enrichment in the flanking sequences for all modifications was particularly notable. Analysis of combined lysine content for all modifications (Figure 3D), all 4-HNE modifications (Figure 3E), and all 4-HHE modifications (Figure 3F) shows high lysine content for all substrates.

Motif analysis using Motif-X revealed three highly enriched motifs for cysteine carbonylation and 1 for lysine modification, with no enriched motifs for histidine modification (Figure 3G). The identified motifs are all based upon the location of neighboring cysteine residues; for cysteine modification, there was a statistically significant enrichment for sites with a cysteine in the +5 position (Figure S2A), the +3 position (Figure S2B), or the -3 position (Figure S2C) and for lysine modification at the +1 position (Figure S2D). Interestingly, ontology analysis of the aligned peptides for each motif indicates that both C-x2-C motifs (Figure S2B, S2C) and motif -KC- (Figure S2D) are driven by zinc finger substrates (Figure S2F-H) while the motif C-x5-C is not (Figure S2E).

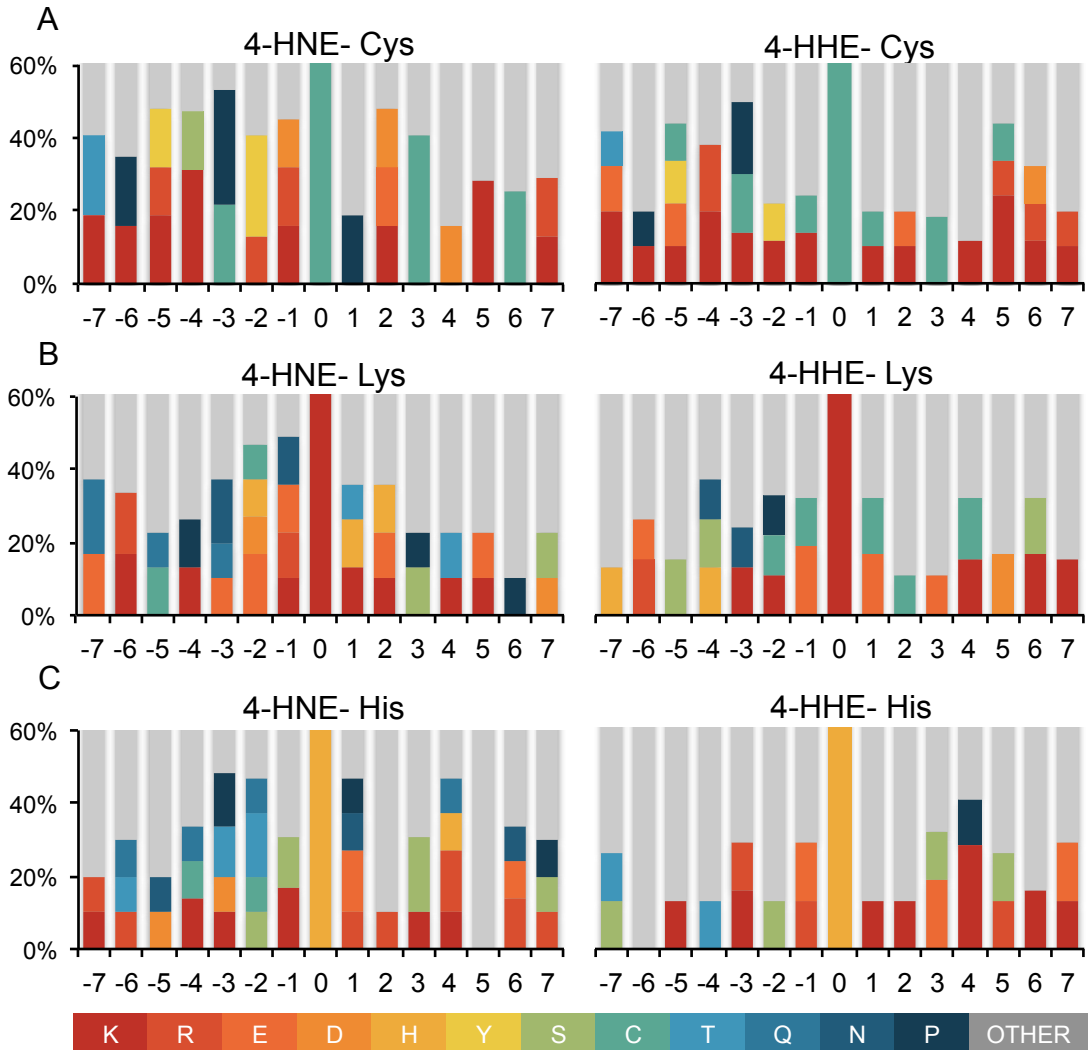
A
4-HNE- Cys
4-HHE- Cys
B
4-HNE- Lys
4-HHE- Lys
C
4-HNE- His
4-HHE- His
60%
40%
20%
0%
-7 -6 -5 -4 -3 -2 -1 0 1 2 3 4 5 6 7
K R E D H Y S C T Q N P OTHER

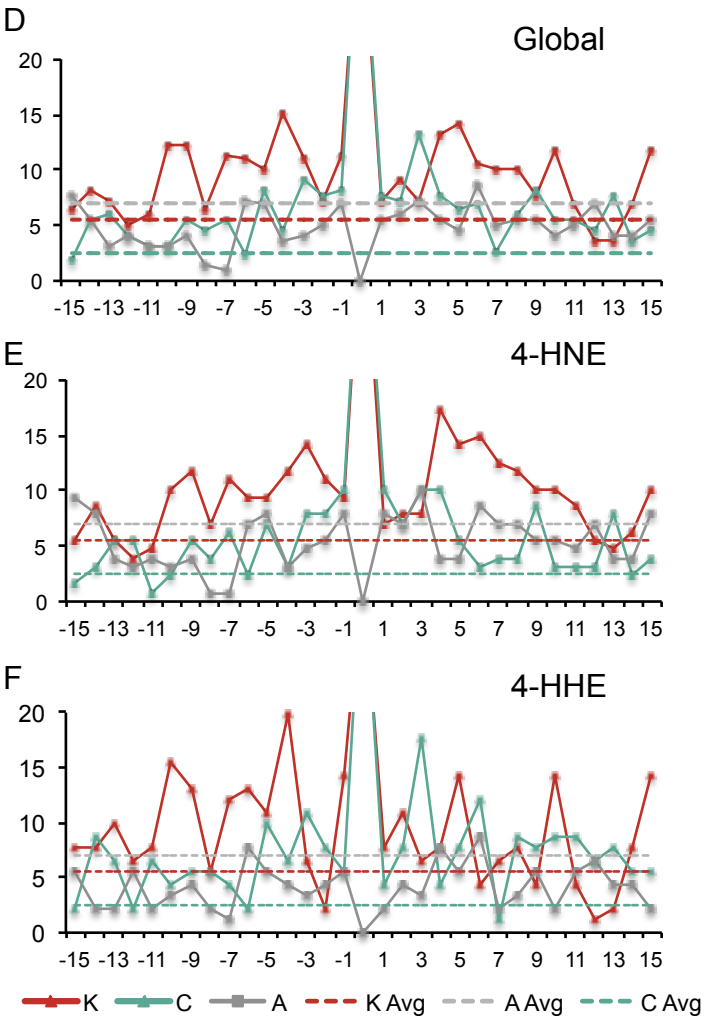

G

Modified AA	Motif	Score	Matched Peptides	Fold Enrichment	Pvalue
Cys	xxxxxxxCxxxxCxx	6.55	17	4.39	<.0006
Cys	xxxxxxxCxxCxxxx	6.47	24	3.21	<.0006
Cys	xxxxCxxCxxxxxxx	6.49	19	3.81	<.0006
Lys	xxxxxxxKCxxxxxx	7.28	16	5.43	<.0009

Figure 3: 4-HNE and 4-HHE modifications exhibit distinct molecular signatures

(A-C) Analysis of the flanking sequences for cysteine (A), lysine (B), and histidine (C) modifications. Site of modification is denoted as position 0 on the x-axis. Bars represent the amino acid frequency at each of position from -7 to +7 among all peptides for each type of modification.

(D-F) Frequency of lysine, cysteine, and alanine across the entire nuclear carbonylome (D), all 4-HNE modified residues (E) and all 4-HHE modified residues (F). Solid line is the frequency of K, C, and A residues in the flanking sequences of carbonylated sites. Dotted lines denote the global frequency of K, C, and A residues across the murine proteome.

(G) Motifs identified using Motif-x. Modifications for Cys, Lys, and His were analyzed separately. No motifs were enriched in the histidine carbonylation dataset.

Zinc-coordinating residues are hotspots for protein carbonylation

Due to the strong enrichment of zinc-coordinating proteins in our proteomic and motif analysis, we explored these proteins further in detail. 93% of 4-HNE- and 87% of 4-HHE-modified zinc-coordinating proteins were zinc-finger containing proteins (Figure 4A). Importantly, 70% of the zinc-binding proteins with 4-HNE adducts were modified within the zinc-binding domain, suggesting that zinc coordination makes residues particularly susceptible to modification (Figure 4B). Roughly a third of 4-HHE adducts on zinc binding proteins were within zinc binding domains (Figure 4B).

Of the zinc fingers identified, 50% (19 proteins) were C2H2 zinc fingers (Figure 4C). The C2H2 zinc finger is a common DNA binding domain that mostly exhibits

the motif C-x3-C-x12-H-x3-H [129], where the 2 cysteines and two histidines coordinate a single zinc ion (Figure 4D). 11 C2H2 zinc fingers had carbonylation sites within the zinc-binding domain. Alignment of these domains showed that the two cysteine residues involved in zinc coordination are common sites for modification (Figure 4E). Interestingly, 7 of these C2H2 zinc fingers were found in proteins that also contain an amino-terminal Krüppel-associated box (KRAB domain)(Figure 4E). An additional three KRAB-containing proteins were also identified (2810021J22RIK, ZFP68, and 2610021A01RIK) with modifications outside of the zinc-coordinating sites. The KRAB domain is generally associated with transcriptional repression through the binding of KAP1 (KRAB-associated protein 1) and subsequent recruitment of chromatin modifying enzymes [130,131]. The enrichment of KRAB containing-proteins is intriguing and suggests a potential role for protein carbonylation in mediating the effects of these transcriptional regulators in adipose tissue.

In addition to the C2H2 zinc fingers, several other types of zinc fingers were identified with modifications including (among others) MATRIN, RING, C3H1, and N4-type domains. Analysis of the sites of modification within the non-C2H2 zinc fingers revealed an additional 12 carbonylated zinc-coordinating sites (Figure 4F-I, Supplementary Table 3).

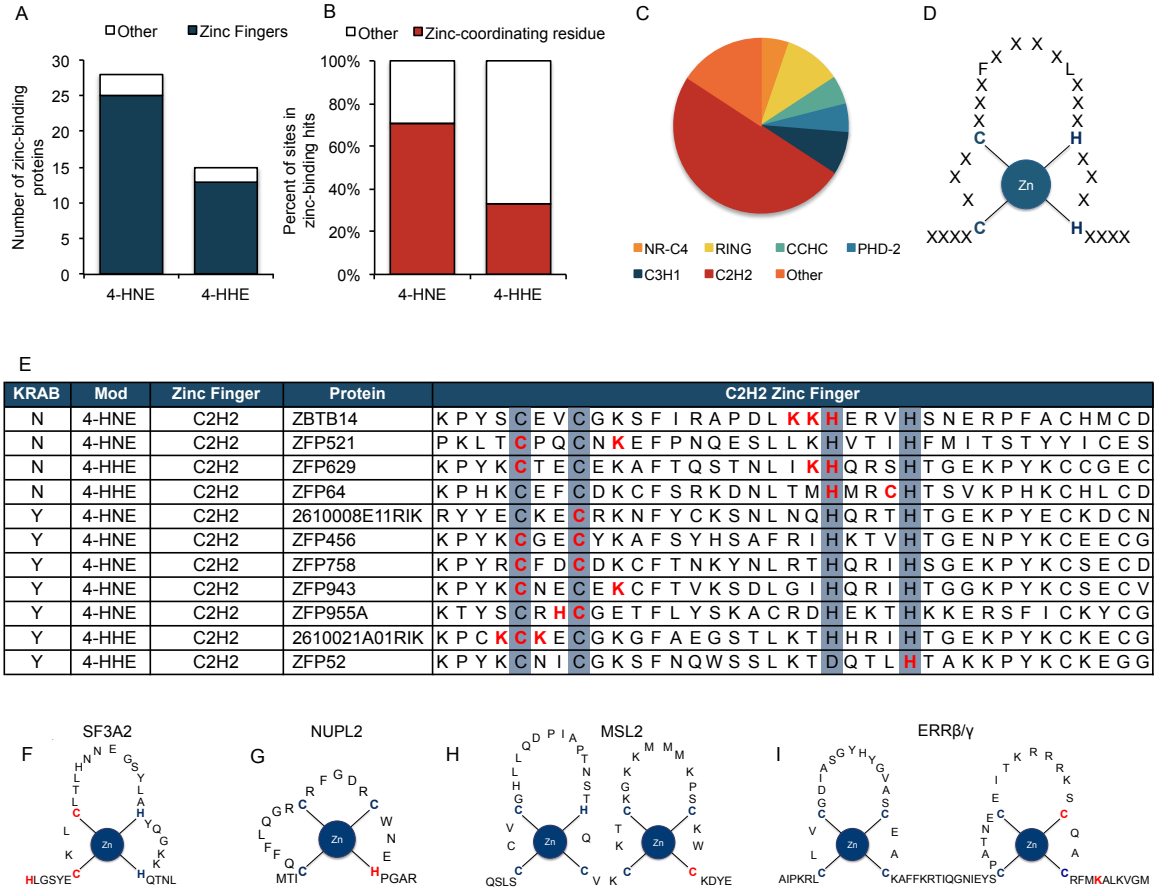

E

KRAB	Mod	Zinc Finger	Protein	C2H2 Zinc Finger
N	4-HNE	C2H2	ZBTB14	K P Y S C E V C G K S F I R A P D L K K H E R V H S N E R P F A C H M C D
N	4-HNE	C2H2	ZFP521	P K L T C P Q C N K E F P N Q E S L L K H V T I H F M I T S T Y Y I C E S
N	4-HHE	C2H2	ZFP629	K P Y K C T E C E K A F T Q S T N L I K H Q R S H T G E K P Y K C C G E C
N	4-HHE	C2H2	ZFP64	K P H K C E F C D K C F S R K D N L T M H M R C H T S V K P H K C H L C D
Y	4-HNE	C2H2	2610008E11RIK	R Y Y E C K E C R K N F Y C K S N L N Q H Q R T H T G E K P Y E C K D C N
Y	4-HNE	C2H2	ZFP456	K P Y K C G E C Y K A F S Y H S A F R I H K T V H T G E N P Y K C E E C G
Y	4-HNE	C2H2	ZFP758	K P Y R C F D C D K C F T N K Y N L R T H Q R I H S G E K P Y K C S E C D
Y	4-HNE	C2H2	ZFP943	K P Y K C N E C E K C F T V K S D L G I H Q R I H T G G K P Y K C S E C V
Y	4-HNE	C2H2	ZFP955A	K T Y S C R H C G E T F L Y S K A C R D H E K T H K K E R S F I C K Y C G
Y	4-HHE	C2H2	2610021A01RIK	K P C K C K E C G K G F A E G S T L K T H H R I H T G E K P Y K C K E C G
Y	4-HHE	C2H2	ZFP52	K P Y K C N I C G K S F N Q W S S L K T D Q T L H T A K K P Y K C K E G G

Figure 4: Zinc-coordinating residues hotspots for protein carbonylation

(A) Quantitation of the number of zinc finger-containing proteins among total zinc binding proteins in the nuclear carbonylome.

(B) Quantitation of the number of sites identified that participate directly in zinc-coordination. Percentage of total sites identified in all zinc-binding proteins.

(C) Distribution of zinc finger domains amongst all zinc finger-containing proteins that were identified.

(D) Model of a typical C2H2 finger. Blue residues coordinate the zinc ion.

(E) Alignment of all C2H2 zinc fingers that with modifications identified within the zinc-binding domain. Blue highlight are zinc-coordinating residues, red letters are sites of modification.

(F-G) Examples of other classes of zinc fingers identified in this study; SFA2 contains a MATRIN TYPE ZF (F), MSL2 contains a RING ZF, NUP2L contains a C3H1 ZF, and ERRβ/γ is a NR-C4-type ZF. Blue residues coordinate zinc, red denotes modified sites.

Functional analysis of estrogen related receptors beta and gamma carbonylation

Due to the central role that zinc-coordination has in stabilizing the DNA-binding capacity of proteins [132,133], we hypothesized that carbonylation of zinc-coordinating residues would disrupt DNA binding. To directly test this hypothesis, we selected estrogen related receptor beta/gamma (ERR-β, ERR-γ) to investigate the functional consequences of the identified modification. The estrogen related receptors are a family of three orphan nuclear receptors that orchestrate transcriptional responses by binding to estrogen-related response elements (ERRE) to activate transcription[134]. Expressed in a variety of tissues, these receptors are critical for maintaining metabolic homeostasis through the regulation of diverse processes including browning, thermogenesis, adipogenesis, oxidative metabolism, and lipid metabolism [135-139]. Importantly, the ERR family of receptors are critical for transcriptional activation of nuclear-encoded mitochondrial genes [134].

Two 4-HHE modifications were identified in the proteomic screen that were located in the DNA binding domain (DBD) of ERR-γ/ERR-β (Figure 5A). Cys155

is the third zinc-coordinating cysteine of the second finger within the DBD while Lys162 is located immediately adjacent to the carboxyl-terminus of the second finger (Figure 5A, 5B). Since the DNA binding domains of ERR-γ and ERR-β are identical, it was not possible to distinguish which of these two proteins resulted in the tryptic peptide carrying the two modifications (Figure 5C). However, since ERR-γ is expressed ubiquitously while ERR-β is expressed primarily in embryonic tissues [134], it is likely that the parent protein is ERR-γ (Figure 5C). Western blots of nuclear lysates from eWAT showed robust protein expression of ERR-γ that is significantly decreased in HFD-fed mice (Figure 5D). Furthermore, treatment of 3T3-L1 adipocytes with a specific ERR-γ inhibitor GSK5182 resulted in decreased expression of known ERR-γ targets Cpt2, Txn2, Atp2a2 and Ndufs2 (Figure S3A).

To confirm that ERR-γ is carbonylated, we isolated nuclei from eWAT depots and used biotin-hydrazide to biotinylate fee protein carbonyls. Affinity purification of the biotinylated substrates followed by western blotting for ERR-γ in both the enriched and supernatant fractions revealed that ERR-γ is detectable in the biotin-labeled fraction, indicating that approximately 30% of ERR-γ is carbonylated in obese eWAT (Figure 5E, left). Since ERR-α is also expressed in white adipose tissue and the sites of modification in ERR-γ are conserved between all three ERR's, we used the same strategy to test whether ERR-α is carbonylated in obese eWAT. Interestingly, a significant pool of ERR-α (~ 50%)

is detectable in the biotinylated fraction, suggesting robust carbonylation in white adipose tissue (Figure 5E, right).

To study the effects of carbonylation on DNA binding, we generated a GST-tagged DNA binding domain from ERR-β (referred to as ERR2-DBD) expressed in *E. coli.* This construct is a good model for binding studies of ERR-γ due to the near-complete conservation of the domain between family members and between mice and humans (Figure S3B). To determine the importance of lysine162 for DNA binding, we mutated K162 to alanine or arginine and performed electrophoretic mobility shift assays (EMSA). Mutation of K162 to alanine results in a nearly complete loss of DNA binding capacity (Figure 5F). Similarly, a lysine to arginine mutation to control for electrostatic differences also led to a significant decrease in DNA-binding, suggesting that K162 not only plays a structural role, but also may play a direct role in sequence-specific DNA recognition (Figure 5F). Next, we in vitro-modified ERR2-DBD with 4-HHE resulting in a robust time-dependent increase in protein carbonylation (Figure 5H). EMSA analysis of the carbonylated and non-carbonylated ERR2-DBD showed a decrease in DNA binding capacity that was dependent on the relative level of 4-HHE modification (Figure 5G, 5I). Collectively, these data suggest that carbonylation of ERRγ functions to inhibit binding to ERRE's in the genome, thereby preventing transcriptional activation of target genes.

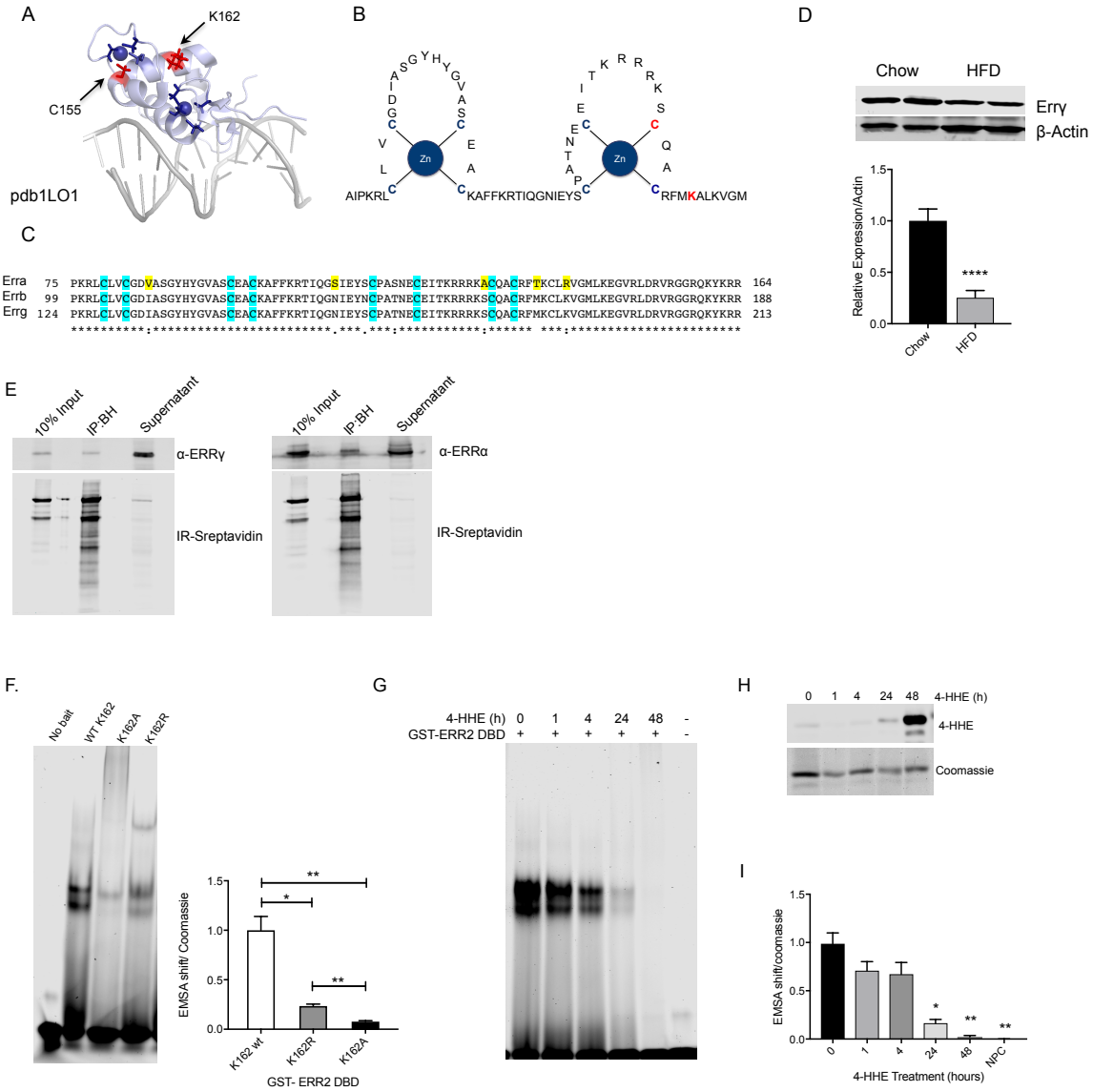
A
K162
C155
pdb1LO1
B
AIPKRL
KAFFKRTIQGNIEYS
RFMKALKVGM
Zn
C
Erra 75 PKRLCLVCGDVASGYHYGVASCEACKAFFKRTIQGSIEYSCPASNECEITKRRRKACQACRFTKCLRVGMLKEGVRLDRVRGGRQKYKRR 164
Errb 99 PKRLCLVCGDIASGYHYGVASCEACKAFFKRTIQGNIEYNCPATNECEITKRRRKSCQACRFMKCLKVGMLKEGVRLDRVRGGRQKYKRR 188
Errg 124 PKRLCLVCGDIASGYHYGVASCEACKAFFKRTIQGNIEYSCPATNECEITKRRRKSCQACRFMKCLKVGMLKEGVRLDRVRGGRQKYKRR 213
D
Chow
HFD
Errγ
β-Actin
Relative Expression/Actin
****
E
10% Input
IP:BH
Supernatant
α-ERRγ
IR-Sreptavidin
α-ERRα
F.
No bait
WT K162
K162A
K162R
EMSA shift/ Coomassie
K162 wt
GST- ERR2 DBD
G
4-HHE (h) 0 1 4 24 48 -
GST-ERR2 DBD + + + + + -
H
4-HHE (h)
4-HHE
Coomassie
I
EMSA shift/coomassie
4-HHE Treatment (hours)
NPC

Figure 5: 4-HHE modification of Estrogen-related receptor beta/gamma disrupts DNA binding

(A) Ribbon diagram of the DNA binding domain (DBD) of ERR-β/-γ. Blue spheres are zinc ions that are each coordinated by 4 cysteine residues in blue. Red are carbonylated sites of modification. Amino acid designations represent the location in ERR-β.
(B) Model of the DBD of ERR-β/-γ.
(C) Alignment of the DBD of the ERR family members. Blue residues coordinate zinc, yellow are those amino acids that differ between ERRα and the other family members.
(D) Western blot of whole cell lysates from chow- and HFD-fed mice (left), and quantitation (right).
(E) Western blot of immunoprecipitated biotin-hydrazide labeled proteins from eWAT of HFD-fed mice. IP:BH is the total immunoprecipitated fraction, supernatant is all protein remaining post-IP. Biotin label is detected with IR Streptavidin. ERRγ (left) and ERRα (right) are both detected in the BH IP lanes.
(F) EMSA of WT ERR2 DBD, K162A, and K162R mutants (left). Probe only control contains no ERR2 DBD. Quantitation normalized to coomassie stain of protein (right).
(G) EMSA of WT ERR2 DBD that has been in vitro modified with .5 mM 4-HHE for 0,2,4,24, or 48 hours.
(H) Western blot of in 4-HHE in vitro modified ERR2-DBD.
(I) Quantitation of (G) normalized to coomassie stain of protein.

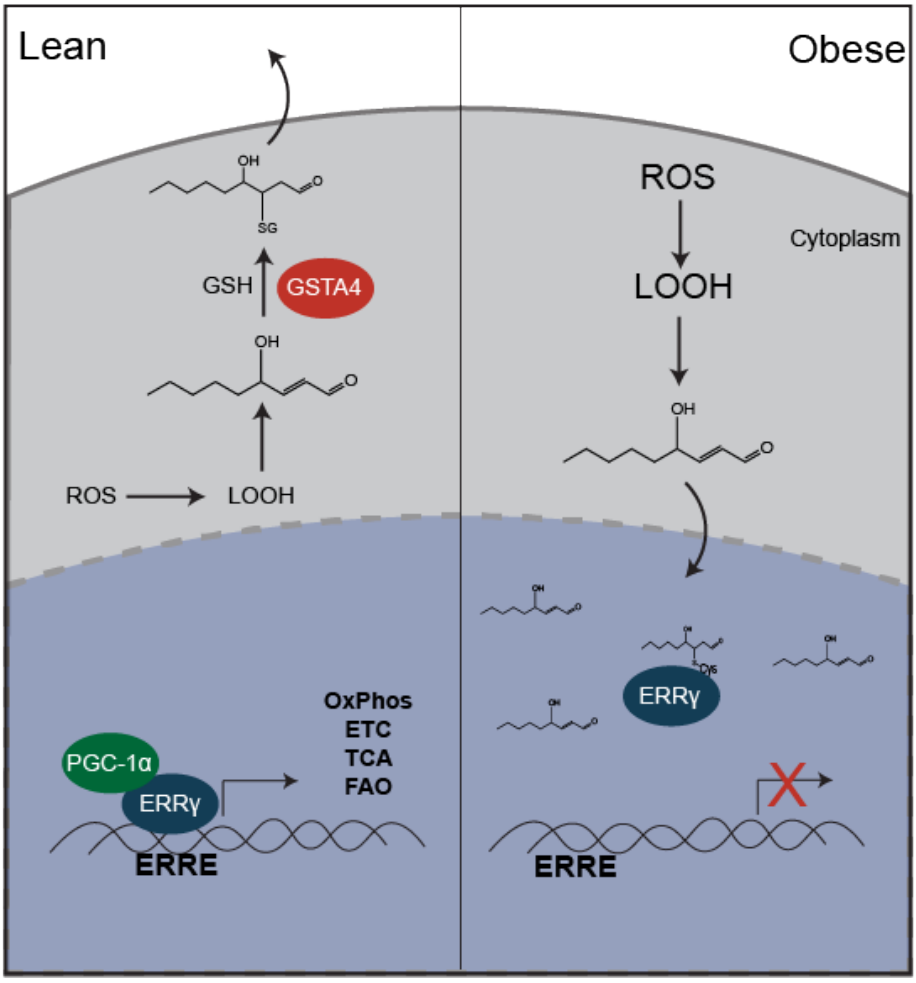

Figure 6. Summary: Protein carbonylation of zinc fingers in the adipocyte nucleus

Under lean conditions, ROS production is balanced by antioxidant capacity. GSTA4 is a major antioxidant responsible for glutathionylation of reactive lipids, allowing for their eventual excretion. Depletion of intracellular antioxidants leads to elevated levels of reactive lipid aldehydes and accumulation of nuclear protein carbonylation in the obese state. ERRγ is a target of this modification, leading to decreased binding capacity to target genes.

Discussion

Protein carbonylation by reactive lipid aldehydes has long been appreciated as a direct consequence of elevated reactive oxygen species [140,141] and/or depletion of glutathione stores. As such, carbonylation targets have been studied at length in tissues and disease models in which oxidative stress is elevated [142]. In obesity-linked insulin resistance a variety of studies have shown that oxidative stress plays a causal role in metabolic dysfunction but the mechanism(s) remains unclear

[7,143]. In the majority of animal models, and in human biology, accumulation of adipose tissue in the visceral depot is a positive risk factor for metabolic disease while subcutaneous adipose tissue is considered to often be protective in the context of obesity [144]. While oxidative stress and glutathione depletion in the visceral depot is linked to insulin resistance, the molecular mechanisms connecting such changes to metabolic dysfunction remain poorly characterized. Herein, we show that protein carbonylation is selectively upregulated in the nucleus of obese eWAT but not in the nuclear fraction of inguinal adipose tissue (Figure 1). Moreover, using 3T3-L1 adipocytes, glutathione depletion using erastin resulted in increased protein carbonylation that localized to the nucleus as well (Figure 1D). Prior work from the laboratory has shown that the expression of key antioxidants such as peroxyredoxin3, glutathione peroxidase4 and glutathione S-transferase4 are selectively down regulated in the visceral, but not subcutaneous, depot of high fat fed mice and that the decreased expression

is correlated with increased levels of reactive aldehydes including 4-HNE [61]. Whereas plasma membrane NADPH oxidase, endoplasmic reticular Ero1, xanthine oxidase/dehydrogenase and the mitochondrial electron transport chain have been considered the major sites for ROS synthesis in adipose tissue, the specific sites for protein carbonylation have been less well characterized. The results of this study are surprising for they point towards the nuclear localization of carbonylated proteins and the potential for transcriptional control by oxidative stress-dependent mechanisms.

Analysis of the adipose carbonylome resulted in the identification of over 100 novel, endogenous targets of protein carbonylation as well as the type of aldehyde (9-carbon 4-HNE or 6-carbon 4-HHE) carrying out the modification. Contrary to previous work on mitochondrial carbonylation that delimited highly enriched pathways [11], the nuclear carbonylome did not exhibit any such bias. This is not unusual for chemically driven modifications where enzymatic regulation is not a driving factor. Our previous studies defining cytoplasmic or mitochondrial protein targets of carbonylation have been limited in depth due to the use of non-specific derivitization methods that do not enable one to distinguish between sites of modification or the many possible types of carbonylation events [8,11]. Our proteomic workflow (Figure 2A) herein differs in several important ways from that utilized previously by our group [11] in that we used an antibody specific for 4-HNE to enrich for carbonylated proteins. This

allowed for enrichment of 4-HNE modified substrates and specific identification of 4-HNE adduction sites. In addition, we enriched at both the protein and the peptide levels. This ensures that even low abundance peptides with the modification will be detected. Importantly, we found that reduction of nuclear extracts using sodium borohydride dramatically increased the reproducibility of analysis and the yield of carbonylated proteins and peptides.

The major protein group we identified as carbonylation targets were zinc-coordinating proteins and that the site of modification was typically a residue on or adjacent to the zinc coordinating amino acids (Figure 2). From this analysis we also defined the protein landscape surrounding carbonylation sites providing for the first time insight into the chemical environment that makes modification favorable by endogenous lipid aldehydes. In general, we found that for both 4-HNE and 4-HHE carbonylation occurred approximately equally on cysteine, histidine and lysine side chains. For cysteine carbonylation, the most striking motif defined by the proteomic analysis was the CX2**C**X2C motif in which for both 4-HNE and 4-HHE modification the central modified cysteine residue was flanked at the +3 or the -3 position by another cysteine residue. While there was no general motif evident from the modification of histidine or lysine side chains, the region surrounding the carbonylated amino acid had a relatively high content of basic lysine residues. Interestingly, analysis of each of the 6 modifications

(Figure 3) revealed the presence of a proline residue within the +7 to -7 region suggesting the potential for a unique structural determinant for carbonylation.

Our results did reveal a strong enrichment of zinc binding proteins with the majority of defined carbonylation sites in zinc-coordinating residues (Figure 4). Zinc coordination is generally achieved via a tetrahedral geometry of 4 residues that typically includes 2-3 cysteine residues [133]. Importantly, the ability of a cysteine to participate in zinc binding is dependent on a completely reduced, unmodified thiol. Redox metabolism that is coupled to zinc binding is not uncommon; indeed there are many proteins that undergo a redox-switch whereby oxidation of a zinc-coordinating residue results in the release of zinc and a conformational change in the protein [132]. For example, heat shock protein 33 (Hsp33) is activated in response to oxidative stress and acts to prevent protein unfolding and aggregatation [145]. Structural studies of the Hsp33 mechanism revealed that under normal conditions, Hsp33 exists in a monomeric state with a tight zinc-coordinating domain on the C-terminus. In response to oxidative stress, one of the four zinc-coordicating cysteins is oxidized, leading to the unfolding of the C-terminal domain and subsequent dimerization of Hsp33 into its active state [145]. Importantly, this is most often a reversible process, as cysteine thiols can readily be re-reduced resulting in restored zinc binding capability [132]. As such, it is possible that carbonylation of the zinc-coordinating residues identified in this study results in the release of zinc and loss of structural

integrity of the domain. However, since there are no known enzymes that can remove 4-HNE and 4-HHE Michael adducts from their substrates, these modifications result in the permanent disruption of secondary structure in those proteins.

Finally, we explored the functional significance of carbonylation of zinc fingers and showed that the ERR family of nuclear receptors are carbonylated in vivo and this leads to a severe impairment in DNA binding capacity. Zinc fingers are most commonly observed in DNA-binding proteins and are critical for sequence-specific DNA binding of a wide variety of proteins involved in transcription, replication, and repair [146,147]. It is appreciated that these proteins are sensitive to oxidative stress though the mechanisms by which this occurs remain elusive [132,148]. Our data strongly supports a model by which oxidative stress results in carbonylation of zinc finger proteins, disrupting their ability to bind DNA resulting in a loss of transcriptional regulation. 4-HHE modification of the ERR-γ is an example of one such event that is of critical importance for energy metabolism. The site of modification of ERR-α/-γ was within or adjacent to the second zinc finger that resides on the helix that caps and is perpendicular to the DNA contacting helix. A large fraction of ERR-α (~ 50%) and ERR-γ (~ 30%) were found to be carbonylated. Consistent with this, many transcriptional targets for ERRs are down regulated in the obese state relative to lean controls including Cpt2, Txn2, Atp2a2, and Ndufs2 [149], leading to the consideration that ERR

carbonylation may be functional and selectively reduce gene expression. The ERR-α and ERR-γ are broadly expressed in tissues that have high bioenergetics demands. Although their specific effects and gene targets are broad, they are most well known for their role in promoting mitochondrial bioenergetics pathways including oxidative phosphorylation, fatty acid oxidation, TCA cycle, and electron transport chain proteins [134]. Our data is consistent with a model in which oxidative stress leads to the carbonylation of ERR-γ/-α leading to impairment in the expression of target genes.

A major unknown revealed by this study is the source of ROS and aldehydes that lead to nuclear carbonylation. When considering either high fat feeding in vivo or glutathione depletion in 3T3-L1 adipocytes, there are numerous sources of ROS that can lead to 4-HNE or 4-HHE production. While superoxide anion is highly labile and has a short half-life, hydrogen peroxide is relatively stable and able to diffuse across membranes to various sites within the cell. Hydroxyl radicals that are the critical ROS agent leading to reactive lipid aldehydes are also highly labile and as such, defining the site of ROS synthesis is critical. In parallel, medium chain lipid aldehydes are also capable of rapid diffusion across biological membranes and therefore, while the nucleus may be the site of protein carbonylation, it is not clear what is the origin of the aldehydes. The results presented herein suggest either reactive aldehyde synthesis in the nucleus or retrograde movement to the nucleus from their site of origin.

Abbreviations and Acknowledgements

Acknowledgements

We would like to thank Peter Wright for the kind gift of the ERR2 DBD construct. We thank the members of the Bernlohr laboratory for helpful discussions during the preparation of this chapter.

Abbreviations

4-HNE – *trans*-4-hydroxy-2-nonenal; 4-HHE – *trans*-4-hydroxy-2-hexenal; ERRγ – Estrogen related receptor gamma; ROS – reactive oxygen species; eWAT – epididymal adipose tissue; iWAT – inguinal white adipose tissue; GSTA4 – glutathione-S-transferase A4; HFD – high fat diet; GO – gene ontology; ZBD – zinc binding domain; KRAB – Krüppel associated box; KAP1 – KRAB associated protein 1; ERRE – Estrogen related response element; DBD – DNA binding domain; SOD1 – Superoxide dismutase 1.

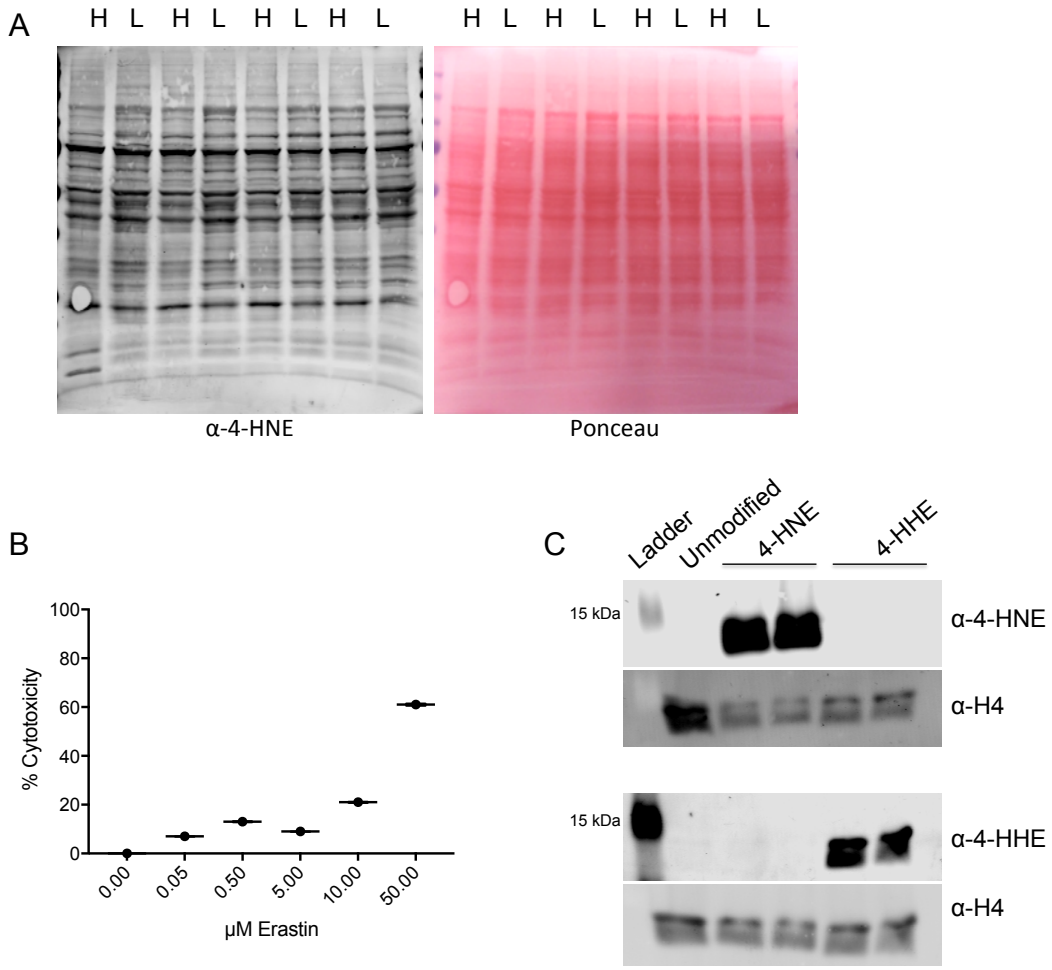

Supplementary Figure 1. Protein carbonylation in adipose tissue.

(A) Western blot of mitochondrial extracts from chow (L) and high-fat (H) fed mice (Left). Ponceau stain of membrane (right)

(B) Western blot of 4-HNE adducts in nuclear lysates and post-nuclear lysates from chow- and HFD-fed mice.

(C) Cytotoxicity assay of erastin-treated 3T3-L1 adipoctyes. Cells were treated with erastin or vehicle (DMSO) for 24 hours.

(D) Western blot of in vitro modified recombinant histone H4 (rH4) with 4-HNE or 4-HHE. Normalized to histone H4.

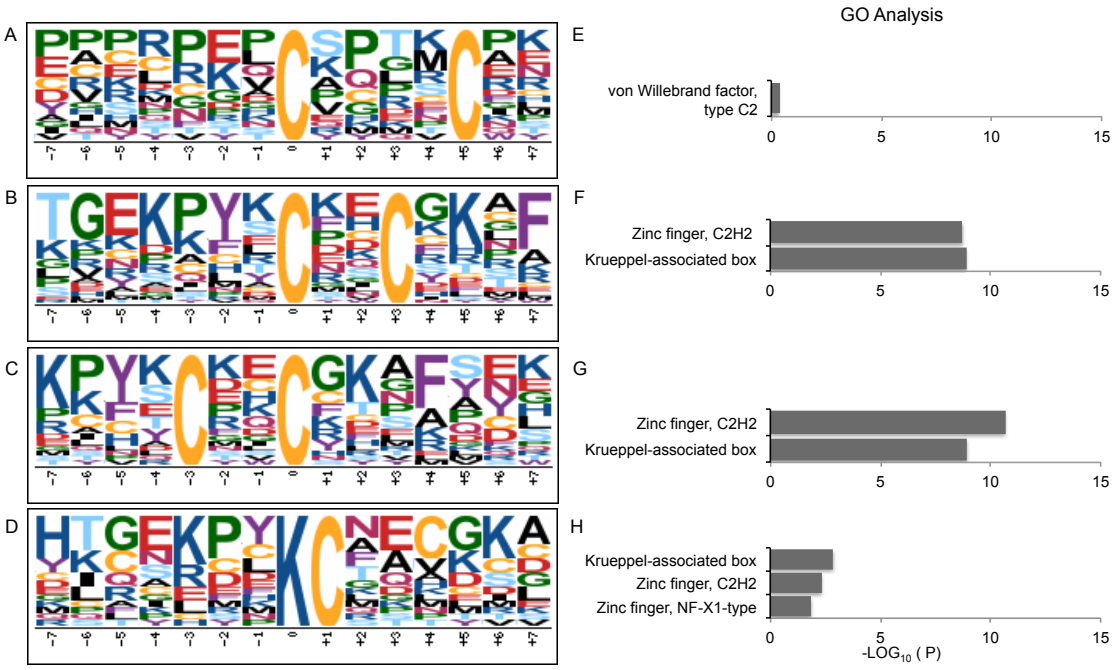

Supplementary Figure 2: Motif analysis of carbonylation sites.

(A-D) Flanking sequence distribution for each of the four motifs identified with motif-x.

(E-H) Gene ontology analysis of the proteins matching each motif with statistical enrichment of structural motifs. (Benjamini-Hochberg adjusted P value).

S2A

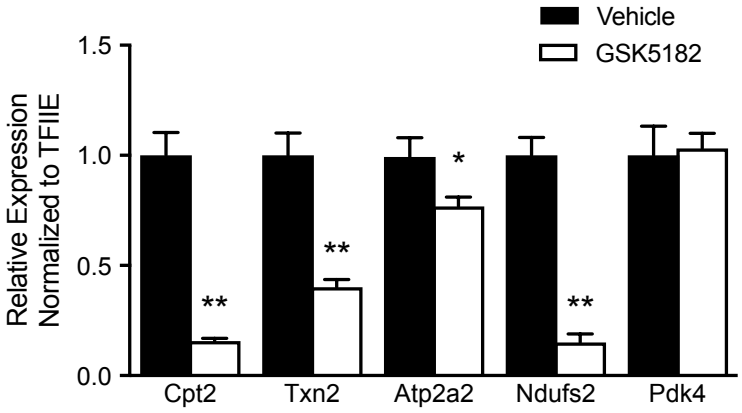

S2B

Seq_1 = mouse ERRg1 NP_036065
Seq_2 = GST-ERR2 DBD (97-194 C163A)

```
Seq_1  124   ------------------------------------------------------------  123
Seq_2  95    LEGAVLDIRYGVSRIAYSKDFETLKVDFLSKLPEMLKMFEDRLCHKTYLNGDHVTHPDFM  154

Seq_1  124   ------------------------------------------------------------  123
Seq_2  155   LYDALDVVLYMDPMCLDAFPKLVCFKKRIEAIPQIDKYLKSSKYIAWPLQGWQATFGGGD  214

Seq_1  124   --------------pkrlclvcgdiasgyhygvasceackaffkrtiqgnieyscpatne  169
                           ||||||||||||||||||||||||||||||||||||||||||||||
Seq_2  215   HPPKSDLVPRGSAIPKRLCLVCGDIASGYHYGVASCEACKAFFKRTIQGNIEYSCPATNE  274

Seq_1  170   ceitkrrrkscqacrfmkclkvgmlkegvrldrvrggrqkykrridaenspylnpqlvqp  229
              ||||||||||||||||| |||||||||||||||||||||:| |||
Seq_2  275   CEITKRRRKSCQACRFMKALKVGMLKEGVRLDRVRGGRQKYKRRLDSENS----------  324

Seq_1  230   akkpynkivshllvaepekiyampdptvpdsdikalttlcdladrelvviigwakhipgf  289
Seq_2  325   ------------------------------------------------------------  324

Seq_1  290   stlsladqmsllqsawmeililgvvyrslsfedelvyaddyimdedqsklaglldlnnai  349
Seq_2  325   ------------------------------------------------------------  324
```

Supplementary Figure 3: ERR family of nuclear receptors are carbonylated in vivo

(A) q-RT-PCR of ERRγ targets in 3T3-L1 adipocytes treated with vehicle or ERRγ inhibitor GSK1582.

(2) Amino acid alignment of the DBD of mouse ERRγ(NP_036065) and GST-ERR2 DBD. Grey highlight denotes the DBD.

Category	Term	Count	%	PValue	Fold Enrichment	Bonferroni	Benjamini	FDR
UP_KEYWORDS	Zinc-finger	37	30.8	1.46E-14	4.47	2.6E-12	3E-12	2E-11
UP_KEYWORDS	Zinc	41	34.2	1.60E-13	3.69	2.8E-11	1E-11	2E-10
UP_KEYWORDS	Metal-binding	50	41.7	3.87E-12	2.78	6.8E-10	2E-10	5E-09
UP_KEYWORDS	Ubl conjugation pathway	10	8.3	0.0061	3.00	6.6E-01	2E-01	7E+00
UP_KEYWORDS	DNA-binding	17	14.2	0.0097	2.00	8.2E-01	3E-01	1E+01
UP_KEYWORDS	Transcription regulation	18	15.0	0.0127	1.89	9.0E-01	3E-01	1E+01
GOTERM	Regulation of transcription, DNA-templated	28	23.3	1.9E-04	2E+00	1E-01	1E-01	3E-01
GOTERM	Negative regulation of NF-kappaB transcription factor activity	4	3.3	6.7E-03	1E+01	1E+00	9E-01	1E+01
GOTERM	Positive regulation of sequence-specific DNA binding transcription factor activity	4	3.3	2.4E-02	6E+00	1E+00	1E+00	3E+01
GOTERM	Response to superoxide	2	1.7	2.9E-02	7E+01	1E+00	1E+00	4E+01
KEGG_PATHWAY	Regulation of lipolysis in adipocytes	3	2.5	0.030	10.69	0.978	0.978	29.890
KEGG_PATHWAY	Progesterone-mediated oocyte maturation	3	2.5	0.065	7.01	1.000	0.985	53.947
KEGG_PATHWAY	NF-kappa B signaling pathway	3	2.5	0.078	6.28	1.000	0.967	61.084
INTERPRO	Zinc finger, C2H2	17	14.1667	1.68E-06	4.31	0.001	0.001	0.002
INTERPRO	Zinc finger C2H2-type/integrase DNA-binding domain	16	13.3333	1.99E-06	4.55	0.001	0.000	0.003
INTERPRO	Zinc finger, C2H2-like	16	13.3333	4.19E-06	4.28	0.001	0.000	0.006
INTERPRO	Zinc finger, RING-type	8	6.6667	8.71E-04	5.19	0.242	0.067	1.169
INTERPRO	Krueppel-associated box	9	7.5000	8.84E-04	4.48	0.245	0.055	1.186
INTERPRO	von Willebrand factor, type C	4	3.3333	1.36E-03	18.10	0.352	0.070	1.823

Table 2. Gene ontology analysis of nuclear carbonylation sites.

Mod	Motif	Protein	Zinc-Coordinating Domain
4-HNE	ZF_FYVE	ZFYVE1	N S Q I L S C N Q C A T S F K D N D T K H H C R A C G E G F C D S C S S K T R P V P E R G W G P A P V R V C D S C Y D A R N
4-HNE	LIM_DOMAIN	GM4907	Y T C Y C C K H P M K E G D P A I Y A E R A G Y S K L W H P A C F I C S I C G E I L V D M I Y F W K N G K L Y C G R H Y C D S E
4-HNE	PHD_2	KMT2C	D N L C P F C G K C Y H P E L Q K D M L H C N M C K R W V H L E C D K P T D Q E L D S Q L K E D Y I C M Y C K H L
4-HNE	ZF_RING_2	MSL2	C C V C G H L L Q D P I A P T N S T C Q H Y V C K T C K G K K M M K P S C S W C K D Y E Q F E E
4-HNE	C3H1	NUPL2	M T I C Q F F L Q G R C R F G D R C W N E H P G A R G A G G A R Q P P P Q Q Q
4-HHE	NR_C4	ESRRB/G	C P A T N E C E I R K R R R K S C Q A C R F M K C L K V G M L K E G V R L
4-HNE	ZF_BBOX	TRIM37	F R C F I C M E K L R D A R L C P H C S K L C C F S C I R R W L T E Q R A Q C P H C R
4-HNE	C3H1	ZC3H14	P S S N G Q L C R Y F P A C K K M E C P F Y H P K H C R F N T Q C
4-HNE	BIR_REPEAT	BIRC3	T G A N D K V K C F C C G L M L D N W K Q G D S P M E K H R K L Y P S C N F V Q
4-HNE	ZF_BBOX	TRIM36	P K V L M C P E H E T E R I N M Y C E L C R R P V C H L C K L G G N H S N H R V T T M
4-HHE	ZF_RING_DEG	RNF144B	P I K Q C P V C R I Y I E R N E G C A Q M M C K N C K H T F C W Y C L Q N L
4-HHE	C2H2 MATRIN	SF3A2	F M K N H L G S Y E C K L C L T L H N N E G S Y L A H Y Q G K K H Q T N L A R

Table 3. Carbonylation of zinc-coordinating residues in non-C2H2 ZF motifs.

CHAPTER THREE

Histone carbonylation is a redox-regulated epigenomic mark that accumulates in obesity and aging

Amy K. Hauck[1], Tong Zhou[1], Raphael Petegrosso[2], , Ambuj Upadhyay[3], Rui Kuang[2], Michael B. O'Connor[3], Yue Chen[1], and David A. Bernlohr[1]

[1]Department of Biochemistry, Molecular Biology, and Biophysics, University of Minnesota, Minneapolis, MN 55455

[2]Department of Computer Science and Electrical Engineering, University of Minnesota, Minneapolis, MN 55455

[3]Department of Molecular Biology, Cell Biology, Developmental Biology, and Genetics, University of Minnesota, Minneapolis, MN 55455

This chapter contains an original research article in preparation to be published.

Tong Zhou performed LC-MS/MS analysis. Raphael Petegrosso perfomed analysis of ChIPseq data. Amy Hauck performed all other experiments, analysis and manuscript preparation.

Summary

Oxidative stress is long-appreciated hallmark of metabolic disease, though the mechanisms that connect oxidative stress to altered metabolism, particularly in the mitochondrion, remain poorly understood. Through the study of protein carbonylation, the modification of proteins by reactive lipids 4-hydroxynonenal (4-HNE) and 4-hydroxyhexenal (4-HHE), we identified a novel class of histone modifications that are dependent upon obesity and aging in white adipose tissue. Using label free proteomics we identified 14 sites of histone carbonylation, including sites from both the N-terminal tails as well as sites contained within the histone fold. These data provide evidence for a new class of epigenomic regulators that has major implications for the progression of metabolic disease.

Introduction

Obesity is a chronic, low grade inflammatory state in which increased pro-inflammatory signaling leads to oxidative stress, altered cellular metabolism, and the development of insulin resistance[150]. Dysregulation at the transcriptional level of major metabolic pathways in response to oxidative stress is a phenotypic hallmark of obesity[102,150]. In particular we have observed down regulation of the mitochondrial antioxidants as well as the enzymes of the branched chain amino

acid and tricarbonxylic acid pathways in response to inflammatory signals[61,95,103]. These data suggest that the mitochondrial proteome is broadly reprogrammed as a consequence of obesity-linked inflammation. Despite these observations, the mechanisms that link inflammation and oxidative stress to an altered transcriptional milieu of metabolic genes in adipose tissue remain unclear.

Oxidative protein damage represents an attractive mechanistic target behind this process because it is directly correlated with the levels of reactive oxygen species (ROS) present [6,28]. In the obese state, oxidative stress is the combined result of increased production of ROS and decreased expression of the major antioxidant enzymes responsible detoxifying these damaging species[1]. The net result is the channeling of ROS towards the formation of the hydroxyl radical[151]. This species cannot be metabolized and is only reduced by the removal of hydrogen atoms from neighboring molecules. Polyunsaturated lipids (either free fatty acids or membrane phospholipids) are particularly susceptible to this type of oxidation, ultimately leading to the formation of highly reactive, diffusible lipid aldehydes. These aldehydes, such as 4-hydroxynonenal (4-HNE), are subject to nucleophilic attack by lysine, cysteine, and histidine residues, resulting covalent lipid adducts [1]. Although the modification is chemical, it is clear that specific proteins are modified. In addition, there is recent evidence that suggests that de-carbonylation is an enzymatically-driven process and that the steady state level

of carbonylation is driven by the balance between chemical modification and enzymatic de-modification [152].

Notably, in the obese state protein carbonylation in adipose tissue is increased up to three-fold, often leading to protein dysfunction and altered mitochondrial output [11,54]. As such, identifying and characterizing carbonylation events in adipose tissue has been the subject of intense study[1]. Recent work from our laboratory has led to the surprising discovery that the major site for differential carbonylation of proteins in adipose is not the mitochondrion, as previously believed, but the nucleus. This was an unanticipated result that has opened the door for a new mechanistic connection between oxidative stress and nuclear regulatory events. Indeed, proteomic evaluation of nuclear carbonylation targets revealed that many transcriptional and chromatin-associated regulatory proteins are modified in the obese state (Bernlohr lab, unpublished).

Here, we expand upon these studies and describe the post-translational modification of histones by reactive lipid aldehydes 4-HNE and 4-HHE. We find that the core histones are specific targets of carbonylation and that these modifications accumulate in adipose tissue as a consequence of high-fat diet (HFD) and of aging. Furthermore, 4-HNE and 4-HHE, despite their chemical similarity, modify different sites, introducing the concept that each oxidation event may initiate distinct signaling outcomes. Finally, we evaluate the functional role of

histone carbonylation by investigating the genomic localization of carbonylation events in comparison to transcriptional outcomes. Together, this work suggests that histone carbonylation is an abundant epigenomic modification that is a critical link between oxidative stress and metabolic dysfunction in adipose tissue.

Materials and Methods

Animals

Wild-type C57Bl/6J mice were weaned at 3 weeks of age and then fed either a high fat diet (20% protein, 35.5% fat, 36.3% carbohydrate; BioServ F3282) or a chow diet for 12 weeks. O*b/ob* mice were obtained at 10 weeks and maintained on chow diet for two weeks prior to sacrifice. Animals were sacrificed by cervical dislocation and epididymal and inguinal white adipose depots were removed for analysis. Experiments were carried out were approved by the University of Minnesota Institutional Animal Care and Use Committee. For the Aging experiment, eWAT tissues were obtained from Yuxiang Sun (Texas A&M University).

Drosophila melanogaster flies (*yw* WT strain) were reared on standard agar-cornmeal medium at 25°C under a 12:12 h light/dark cycle. Male and female flies were collected within 24-hours of eclosion and housed separately (50-60 flies per vial). Flies were counted and transferred to new vials every two days for the duration of the experiment. At the appropriate time points, flies were collected, snap-frozen in liquid nitrogen, and stored at -80°C until processing.

Cell Culture

3T3-L1 fibroblasts were grown to confluence and differentiated as previously described[108] using the standard differentiation cocktail consisting of dexamethasone, methylisobutylxanthine, and insulin. On day 7 of differentiation, cells were treated with 10 uM erastin (Cayman Chemical 177754) or vehicle (DMSO) in DMEM +5%FBS for 24 hours before harvesting.

Histone Preparation

From mice, fresh tissue was minced on ice in hypotonic lysis buffer (10 mM Tris-Cl pH 8.0, 1 mM KCl, 1.5 mM MgCl2, 1mM DTT) with protease and phosphatase inhibitors. Tissue was homogenized with a glass-Teflon system using an electric homogenizer (8 strokes, 1600 rpm). Samples were spun at 1000 rpm at 4°C for 10 minutes and the fat cake was discarded. Then, samples were briefly vortexed and spun at 3700 rpm at 4°C for 10 minutes to collect nuclei. Histones were purified using acid extraction, reduced in 15mM $NaBH_4$, and quantitated using the BCA assay (Sigma Aldrich). Where indicated, histones were salt-purified using the method described by Schecter et, al.[153]

From flies, frozen pellets were ground using mortar/pestle in hypotonic lysis buffer supplemented with 1% NP40 and .1% SDS. Insoluble debris was cleared

and nuclei were collected by centrifugation. Histones were prepared as described above.

Western blotting analysis

Samples were prepared for western blot by mixing normalized samples with 4X loading buffer. Samples were resolved by SDS-PAGE, wet transferred to nitrocellulose membrane, blocked for 1 hour with blocking buffer (LI-COR 927-4000) and incubated with primary antibodies overnight at 1:1000 dilutions in TBS-T + 5% BSA. Membranes were then washed 3X in TBS-T and incubated for 1 hour with fluorescently labeled secondary antibodies (LI-COR) and imaged using the LI-COR Odyssey Imager. Antibodies used include 4-HNE (Millipore, 393207), 4-HHE (non-commercial), Histone H3 (abcam 10799), and Histone H4 (Cell Signaling 2935S).

In vitro modification of purified histones

Acid extracted histones were resuspended in Adduction Buffer (100 mM potassium phosphate pH 7.4, 150 mM NaCl). Samples were then incubated at 37°C with the indicated concentrations of 4-HNE (Cayman Chemical 32100) and 4-HHE (Cayman Chemical 32060). Reaction was quenched with 5 mM DTT. Modification was verified by western blotting.

Chromatin and Nucleoplasm Separation

Cells were washed 3X with PBS and lysed in hypotonic lysis buffer (10 mM Tris-Cl pH 8.0, 1 mM KCl, 1.5 mM MgCl2, 1mM DTT) with protease and phosphatase inhibitors. Nuclei were collected by centrifugation (10 minutes, 10,000 rpm at 4°C) and washed 2X with hypotonic lysis buffer. Nuclei were then resuspended in low salt buffer (10 mM Tris-Cl pH 7.4, .2 mM $MgCl_2$, 1% Triton X-100, protease & phosphatase inhibitors) and incubated on ice for 15 minutes. Samples were spun at 14,000 rpm for 10 minutes at 4°C. The supernatant (nucleoplasmic fraction) was collected and concentrated prior to analysis. The pellet (chromatin fraction) was resuspended directly into 1X loading buffer. The entire sample for each fraction loaded into each lane and resolved by SDS-PAGE into order to appropriately compare histone content.

Immunoprecipitation of carbonylated proteins

For IP of proteins, 10-20 ug of reduced, purified histones were diluted to 500 ul with a PBS+ 1% NP40 and then pre-cleared with protein A/G agarose resin (Sant Cruz sc-2004). 4-HNE primary antibody (Millipore 393207) was cross-linked to protein A/G agarose resin using DMP imidoester crosslinking reagent (Thermo Scientific) according to manufacturer's instructions. Cross-linked antibody/resin was incubated with histones overnight. The next day, resin was washed 3X with RIPA buffer and proteins were eluted by boiling in 4X DNS. Samples were

resolved by SDS-PAGE and stained with Imperial Protein Stain (Thermo Scientific) prior to in gel digestion.

In gel digestion

SDS-PAGE gel bands (H1,H2A/B &3, H4) were first washed by 50% EtOH in water for overnight and then washed by water for an hour. Each gel band was cut into small pieces and then dehydrated by acetonitrile. Proteins were reduced and alkylated at room temperature in dark by TCEP (15 mM) and iodoacetimide (45 mM) in PBS. Then the gel pieces were washed sequentially by 50 mM ammonia bicarbonate, 100% acetonitrile, and dried completely by SpeedVac (ThermoFisher). Trypsin stock solution (Promega) was reconstituted in 50 mM ammonia bicarbonate buffer to 10 ng/μl and applied to digest proteins in-gel for overnight at 37 °C. Peptides were extracted sequentially by Extraction Buffer (5% trifluoroacetic acid and 50% acetonitrile in water, v/v) and 100% acetonitrile. The pooled peptide extracts were dried in SpeedVac and then desalted by C18 Stagetip as previously described.[109]

LC-MS/MS

Peptides were reconstituted in HPLC buffer A (0.1% formic acid in water, v/v) and injected into a Proxeon Easy nLC 1000 HPLC system (ThermoFisher) by

autosampler. Peptides were separated by C18 column packed in-house (15 cm × 75 μm, ReproSil-Pur Basic C18, 2.5 μm, Dr. Maisch GmbH) with a linear gradient of 5%-35% HPLC buffer B (0.1% formic acid in acetonitrile, v/v) at a flow rate of 200 nl/min. Eluted peptides were directly electrosprayed into the Fusion Orbitrap mass spectrometry (ThermoFisher). The instrument was operated in a data-dependent mode with full mass spectra were acquired with a resolution of 120,000 FWHM at 200 m/z and MS/MS spectra were acquired using collision-induced dissociation (CID) with 35% collision energy for detection in the ion trap.

MS data processing

Raw MS data were processed by MaxQuant software (v 1.5.3.12) for protein identification.[110] Variable modifications include carbamidomethylation on cysteine and lysine, methionine oxidation, protein N-terminal acetylation, HNE and reduced HNE on cysteine, histidine and lysine, as well as HHE and reduced HHE on cysteine, histidine and lysine. Trypsin was selected as the proteolytic enzyme and a maximum of two missing cleavages were allowed. The precursor ion mass tolerance was set to +/-4.5 ppm and the fragment ion mass tolerance was set to +/-0.6 Da. MS data were searched against the Uniprot mouse database (released on 2013/09/27 and containing 43310 sequences). Peptides were filtered with a 1% False Discovery Rate (FDR) at the peptide, protein and modification site levels. A minimum Andromeda score of 40 was required for the identification of modified peptides.

Preparation of sheared chromatin

3T3-L1 cells were grown in 10 cm plates, differentiated according to normal protocol and treated on day 7 with erastin (Cayman Chemical 177754) or vehicle (DMSO). Cells were washed 2X with ice cold PBS. Cells were harvested by scraping into .5 mL of lysis buffer (0.1% SDS, 1% Triton X-100, .15 M NaCl, 1 mM EDTA, 20 mM Tris pH 8) and incubated on ice for 30 minutes. Cells were homogenized on ice with 10 strokes using a glass manual homogenization system. Nuclei were collected by centrifugation for 10 minutes at 5000 rpm at 4°C. Nuclei pellets were resuspended in 15 mM $NaBH_4$ and incubated at RT for 20 minutes for aldehyde reduction. Nuclei were collected by centrifugation and washed 3X with PBS. Chromatin was sheared enzymatically using the ChIP-IT Express Enzymatic Shearing Kit (Active Motif 53035) according to manufacturer's instruction. The shearing reaction was incubated at 37°C for 10 min with vortexing every two minutes. The reaction was stopped with EDTA and incubated on ice for 10 minutes. Insoluble material was cleared by centrifugation and chromatin was stored at -80°C until it was used for ChIP experiments.

ChIP-PCR and ChIP-seq

Sheared chromatin was immunoprecipitated with antibodies for 4-HNE (Millipore, 393207), H3 (abcam 1791), H3K27me^3 (Active Motif 39156), H3K4me^3 (abcam 8580), rabbit IgG (abcam, 171870). Protein A Dynabeads (novex 100001D) were

used to magnetically capture immune complexes. Samples were then eluted with 1% SDS and .1M $NaHCO_3$ followed by DNA precipitation.

For ChIP-seq, ChIP was carried out independently for 6 samples each of erastin- and vehicle-treated cells. 3 ChIP reactions were pooled together for each condition prior to library preparation and sequencing. Library preparation (Thruplex ChIPseq libraries) and deep sequencing (HiSeq 2500, 50-bp single read) was carried out at the University of Minnesota Genomics Core.

For ChIP-PCR, the immunoprecipitated DNA and input DNA amplified using a Bio-Rad iCycler thermocycler with iQ SYBR Green Supermix. Control primers for a gene desert on chromosome 6, Pax-2, and Actb-1 were purchased from Active Motif (71011,71020, 71015). All other primers are listed in Table 1.

Gene	Primer Sequence
Nrf2A fwd	CGAGCATATCTCCTAGT
Nrf2A rev	CTACTTGCAGAGGTGAG
Ndufa2 fwd	CACTACGCACTACGCAACTA
Ndufa2 rev	GCCTCTCTTTTAGGGACGTG
Mfn2 fwd	TCCCTTTGAAGACACTCGGA
Mfn2 rev	ACGACAAGGGTACCGATTAG

Table 1. q-RT-PCR primer pairs

Results

The core histones are carbonylated in vitro and in vivo

Recent work from the Bernlohr lab demonstrated that protein carbonylation is elevated in the nucleus of adipocytes in from obese animals compared to lean controls. In agreement with this data, Figure 1A shows that nuclear carbonylation is markedly increased as a consequence of high fat diet feeding. Previously,

studies have shown that visceral adipose depots exhibit a strong oxidative stress phenotype in obese mice and humans, while subcutaneous depots do not[61]. Consistent with these data, the elevation in carbonylation in obese mice is specific to epididymal depots (eWAT) and is not observed in the inguinal depot (iWAT) (Figure 1A).

The core histones are relatively small proteins (10-15 kDa) and are among the most abundant proteins in the nucleus. Analysis of nuclear of protein carbonylation by western blot left us intrigued about the low M_r carbonylated proteins, hypothesizing that the core histones are targets of 4-HNE modification in obese eWAT (Figure 1A). To test this, we purified histones by acid extraction from eWAT and iWAT depots of lean and obese mice. We observed a significant increase in 4-HNE adducts on all core histones from eWAT depots of HFD-fed mice compared to lean controls (Figure 1B, 1D). To rule out diet-specific effects, we performed the same analysis with wild type (WT) and *ob/ob* mice. The *Ob/ob* mouse model is a well-characterized genetic model of obesity in which the mice are fed the same chow diet as controls but become obese due to an extreme increase in caloric intake[154,155]. Ob/ob mice exhibited a similar increase in histone carbonylation in eWAT but not in iWAT, indicating that histone carbonylation is not an artifact of the HFD but is the result of increased adiposity (Figure 1C, 1E).

To assess the relative stoichiometry of 4-HNE modification, we purified histones and from eWAT and subsequently immunoprecipitated 4-HNE Michael adducts. Roughly 33% of the total histone pool was present in the IP fraction compared to the unmodified (supernatant) fraction, indicating that 4-HNE modification occurs a significant population of total histones in eWAT.

To investigate histone modification further, we turned to models of oxidative stress in cultured cells. In 3T3-L1 adipocytes, treatment of cells with inflammatory cytokine TNF-α, knockdown of key antioxidant glutathione-S-transferase A4 (GSTA4), and treatment with erastin, which leads to depletion of intracellular glutathione[121], all result in elevated 4-HNE modification of histones (Supplementary figure 1A-C). Together these data indicate that histone carbonylation is a dynamic redox sensitive modification that occurs in adipocytes in vivo.

We next wondered whether 4-HNE modification was occurring primarily on chromatin-associated histones or free histones. To test this, we isolated chromatin and nucleoplasm fractions of eWAT from mice fed a HFD. We could not detect a significant pool of free core histones, modified or unmodified in the nucleoplasm, suggesting that histone carbonylation is primarily occurring on chromatinized histones in adipocytes.

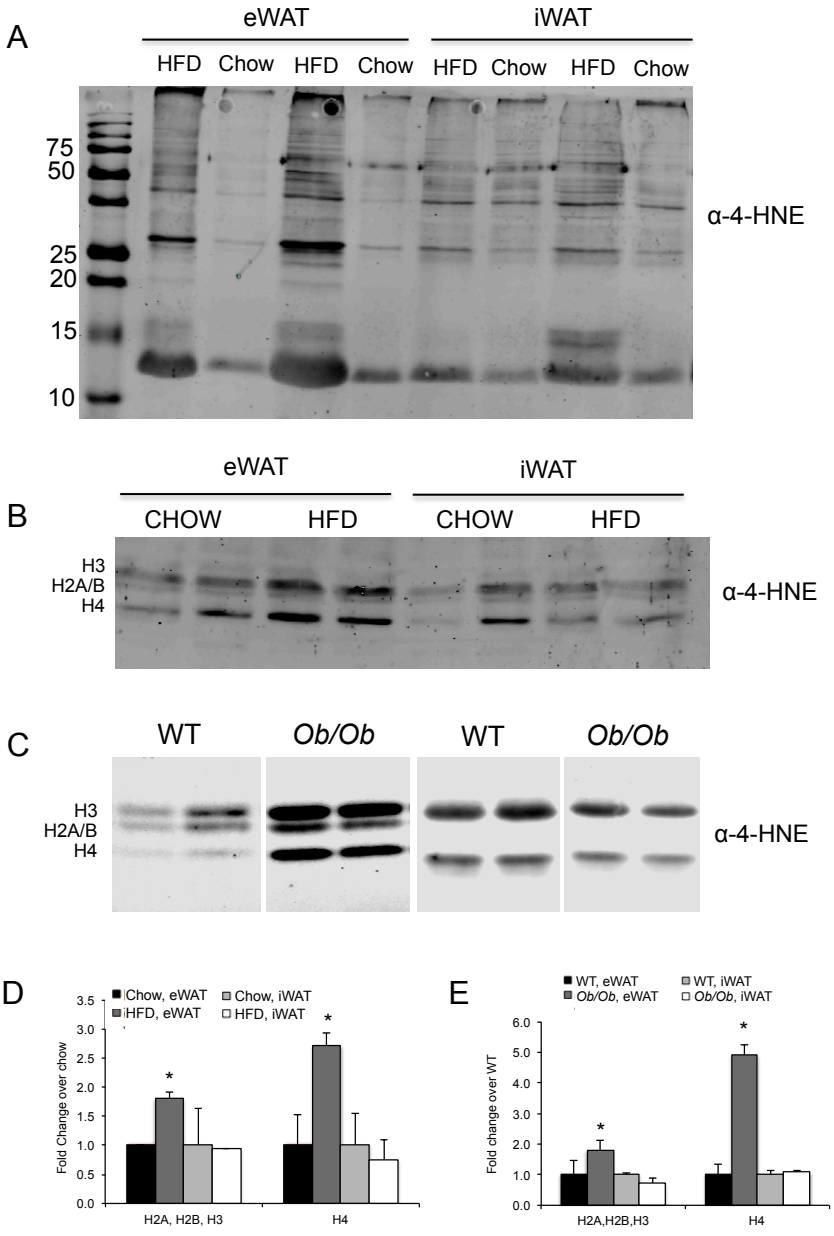
A
eWAT
iWAT
HFD Chow HFD Chow HFD Chow HFD Chow
75
50
25
20
15
10
α-4-HNE
B
eWAT
iWAT
CHOW HFD CHOW HFD
H3
H2A/B
H4
α-4-HNE
C
WT Ob/Ob WT Ob/Ob
H3
H2A/B
H4
α-4-HNE
D
Chow, eWAT
Chow, iWAT
HFD, eWAT
HFD, iWAT
Fold Change over chow
H2A, H2B, H3
H4
E
WT, eWAT
WT, iWAT
Ob/Ob, eWAT
Ob/Ob, iWAT
Fold change over WT
H2A,H2B,H3
H4

F

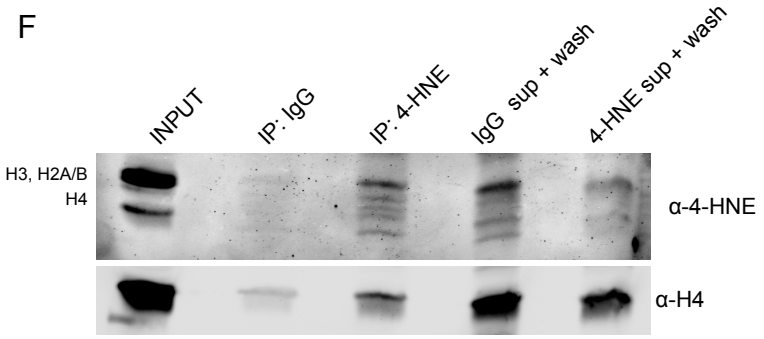
INPUT
IP: IgG
IP: 4-HNE
IgG sup + wash
4-HNE sup + wash
H3, H2A/B
H4
α-4-HNE
α-H4

G

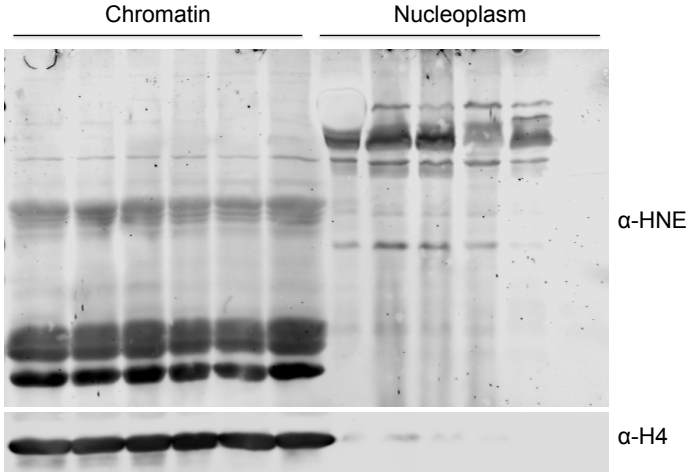
Chromatin
Nucleoplasm
α-HNE
α-H4

Figure 1. 4-HNE modification of histones occurs in vivo and is increased in obese animals

(A) 4-HNE modification in crude nuclear extracts from high-fat (HFD) and chow-fed mice in eWAT and iWAT.

(B) 4-HNE modification of histones purified from eWAT and iWAT of HFD and chow mice

(C) 4-HNE modification of histones purified from eWAT and iWAT of WT and Ob/Ob mice

(D,E) Quantitation of (B,C, respectively). Relative level 4-HNE modification in obese mice relative to lean controls. Normalized to histone H4. P <.05.

(G) Chromatin and nucleoplasm fraction of eWAT from HFD-fed mice.

(F) Immunoprecipitation of histones with 4-HNE modifications (IP:4-HNE) and an IgG isotype control IP (IP:IgG). Sup+wash (lanes 4-5) refer to all proteins remaining in the supernatant following IP plus proteins in the first two wash steps following IP.

Histone carbonylation accumulates in aged flies and mice

The observation that histone carbonylation is induced in models of obesity led us to wonder if these modifications are unique to the obesity phenotype. As such, we set out to test other models in which oxidative stress plays a defining role. Aging is a complex process that involves many different metabolic perturbations, one of which is elevated oxidative stress[156]. Several studies demonstrate the age-dependent increase in ROS and ROS-related damage including modification of proteins by lipid electrophiles[157-159]. As such, we decided to test whether aging led to an accumulation of 4-HNE modified histones. To test this, we aged WT male and female (*yw/yw*) *drosophila melanogaster* flies for 8 weeks and

assessed the level of 4-HNE modification of histones from whole animals at 0,2,4,6,and 8 weeks (Figure 2A). No change was detectable in female flies at any point over the course of 8 weeks (Figure 2B, 2D), but male flies showed a significant increase in the modification of all core histones at 6 weeks (Figure 2C, 2E). Interestingly, modification of histone H4 displayed the most significant increase starting at 2 weeks of age (Figure 2C, 2E).

Consistent with this, in male mice aged 3,6,12,and 18 months, there was a significant increase in the level of histone modification beginning at 12 months (Figure 2F, 2G). Together, these data provide evidence that 4-HNE modification of histones is an evolutionarily conserved process that increases as a consequence of age.

A

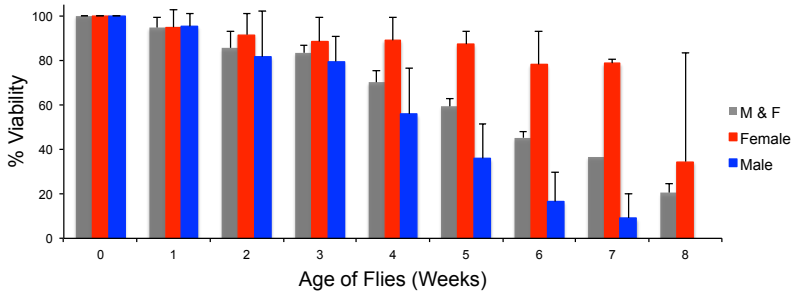

B

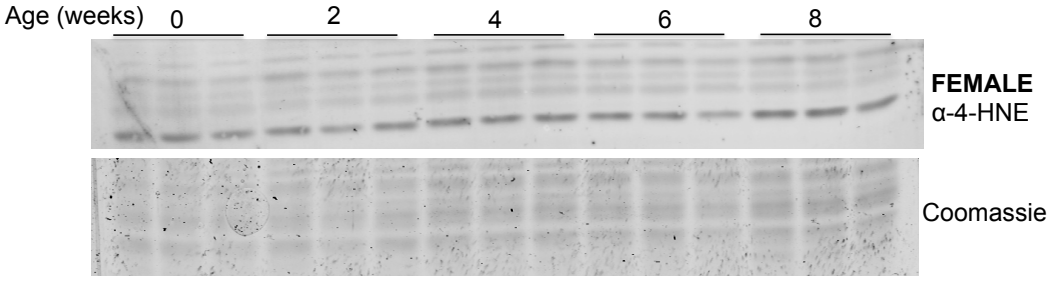
Age (weeks)
0
2
4
6
8
FEMALE
α-4-HNE
Coomassie

C

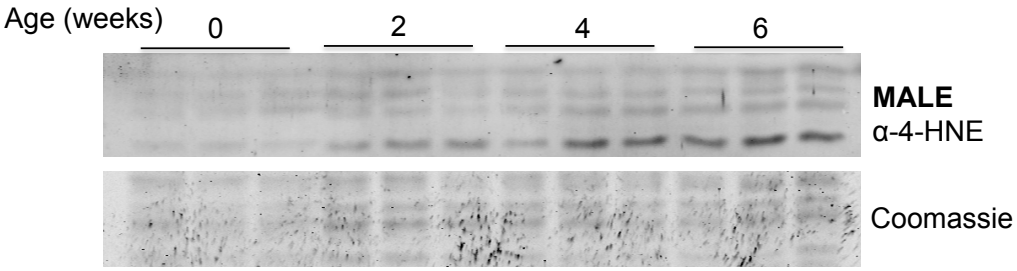
Age (weeks)
0
2
4
6
MALE
α-4-HNE
Coomassie

D

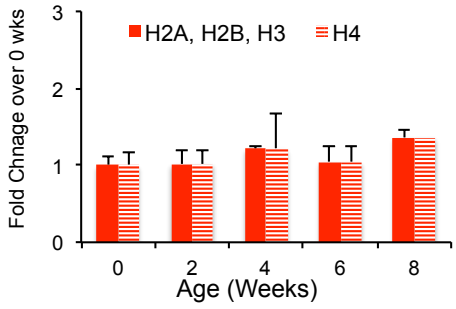
H2A, H2B, H3
H4
Fold Chnage over 0 wks
0
1
2
3
0
2
4
6
8
Age (Weeks)

E

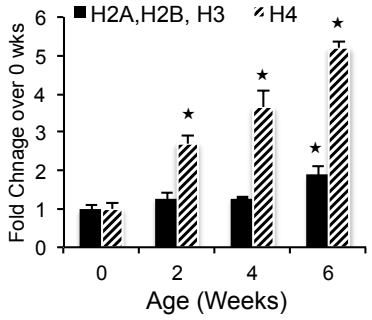
H2A,H2B, H3
H4
Fold Chnage over 0 wks
0
1
2
3
4
5
6
0
2
4
6
Age (Weeks)

F

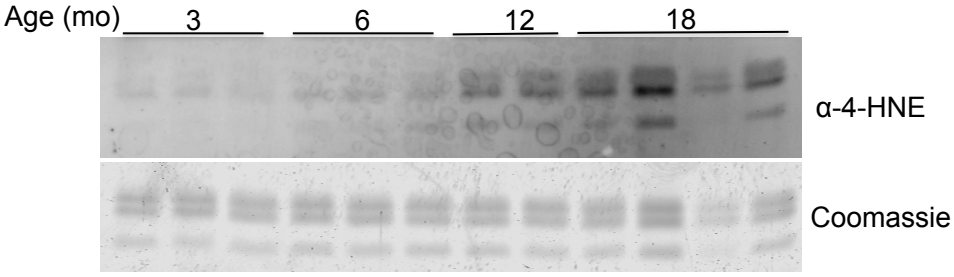
Age (mo)
3
6
12
18
α-4-HNE
Coomassie

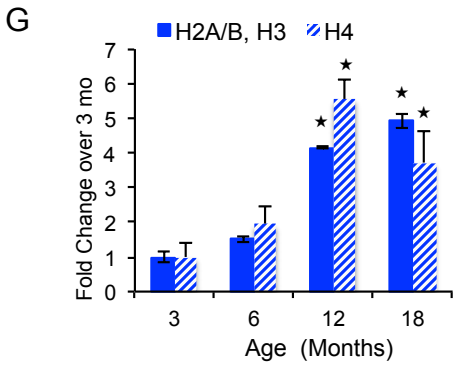

Figure 2: Histone carbonylation is increased with aging in mice and flies

(A) Survival curve of flies over the course of 8 weeks. Total percent of surviving male and female flies during each experimental week.

(B,D) 4-HNE modification of histones purified from total fly homogenate for females (B) and males(D)

(C,E) Quantitation of histone carbonylation in female (C) and male (E) aged flies compared to newly hatched flies (week 0). Normalized to coomassie stain, significance is set at P<.05.

(F) 4-HNE modification of histones purified from eWAT of mice aged 3-18 months.

(G) Quantitation of (F). Normalized to coomassie, significance is set at P<.05.

Proteomic analysis of histone carbonylation sites in vitro

We next sought to identify specific sites of histone modification by 4-HNE. Recently, our lab developed a technique to perform label-free proteomic analysis of protein carbonylation (unpublished data). Here, we adapted this method to study histone modifications. First, we generated a positive control by in vitro modifying histones purified from WT-3T3-L1 fibroblasts. In vitro modification led to the robust modification of all core histones (Figure 3A, 3B). Modification for all histones occurred at the same rate, indicating that in vitro, there is not a detectable site preference for 4-HNE modification (Figure 3A). Proteomic analysis of the positive control revealed sites on all four core histones (Figure 3D). 4-HNE modification of proteins can occur as either a Michael adduct on lysine, histidines, and cysteines or as a Schiff base on lysine residues (Figure 3C). We detected both types of adducts on all core histones, but the majority of identified sites were Michael adducts (Figure 3E). This data is consistent with previous work that indicates that Schiff bases are more labile in nature, while Michael adducts are stable.

The core histone proteins share in common the basic structure of a C-terminal globular histone fold domain and an N-terminal, unstructured, lysine-rich tail. The lysine residues of the histone tail have been the subject of intense study due to their role in replication and transcriptional regulation. Interestingly, over 90% of the sites identified in this study mapped to the globular histone-fold domain rather

than the N-terminal lysine-rich tail (Figure 3F, 3G, Supplementary Table 1). Modifications were identified on all faces of the nucleosome, including residues involved in histone-histone interaction, nucleosome-DNA interaction on the lateral surface, and solute accessible surfaces (Figure 3F-H). In sum, these data show that histones are robustly modified by 4-HNE in vitro and these modifications are readily detectable using the described methodology.

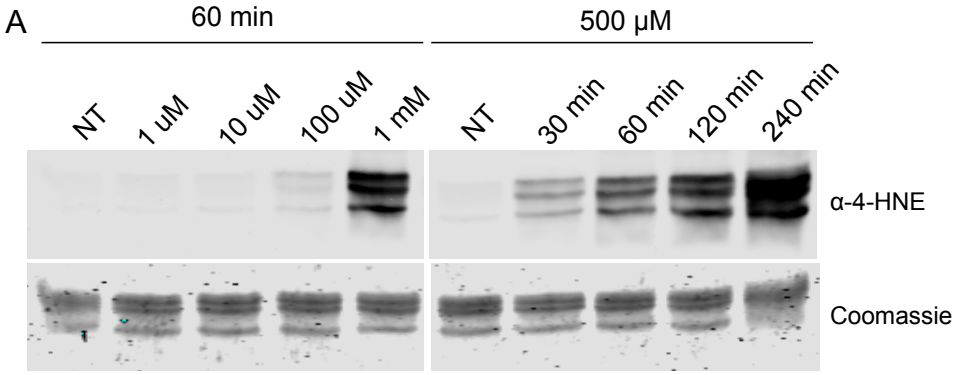
A
60 min
500 μM
NT
1 uM
10 uM
100 uM
1 mM
NT
30 min
60 min
120 min
240 min
α-4-HNE
Coomassie

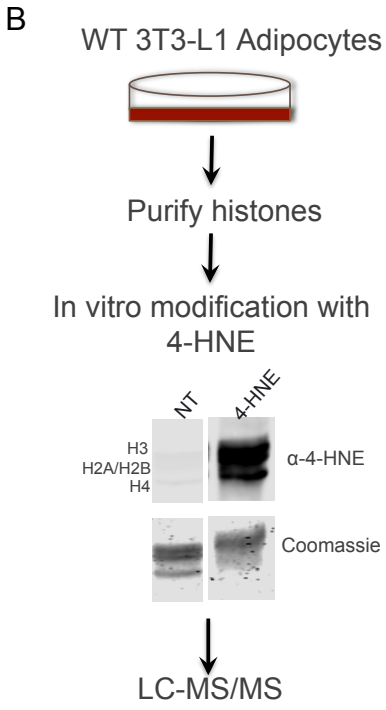
B
WT 3T3-L1 Adipocytes
Purify histones
In vitro modification with 4-HNE
NT
4-HNE
H3
H2A/H2B
H4
α-4-HNE
Coomassie
LC-MS/MS

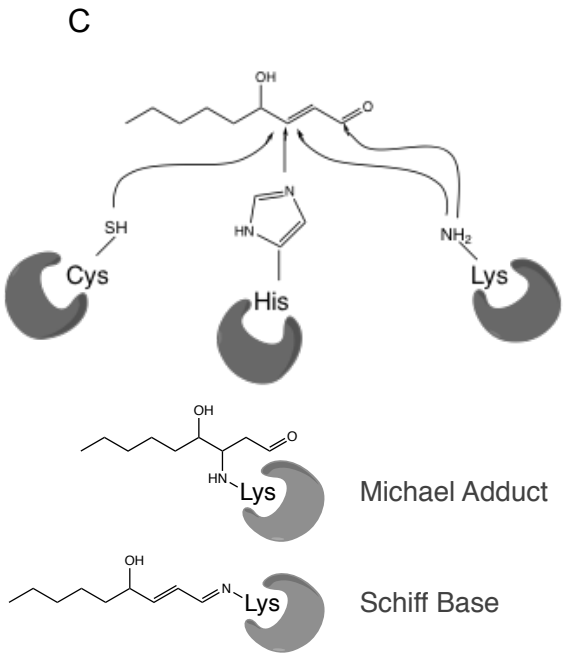
C
OH
O
SH
HN
N
NH2
Cys
His
Lys
OH
O
HN
Lys
Michael Adduct
OH
N
Lys
Schiff Base

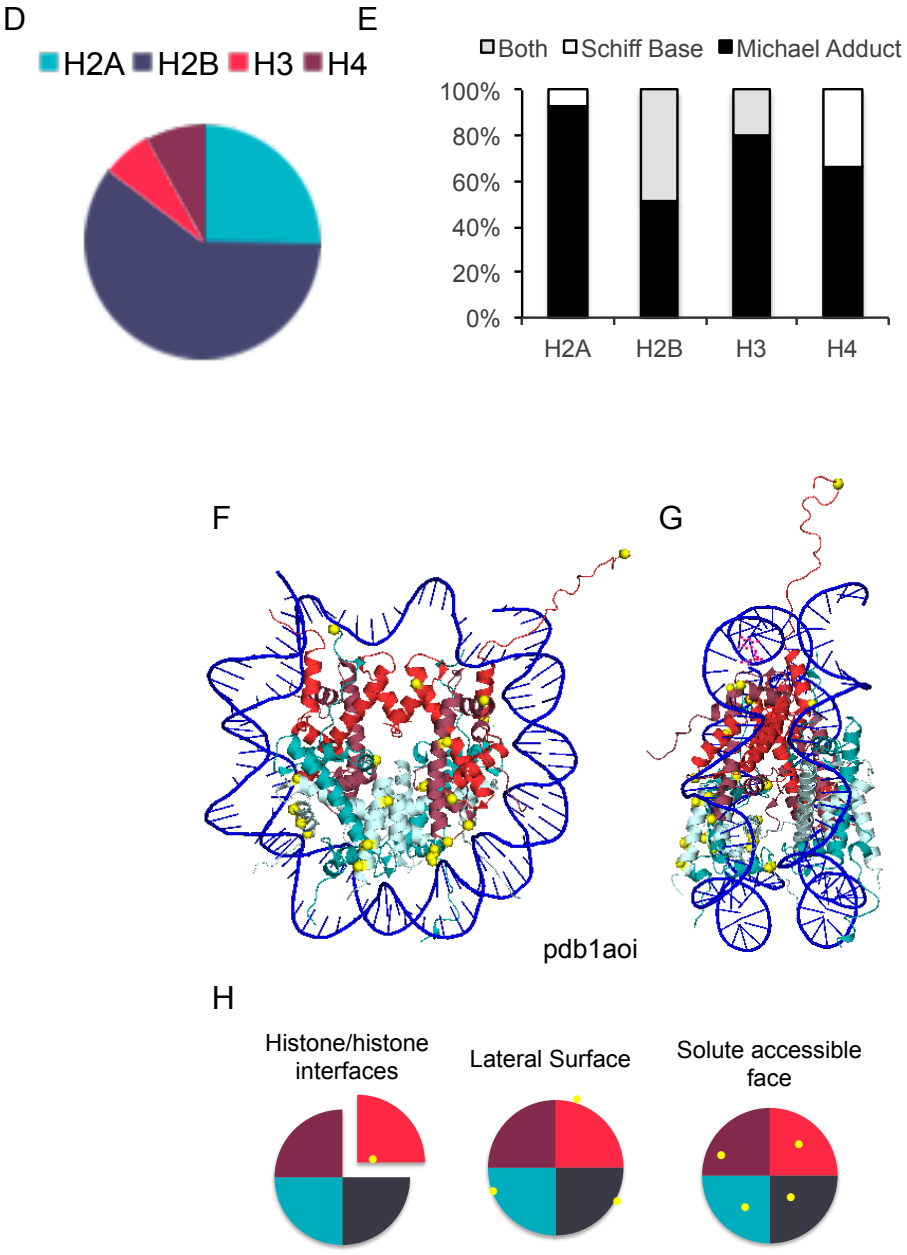
D
H2A H2B H3 H4
E
Both Schiff Base Michael Adduct
100%
80%
60%
40%
20%
0%
H2A
H2B
H3
H4
F
G
pdb1aoi
H
Histone/histone interfaces
Lateral Surface
Solute accessible face

Figure 3: Proteomic evaluation of 4-HNE adducts on in vitro modified core histones

(A) In vitro modification of purified histones with 4-HNE. Titration of 4-HNE concentration (left) and reaction time (right).
(B) Flow diagram of LC-MS/MS workflow for proteomic analysis of modified sites.
(C) Nucleophilic attack of 4-HNE by the side chains of Cys, His, and Lys can result in Michael adduct formation or Schiff base formation.
(D) Distribution of identified sites on the core histones
(E) Percentage of Michael adducts and Schiff bases identified in this screen.
(F,G) Ribbon diagram of the nucleosome. Front (F) and Side (G) view. Sites of modification are in yellow.
(H) Depiction of the localization of identified sites on the nucleosome structure.

Proteomic analysis of in vivo histone carbonylation sites

We next investigated sites of protein carbonylation in vivo. To do this, we performed analysis of samples using an unbiased approach in which total histones were purified from eWAT and resolved by SDS-PAGE prior to in gel-digestion and LC-MS/MS (Figure 4A). We also utilized an enrichment approach whereby 4-HNE-modifed proteins were immunoprecipitated from the total histone pool prior to SDS-PAGE (Figure 4A). Together, these studies led to the identification of 21 histone modifications including 14 sites on the core histones and 7 sites on linker histone H1 (Figure 4B, Supplementary Table 1). Of these, 20 are novels sites. H2BK117 has previously been reported as 4-oxononenal (4-ONE) target site in in-vitro modified cells[160].

In contrast to the in vitro modified histones, we observed 7 sites localized to the N-terminal histone tail including critical regulatory sites H3K4, H3K9, H3K36 and H2BK5. Interestingly, there were no overlapping sites identified between 4-HNE and 4-HHE modifications.

We next tested the relative abundance of these modifications in lean vs. obese eWAT. Only four sites were identified in both lean and obese samples. Of these, we observed elevated stoichiometry of modification in obese relative to lean controls for H2AK73$^{4\text{-HHE}}$, H2AK125$^{4\text{-HHE}}$, and H4K31$^{4\text{-HNE}}$ (Figure 4C, Supplementary table 2).

Interestingly, the 4-HHE sites were all located within the C-terminal histone fold domain while the 4-HNE modifications were localized primarily to the N-terminal histone tail (Figure 4B). Consistent with these data, analysis of histones from WT and *ob/ob* mice by western blot indicates that 4-HNE modification is more heavily localized to H3 and H4, while 4-HHE is predominately on H2A/B and H4 (Figure 4D). Moreover, treatment of 3T3-L1 adipocytes with either 4-HNE or 4-HHE results in distinct carbonylation signatures of the core histones (Figure 4E). This is in contrast to purified histones modified in vitro (Figure 4E). Together these data suggest a previously unappreciated specificity for 4-HNE vs. 4-HHE modifications.

A

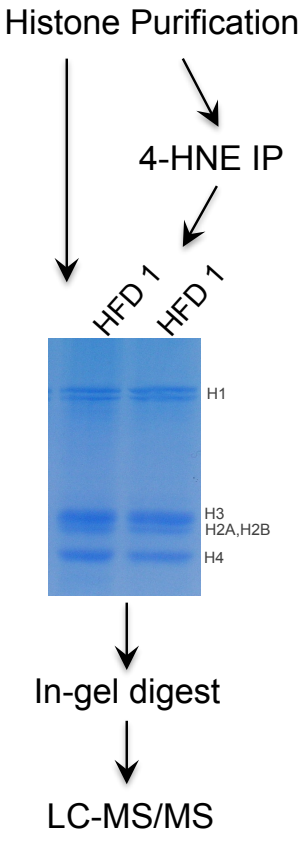
Histone Purification
4-HNE IP
HFD 1
HFD 1
H1
H3
H2A,H2B
H4
In-gel digest
LC-MS/MS

B

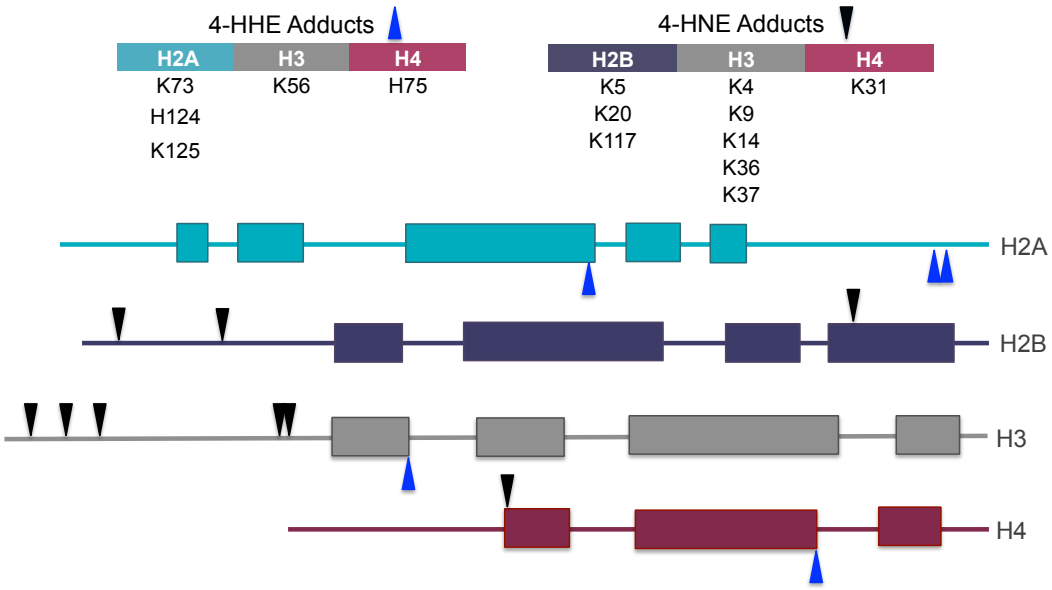
4-HHE Adducts
H2A
H3
H4
K73
H124
K125
K56
H75
4-HNE Adducts
H2B
H3
H4
K5
K20
K117
K4
K9
K14
K36
K37
K31
H2A
H2B
H3
H4

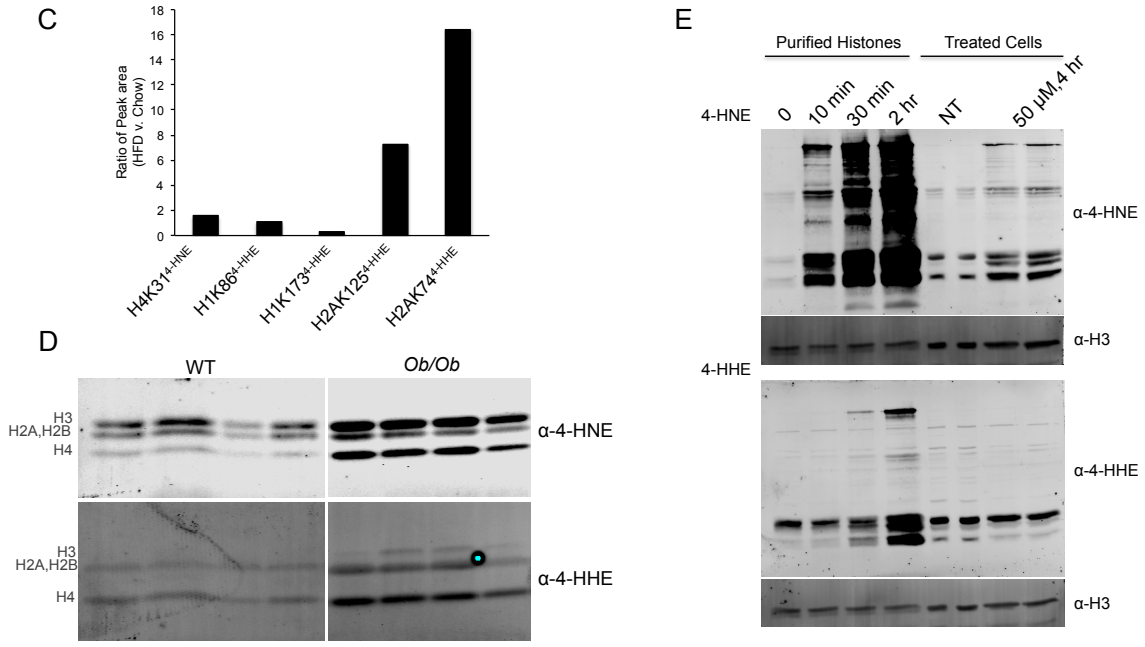

Figure 4: Identification of carbonylation sites in vivo

(A) Proteomic workflow for identification of sites. Both unenriched and immunoaffinity enrichment for 4-HNE modified histones were resolved by SDS-PAGE, in gel digested, and analyzed by LC-MS/MS.

(B) Cartoon diagram of the sites identified in this screen. Both 4-HHE adducts and 4-HNE adducts were identified.

(C) Relative abundance of carbonylation events identified in eWAT from both lean and obese mice. Values represent the peak width of the identified site normalized to the abundance of each protein detected in individual samples.

(D) 4-HHE and 4-HNE modification of histones from eWAT for WT and *ob/ob* mice.

(E) In vitro modification of purified histones with 4-HNE (upper panel) and 4-HHE (lower panel), lanes 1-4. Treatment of 3T3-L1 adipocytes with 4-HNE and 4-HHE (lanes 5-8).

ChIP-seq of 4-HNE modified sites (currently underway)

Histones are essential regulators of chromatin structure and organization and the dynamic post-translational modification of histones is responsible for orchestrating gene expression in every human cell type. The identification of carbonylation sites on known regulatory residues led us to hypothesize that carbonylation of these site would impact transcriptional outcomes in adipose tissue.

To investigate this potential functional role of histone carbonylation, we first set out to determine the genomic localization of the modifications by chromatin immunoprecipitation followed by deep sequencing (ChIP-seq). The workflow we used differs from traditional ChIP in several important ways (Figure 5A). First, we did not include a crosslinking step. Recent work from our lab demonstrated that many chromatin-associated proteins are carbonylated. Crosslinking would result in the capture and eventual IP of any non-histone carbonylation targets. Due to the lack of a crosslinking step, a more gentle shearing protocol was essential for maintenance of nucleosome-DNA complexes. As such, we utilized micrococcal nuclease digestion for DNA shearing followed by chromatin immunoprecipitation. Analysis of sheared DNA by agarose gel electrophoresis indicates that this strategy results in appropriately sheared mono- and di-nucleosome fragments (Figure 5B).

For this initial study, we utilized 3T3-L1 adipocytes treated with vehicle (DMSO) or pro-oxidant erastin. For each sample we carried out ChIP for 4-HNE adducts, histone H3, H3K4me^3, H3K27me^3, and IgG isotype control (Figure 5A). H3K4me^3 and H3K27me^3 are modifications that have been extensively studied and are markers for active and repressed chromatin, respectively. Comparison of ChIP peaks for 4-HNE with these marks will be informative as to the chromatin landscape surrounding carbonylation sites. To ensure the quality of ChIP-DNA we analyzed samples by q-RT-PCR. Generally, PCR targets are chosen that are expected to be enriched (or serve as a negative control) for a given sample. Since there are no known targets of 4-HNE modification, we are unable to assess the ChIP with q-RT-PCR. However, we did perform this analysis with ChIP-DNA from IgG, H3K4me^3 and H3K27me^3.

As expected, H3K4me^3 was enriched at Actb, Nrf2, Mfn2, and Ndufa2 but not at a gene dessert on chromosome 6 (Chr6D). Likewise, H3K27me^3 was enriched at Pax2 and Chr6D, both loci that are not actively expressed in 3T3-L1 adipocytes. Interestingly, both erastin treatment and 4-HNE treatment of 3T3-L1's led to a decrease in H3K4me^3 at Nrf2, Mfn2, and Ndufa2 compared with control cells (Figure 5C). These are genes encoding mitochondrial proteins that are known to be down regulated in obesity, and these observations indicate that oxidative challenge to adipocytes results in an altered chromatin state with loss of the activating H3K4me^3 mark.

Library preparation and barcoding was performed using ThruPLEX chemistry at the University of Minnesota Genomics Core followed by deep sequencing on the Illumina HiSeq 2500 sequencer on 50-bp single-read run. 24-39 million unmapped reads were generated for each sample (Figure 5E). The ongoing analysis of this data will provide novel insights into the functional significance of the modifications identified in this study.

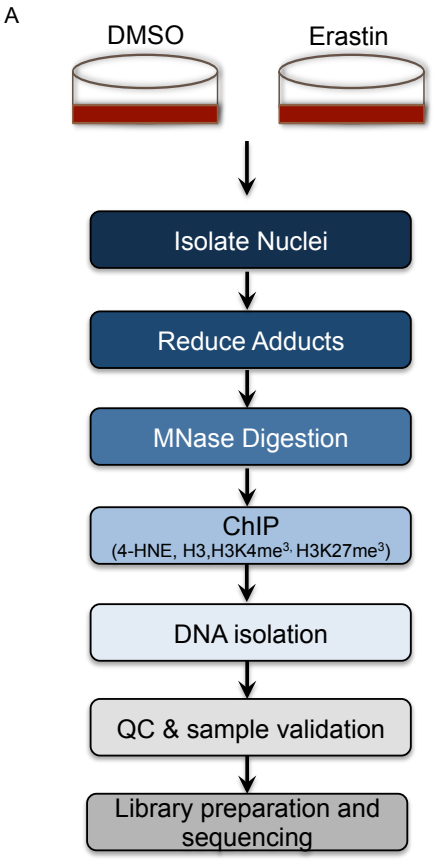

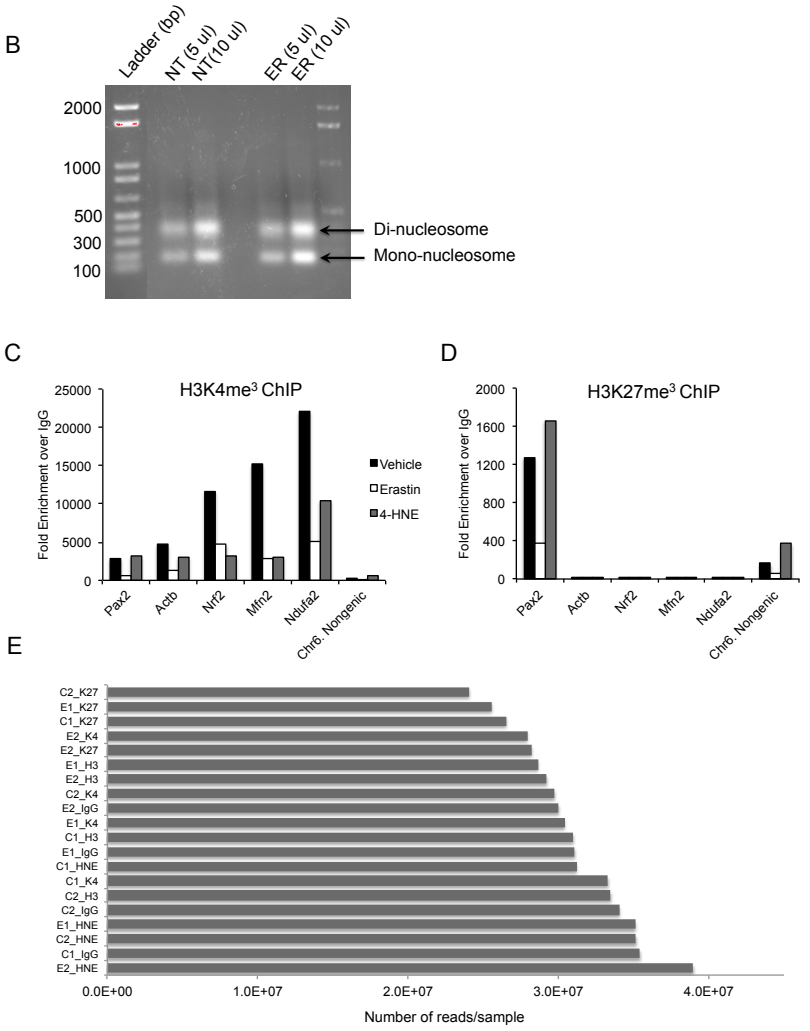

Figure 5. Functional analysis of histone carbonylation with ChIP-seq

(A) Basic workflow for preparation of ChIP-DNA from control (DMSO) and erastin-treated 3T3-L1 adipocytes

(B) Agarose gel of DNA fragments precipitated after enzymatic shearing with MNase.

(C,D) ChIP-PCR of H3K4me^3 (left) and H3K27me^3 ChIP'd DNA from control (DMSO), erastin, and 4-HNE treated 3T3-L1 adipoctyes. Y axis indicates enrichment over IgG isotype control ChIP.

(E) Number of unmapped reads generated for each sample. Samples were run on a HiSeq 2500, 50-bp single read run.

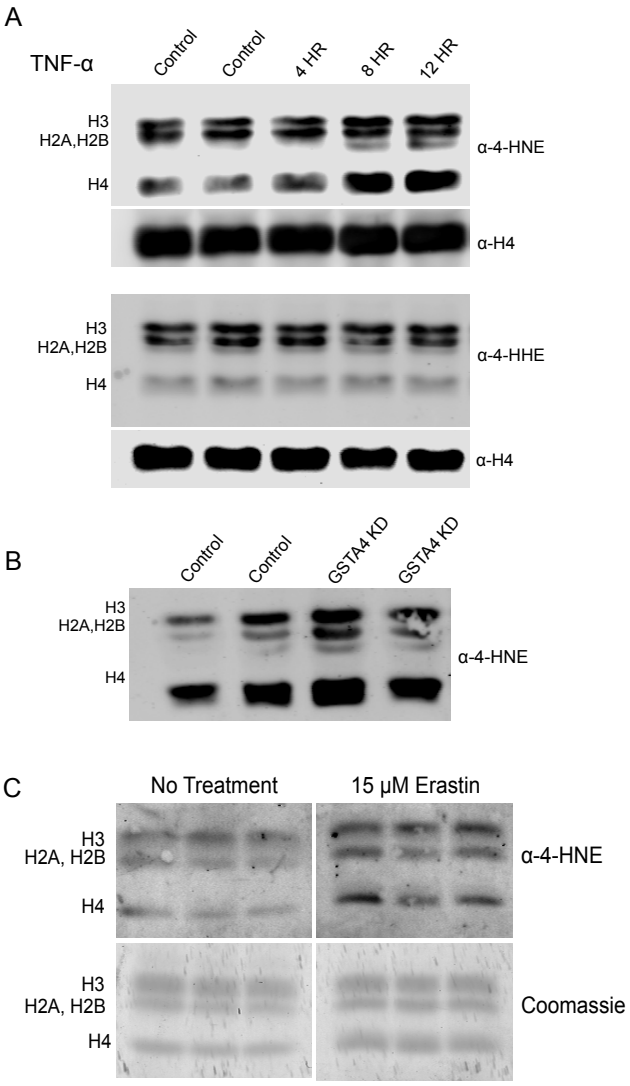

Supplementary Figure 1. Oxidative stress induces histone modification in cultured models of oxidative stress in adipocytes

(A) 3T3-L1 adipocytes treated with .5nM TNF-α on day 8 of differentiation for 4,8, and 12 hours. 4-HNE (upper) and 4-HHE (lower) modifications on purified histones.

(B) 4-HNE adducts on histones from Scr control and GSTA4 knockdown cells.

(C) 4-HNE adducts on histones from cells treated with DMSO (no treatment) or 15 μM erastin for 24 hours.

Table 2. Histone carbonylation sites identified in eWAT from HFD-fed mice

Modification	Histone	Positions within proteins	Protein	Score	Amino acid	HHE (K) Probabilities	Charge	Mass error [ppm]
4-HHE	H1	64	gi|254588110|ref|NP_663759.3|	90.259	K	K(1)ALAAAGYDVEKNNSR	3	0.23424
re-4-HHE	H1	161	gi|74206882|dbj|BAE33250.1|	57.174	K	AK(0.035)K(0.965)PAAAAGAK	2	-0.69731
4-HHE	H1	77	gi|254588110|ref|NP_663759.3|	81.565	K	ALAAAGYDVEK(1)N	2	0.81313
4-HHE	H1	173	gi|254588110|ref|NP_663759.3|	93.143	K	K(0.025)K(0.025)VSK(0.95)SPK	2	-0.039071
4-HHE	H1	92	gi|21426823|ref|NP_085112.1|	99.752	K	LVNK(1)GTLVQTK	2	-0.64027
4-HHE	H1	173	gi|254588110|ref|NP_663759.3|	111.74	K	K(0.001)K(0.015)VSK(0.984)SPK	2	0.16394
re-4-HHE	H1	12	gi|26354855|dbj|BAC41054.1|	81.525	K	STSAPAAK(1)PK	2	0.34012
4-HHE	H2A	73	gi|26347279|dbj|BAC37288.1|	93.374	K	DNK(0.088)K(0.912)ARIA	2	0.11522
4-HHE	H2A	124	gi|28316756|ref|NP_783589.1|	86.136	H	KTESH(1)K(1)SQT	2	-0.24058
4-HHE	H2A	125	gi|28316756|ref|NP_783589.1|	86.136	K	KTESH(1)K(1)SQT	2	-0.24058
4-HNE	H2B	5	gi|117580250|gb|AAI15793.1|	43.442	K	PAK(1)SAPAPK	2	0.098394
4-HNE	H2B	20	gi|28316760|ref|NP_783595.1|	40.103	K	AISK(0.981)AQK(0.019)	2	1.5638
re-HNE	H2B	117	gi|117580250|gb|AAI15793.1|	68.016	K	SEGTK(1)AVTK	2	-0.64868
4-HHE	H3	56	gi|74204635|dbj|BAE35387.1|	113.62	K	QK(1)STELLIR	2	-0.21472
4-HNE	H3	9	gi|82951200|ref|XP_889622.1|	51.066	K	K(1)STGDK(1)APR	2	-1.5724
4-HNE	H3	14	gi|82951200|ref|XP_889622.1|	51.066	K	K(1)STGDK(1)APR	2	-1.5724
re-HNE	H3	36	gi|149255259|ref|XP_897119.3|	88.056	K	SAPSTGGVK(0.5)K(0.5)PY	3	-1.9279
re-HNE	H3	37	gi|149255259|ref|XP_897119.3|	88.056	K	SAPSTGGVK(0.5)K(0.5)PY	3	-1.9279
4-HNE	H3	4	P02301	58.917	K	ALTK(1)QTAR	2	0.021419
4-HHE	H4	75	gi|141794860|gb|AAI15447.1|	65.252	H	TYTEH(1)AKR	2	-0.33905
HNE	H4	31	gi|148700589|gb|EDL32536.1|	67.214	K	DNIQGITK(1)PAIR	3	-0.21294

Table 3. Stoichiometric comparison of sites identified in both lean and obese eWAT

Histone	Site	Peptide	Peak Area (High Fat)	Peak Area (Low Fat)	Protein ratio for normalization	Ratio (HF/LF)
H1.1	K86	LVNK(hhe)GTLVQTK	2691238	3208132	0.74	1.14
H1.3	K173	KKVSK(hhe)SPK	10179121	40458608	0.74	0.34
H2A	K125	KTESH(hhe)K(hhe)SQT	31146776	11591858	0.37	7.31
H2A	K73	DNKK(hhe)ARIA	81172464	13417783	0.37	16.46
H4	K31	DNIQGITK(rehne)PAIR	5669262	761061	4.54	1.64

Discussion

The molecular and mechanistic linkage between environmental queues and metabolic disease and aging is complex and likely brought about by a combination of hormonal, metabolic and genetic determinants[162-165]. A common theme in many metabolic diseases is oxidative stress and downstream events linked to redox biology[143,166]. Here we examine the role of one such redox event--protein carbonylation-the covalent modification of proteins with reactive lipid aldehydes and its primary detoxification enzyme, Gsta4, as a major regulatory mechanism linking mitochondrial oxidative stress to the epigenome.

In this study, we show that the core histones are differentially modified by reactive lipid species 4-HNE and 4-HHE in obese white adipose depots. Furthermore, we show that these modifications are elevated in WAT as a consequence of age. These effects are specific to epididymal depots, where previous work demonstrates a significant down regulation of Gsta4 in obesity[61].

Furthermore, it is interesting to note that carbonylation was not elevated in aged female flies while there was a significant increase in males. It is well documented that women have a longer life expectancy than males[167]. This has been attributed to a variety of factors, but it has been demonstrated that females generally express higher levels of antioxidants and therefore have less ROS productions than males[168]. This effect likely mitigates the deleterious effects of ROS and prevents modification of histones in females during the aging process.

Importantly, one other recent study has also indicated that histone proteins are susceptible to this type of modification[160]. In that study, RKO cells were treated with exogenous 4-HNE and 4-ONE. This resulted in robust modification of histones and the identification of several sites by LC-MS/MS. Our study expands upon these findings to demonstrate that histones modification occurs in vivo.

The epigenome is operationally defined by a complex and highly regulated series of biochemical modifications focused on the covalent modification of DNA or DNA binding proteins (largely histones)[169-171]. Such modifications lead to the recruitment and assembly of transcription factors and DNA binding proteins affecting either activation or repression of nearby genes. Indeed, while histone modification by methylation and acetylation are widespread and function in the control of chromatin organization and transcription, expanded analysis advanced via proteomic technology has revealed a series of additional modifications whose

role(s) are less widely understood[169,172].

In this study, we identify 14 novel epigenomic modifications including critical regulatory sites H3K4^{HNE}, H3K9^{HNE}, H3K36^{HNE}, H4K31^{HNE}, and H3K56^{HHE}. The breadth of sites found in this study and their importance in the regulation transcription underlie the functional importance of these findings. For example, H3K4me^3 is a canonical activating mark[173] that is estimated to be present on up to 75% of human gene promoters[174,175]. In contrast, H3K9me^3 is a strongly repressive mark when localized to promoter regions[176]. These modifications are dynamic and highly regulated by specific methyltransferases and demethylases. Importantly, the carbonylation of lysine residues via a Michael addition reaction is a covalent modification for which there are currently no known removing enzymes. This is critical for it implies that histone carbonylation is a stable epigenomic mark that persists under a variety of metabolic conditions until the histone protein itself is degraded. Moreover, since the reaction is non-reversible, it negates target sites from subsequent modification and further epigenomic control, potentially leading to prolonged impact on transcriptional regulatory mechanisms.

The next phase of this project will be particularly informative, as identification of genomic sites of protein carbonylation combined with expression analysis will shed light on the specific role of this type of event. Moreover, it is unclear if

histone carbonylation is in some way targeted to sites in the genome. These studies will allow us to examine if histone carbonylation is a random and global type of damage that occurs or whether it accumulates in certain chromatin landscapes. Finally, the differences in 4-HHE and 4-HNE modification is striking- both in western blots and by proteomic evaluation of the sites modified. It is unclear why or how this selectivity occurs, particularly as carbonylation is a chemically driven process. These observations suggest that there is an unappreciated regulatory mechanism that directs these modifications.

Oxidative stress is a hallmark of metabolic dysfunction and understanding the mechanisms by which it contributes to metabolic disease is an important goal. In this study, we introduce a novel concept in regulatory biology that extends work on mitochondrial oxidative stress and protein carbonylation to epigenomic regulation of transcription in adipose tissue.

Abbreviations and Acknowledgements

Acknowledgements

We thank Yuxiang Sun for kindly providing aged eWAT for these studies, Ajeetha Joseph Rajan for her assistance with confocal microscopy, the University of Minnesota Imaging Center, and the University of Minnesota Genomics Core.

Abbreviations

4-HNE – *trans*-4-hydroxy-2-nonenal; 4-HHE – *trans*-4-hydroxy-2-hexenal; ROS – reactive oxygen species; eWAT – epididymal adipose tissue; iWAT – inguinal white adipose tissue; GSTA4 – glutathione-S-transferase A4; HFD – high fat diet; 4-ONE – 4-trans-oxo-2-nonenal; ChIP-seq – chromatin immunoprecipitation sequencing; MNase – micrococcal nuclease.

CHAPTER FOUR

Conclusions and Perspectives

Amy Hauck wrote this chapter

As the global incidence of metabolic disease continues to rise, the importance of understanding and defining how to maintain metabolic homeostasis in the face of environmental stressors becomes increasingly evident. While metabolic perturbation takes on distinct phenotypes depending on the tissue and type of stress, one thing shared in common is an altered cellular redox environment. As such, study of the redox mechanisms that define the metabolic state of a cell type or tissue is a necessary step in the pursuit of understanding metabolic changes during health and disease.

The work described here addressed this problem through the study of protein carbonylation in adipose tissue. We found that the post-translational modification of proteins by 4-HNE and 4-HHE were highly enriched in the nucleus of the adipocyte in the obese state. This observation led to interest in development of a proteomic method to identify the sites of modification. We designed the method with the goal of being able to determine a comprehensive lipid modification map that would allow for identification not only of the proteins modified, but also the residues and the specific lipid species. Collaboration with the laboratory of Dr. Yue Chen led to the successful use of affinity purification followed by LC-MS/MS to identify many novel targets.

This technological innovation enabled the focused study of 4-HNE and 4-HHE modified proteins that led to several important observations. First, zinc-coordinating residues are hotspots for lipid electrophile adduction. This finding has important implications for several reasons; zinc ions stabilize protein

structure and their coordination requires unmodified thiols[133]. As such, permanent modification of coordinating residues will result in the release of the zinc ion and likely have a large impact on protein structure and stability. In addition, in the nucleus there are many zinc finger proteins and these are essential for sequence-specific DNA binding[129]. As an example, we have highlighted the estrogen-related receptor family of nuclear receptors and shown that carbonylation of the zinc finger within the DNA binding domain results in complete inhibition of DNA binding. It is likely that modification of the other zinc-finger proteins identified in these studies would result in similar effects and future study of the biological implications of those modifications will be important.

A second major finding of this work is that histones are dynamically modified by 4-HNE and 4-HHE in conditions of oxidative stress. In particular, the identification of histone-tail residues as carbonylation targets has spurred our interest in defining a functional role for these modifications. We generally hypothesize that histone carbonylation will disrupt normal regulatory mechanisms that govern transcription outcomes in adipose; if a lysine is carbonylated, it cannot be acetylated or methylated. Thus far, it is difficult to predict the specific transcriptional effect (up regulation vs. down regulation) these modifications will incur, though I hypothesize that the permanent addition of a nine-carbon or 6-carbon lipid to lysine residues will result in the interruption of DNA-nucleosome contact much in the same way that lysine acetylation has been shown to do.

To address these questions, we have initiated the first ever ChIP-seq experiment for 4-HNE modified histones. While this work is still underway, it will inform us as to the genomic localization of the modifications and what type of chromatin environment it occurs in. Major questions that we hope to answer include whether or not the modification is specific to active or repressed chromatin (or if it occurring randomly throughout the genome). In addition, we plan to evaluate expression of genes in close proximity to peaks identified in the ChIP-seq experiment to correlate protein carbonylation to the regulation of gene expression.

Finally, we have begun the process of generating site-specific antibodies directed against several of the histone modifications that we identified. These antibodies will be a unique and exceptional tool to evaluate the functional role of specific modifications. Moreover, to our knowledge, these will be the first example of a tool to investigate single sites of modification. It will be very exciting to biochemically interrogate histone carbonylation with this new resource.

In addition to the experiments described above that stem neatly from these studies, there are several more biological questions that this work has precipitated that will be interesting and informative pursuits in the future:

Site of ROS production and reactive lipid formation

The observation that the nucleus is a major site for protein carbonylation was unexpected. For many years the mitochondrion has been the focus of oxidative

stress studies. This is for good reason, because while there are many sources of intracellular ROS, the mitochondria remains a major and prominent source[177]. Now, a key question to be answered is what the source of ROS is for nuclear protein carbonylation. It is possible that the lipids are formed inside of the mitochondria and diffuse to the nucleus, but this is hard to justify with the lack of differential carbonylation of the cytoplasmic fraction in lean vs. obese eWAT. Another possibility is that the lipids form outside of the mitochondria, potentially in the endoplasmic reticulum (ER), which is another ROS-rich microenvironment. Finally, it could be that the lipids are formed in the nucleus itself, though it is unclear what the source of ROS might be in this case. Potential experiments to address this question might include fluorescent tracking of various ROS intermediates upon oxidative stimuli of cultured cells. In addition, cells can be treated with organelle-specific ROS-inducing compounds (for example, Antimycin A for mitochondrial ROS and tunicamycin for ER ROS). Analysis of carbonylation patterns by confocal microscopy following these treatments could shed light as to the most likely source of ROS. Furthermore, careful fractionation followed by biochemical evaluation of lipid species could help determine whether free reactive lipid aldehydes are increased in the nucleus relative to other cellular compartments.

The site of reactive lipid formation has important implications for another reason: these lipids are generated through the damage of poly-unsaturated fatty acids in

lipid membranes. Something that is underappreciated about this is that when 4-HNE and other free aldehydes are cleaved from phospholipids, it leaves behind a damaged lipid in the membrane[142]. Elegant work has shown that the presence of these oxidized lipids can have profound effects on membrane dynamics, particularly in the mitochondria[178]. Since reactive lipid aldehydes are readily formed in adipocytes under oxidative stress, it follows that there is also significant damage to phospholipids and membrane structures. As such, a better understanding of the source of reactive lipid aldehydes in the adipocyte is an important and intriguing avenue of inquiry that may yield insights into metabolic dysfunction in these cells.

Longevity and quality control of modified proteins

For decades, protein carbonylation has been described as a permanent modification to proteins that generally leads to damage, unfolding, aggregates and proteasomal degradation. Despite this, the mechanistic details of this process are still under debate[142]. The discovery of histones as a prominent target precipitated much thought surrounding these processes. It will be exciting to investigate whether or not histone carbonylation is reversible (either enzymatically or as a result of histone turnover). While still controversial, a recent study demonstrated enzymatically driven de-carbonylation of in-vitro modified substrates[179]. If it is verified that these enzymes exhibit de-carbonylase activity in vivo, it would have enormous implications in the field of redox biology, as it would

suggest that carbonylation is a signaling event rather than an end-point of oxidative damage. Furthermore, it would help to explain why we consistently see the modification of specific proteins rather than random global modification. These questions are particularly relevant in the field of obesity. For example, if histone modifications accumulate during obesity, will exercise and diet interventions reverse this effect? This type of experiment can readily be carried out with mouse models. In addition, it will be necessary to perform careful evaluation of histone turnover, as it is unclear what the half-life of histone proteins is in a terminally differentiated adipocyte.

4-HNE and 4-HHE similarities and differences

A common theme in much of the work described here is that 4-HNE and 4-HHE modify different proteins. These two lipids are chemically very similar and it is unclear how a chemically driven process would result in the observed selectivity. The proteomic evaluation of nuclear targets did suggest differences in the chemical microenvironment for the two modifications, but there are many questions that remain. Moving forward study of the mechanisms, whether chemical or potentially enzymatic, that drive these differences will be important.

Antioxidant expression in obese adipose tissue

A number of studies from our lab and others indicate that metabolic disease is coincident with elevated oxidative stress in metabolic tissues such as liver, brain, skeletal muscle, cardiac muscle, pancreas, and adipose tissue[102,143]. Normally, acute oxidative stress leads to activation of transcription factor Nrf2, which subsequently stimulates expression of antioxidants to prevent and repair damage from various forms of ROS. However, in many pathological states and tissues, it is clear that metabolic disease coincides with transcriptional down regulation of antioxidant enzymes such as Gsta4, Gpx4, Prdx3, catalase, thioredoxins, and aldehyde dehydrogenases[1,143]. The decreased cellular antioxidant capacity is a major contributor to oxidative stress, though the mechanism by which it occurs is not well understood. Moreover, the unattenuated production of ROS leads to a futile loop in which the ROS damages cellular machinery, particularly in the mitochondrion, which leads to more ROS production. As such, the antioxidants sit at a critical nexus in cellular metabolism and understanding how they are transcriptionally regulated is an important and relevant course of study.

In summary, the work described herein was designed and carried out to investigate the link between oxidative stress and metabolic dysfunction in adipose tissue. This led to several important discoveries on the role of protein carbonylation in the obese adipose tissue and has generated many new investigatory paths to pursue in the future.

Abbreviations

4-HNE – *trans*-4-hydroxy-2-nonenal; 4-HHE – *trans*-4-hydroxy-2-hexenal; ROS – reactive oxygen species; ER – endoplasmic reticulum; eWAT – epididymal adipose tissue; iWAT – inguinal white adipose tissue; ChIP-seq – chromatin immunoprecipitation sequencing.

Complete Bibliography

1. Curtis, J. M. *et al.* Protein carbonylation and metabolic control systems. *Trends in Endocrinology & Metabolism* **23,** 399–406 (2012).
2. Castegna, A. *et al.* Proteomic identification of oxidatively modified proteins in Alzheimer's disease brain. Part II: dihydropyrimidinase-related protein 2, alpha-enolase and heat shock cognate 71. *J. Neurochem.* **82,** 1524–1532 (2002).
3. Choi, J. *et al.* Oxidative modifications and aggregation of Cu,Zn-superoxide dismutase associated with Alzheimer and Parkinson diseases. *J. Biol. Chem.* **280,** 11648–11655 (2005).
4. Barreiro, E., Gea, J. & Matar, G. Expression and carbonylation of creatine kinase in the quadriceps femoris muscles of patients with chronic obstructive pulmonary disease. *American J. Resp. Cell and Mol. Biol.* **33**, 636-642 (2005).
5. Marin-Corral, J. *et al.* Redox balance and carbonylated proteins in limb and heart muscles of cachectic rats. *Antioxidants & Redox Signaling* **12,** 365–380 (2010).
6. Grimsrud, P. A., Picklo, M. J., Griffin, T. J. & Bernlohr, D. A. Carbonylation of adipose proteins in obesity and insulin resistance: identification of adipocyte fatty acid-binding protein as a cellular target of 4-hydroxynonenal. *Mol. Cell Proteomics* **6,** 624–637 (2007).
7. Houstis, N., Rosen, E. D. & Lander, E. S. Reactive oxygen species have a causal role in multiple forms of insulin resistance. *Nature* **440,** 944–948 (2006).

8. Xu, Q., Hahn, W. S. & Bernlohr, D. A. Detecting protein carbonylation in adipose tissue and in cultured adipocytes. *Meth. Enzymol.* **538,** 249–261 (2014).
9. Singh, P. P., Mahadi, F., Roy, A. & Sharma, P. Reactive oxygen species, reactive nitrogen species and antioxidants in etiopathogenesis of diabetes mellitus type-2. *Indian J Clin Biochem* **24,** 324–342 (2009).
10. Evans, M. D., Dizdaroglu, M. & Cooke, M. S. Oxidative DNA damage and disease: induction, repair and significance. *Mutation research* **567,** 1–61 (2004).
11. Curtis, J. M. *et al.* Protein Carbonylation and Adipocyte Mitochondrial Function. *Journal of Biological Chemistry* **287,** 32967–32980 (2012).
12. Barzilai, A. & Yamamoto, K.-I. DNA damage responses to oxidative stress. *BRIDGE OVER BROKEN ENDS - The Cellular Response to DNA Breaks in Health and Disease* **3,** 1109–1115 (2004).
13. Thannickal, V. J. & Fanburg, B. L. Reactive oxygen species in cell signaling. *Am. J. Physiol. Lung Cell Mol. Physiol.* **279,** L1005–28 (2000).
14. Sena, L. A. & Chandel, N. S. Physiological Roles of Mitochondrial Reactive Oxygen Species. *Molecular Cell* **48,** 158–167 (2012).
15. Brand, M. D. The sites and topology of mitochondrial superoxide production. *Special Issue: Mitochondria in aging and age-related disease* **45,** 466–472 (2010).
16. Bienert, G. P. *et al.* Specific aquaporins facilitate the diffusion of hydrogen peroxide across membranes. *J. Biol. Chem.* **282,** 1183–1192 (2007).
17. Miller, E. W., Dickinson, B. C. & Chang, C. J. Aquaporin-3 mediates hydrogen peroxide uptake to regulate downstream intracellular signaling. *Proceedings of the National Academy of Sciences* **107,** 15681–15686 (2010).
18. Rhee, S. G., Woo, H. A., Kil, I. S. & Bae, S. H. Peroxiredoxin functions as a peroxidase and a regulator and sensor of local peroxides. *J. Biol. Chem.* **287,** 4403–4410 (2012).

19. Gardner, H. W. Oxygen radical chemistry of polyunsaturated fatty acids. *Free Radic. Biol. Med.* **7,** 65–86 (1989).
20. Vigo-Pelfrey, C. *Membrane lipid oxidation*. (1990).
21. Pawlosky, R. J., Bacher, J. & Salem, N. Ethanol consumption alters electroretinograms and depletes neural tissues of docosahexaenoic acid in rhesus monkeys: nutritional consequences of a low n-3 fatty acid diet. *Alcohol. Clin. Exp. Res.* **25,** 1758–1765 (2001).
22. Salem, N., Litman, B., Kim, H. Y. & Gawrisch, K. Mechanisms of action of docosahexaenoic acid in the nervous system. *Lipids* **36,** 945–959 (2001).
23. Lim, S.-Y., Doherty, J. D. & Salem, N. Lead exposure and (n-3) fatty acid deficiency during rat neonatal development alter liver, plasma, and brain polyunsaturated fatty acid composition. *J. Nutr.* **135,** 1027–1033 (2005).
24. Long, E. K. *et al.* Trans-4-hydroxy-2-hexenal is a neurotoxic product of docosahexaenoic (22:6; n-3) acid oxidation. *J. Neurochem.* **105,** 714–724 (2008).
25. Ahn, B.-H. *et al.* A role for the mitochondrial deacetylase Sirt3 in regulating energy homeostasis. *Proceedings of the National Academy of Sciences* **105,** 14447–14452 (2008).
26. Kontrová, K. *et al.* CD36 regulates fatty acid composition and sensitivity to insulin in 3T3-L1 adipocytes. *Physiol Res* **56,** 493–496 (2007).
27. Malcom, G. T. *et al.* Fatty acid composition of adipose tissue in humans: differences between subcutaneous sites. *Am. J. Clin. Nutr.* **50,** 288–291 (1989).
28. Long, E. K., Olson, D. M. & Bernlohr, D. A. High-fat diet induces changes in adipose tissue trans-4-oxo-2-nonenal and trans-4-hydroxy-2-nonenal levels in a depot-specific manner. *Free Radic. Biol. Med.* **63,** 390–398 (2013).
29. Schaur, R. J. Basic aspects of the biochemical reactivity of 4-hydroxynonenal. *Molecular Aspects of Medicine* **24,** 149–159 (2003).
30. Long, E. K., Rosenberger, T. A. & Picklo, M. J. Ethanol withdrawal

increases glutathione adducts of 4-hydroxy-2-hexenal but not 4-hydroxyl-2-nonenal in the rat cerebral cortex. *Free Radic. Biol. Med.* **48,** 384–390 (2010).

31. Hubatsch, I., Ridderström, M. & Mannervik, B. Human glutathione transferase A4-4: an alpha class enzyme with high catalytic efficiency in the conjugation of 4-hydroxynonenal and other genotoxic products of lipid peroxidation. *Biochem. J.* **330 (Pt 1),** 175–179 (1998).
32. Zhong, L. *et al.* Aldo-keto reductase family 1 B10 protein detoxifies dietary and lipid-derived alpha, beta-unsaturated carbonyls at physiological levels. *Biochemical and Biophysical Research Communications* **387,** 245–250 (2009).
33. Singhal, S. S., Yadav, S., Roth, C. & Singhal, J. RLIP76: A novel glutathione-conjugate and multi-drug transporter. *Biochem. Pharmacol.* **77,** 761–769 (2009).
34. Renes, J. *et al.* Multidrug resistance protein MRP1 protects against the toxicity of the major lipid peroxidation product 4-hydroxynonenal. *Biochem. J.* **350 Pt 2,** 555–561 (2000).
35. Furukawa, S. *et al*. Increased oxidative stress in obesity and its impact on metabolic syndrome. *J. Clin. Invest.* **114,**1752-1761 (2004).
36. Chung, H. Y. *et al.* Xanthine dehydrogenase/xanthine oxidase and oxidative stress. *Age (Omaha)* **20,** 127–140 (1997).
37. Cheung, K. J. *et al.* Xanthine oxidoreductase is a regulator of adipogenesis and PPARgamma activity. *Cell Metabolism* **5,** 115–128 (2007).
38. Tsushima, Y. *et al.* Uric acid secretion from adipose tissue and its increase in obesity. *Journal of Biological Chemistry* **288,** 27138–27149 (2013).
39. Monteiro, R. & Azevedo, I. Chronic Inflammation in Obesity and the Metabolic Syndrome. *Mediators of Inflammation* **2010,** 1–10 (2010).
40. Xu, H. *et al.* Chronic inflammation in fat plays a crucial role in the

development of obesity-related insulin resistance. *J. Clin. Invest.* **112,** 1821–1830 (2003).

41. Fisher-Wellman, K. H. & Neufer, P. D. Linking mitochondrial bioenergetics to insulin resistance via redox biology. *Trends Endocrinol. Metab.* **23,** 142–153 (2012).
42. Huh, J. Y. *et al.* Peroxiredoxin 3 is a key molecule regulating adipocyte oxidative stress, mitochondrial biogenesis, and adipokine expression. *Antioxid Redox Signal* **16,** 229–243 (2012).
43. Styskal, J., Van Remmen, H., Richardson, A. & Salmon, A. B. Oxidative stress and diabetes: what can we learn about insulin resistance from antioxidant mutant mouse models? *Free Radic. Biol. Med.* **52,** 46–58 (2012).
44. Vance, J. E. & Vance, D. E. *Biochemistry of Lipids, Lipoproteins and Membranes*. (Elsevier, 2008).
45. Peraldi, P. & Spiegelman, B. TNF-alpha and insulin resistance: summary and future prospects. *Mol. Cell. Biochem.* **182,** 169–175 (1998).
46. Wajchenberg, B. L. Subcutaneous and Visceral Adipose Tissue: Their Relation to the Metabolic Syndrome. *Endocr Rev* **21,** 697–738 (2015).
47. McLaughlin, T., Lamendola, C., Liu, A. & Abbasi, F. Preferential Fat Deposition in Subcutaneous Versus Visceral Depots Is Associated with Insulin Sensitivity. *J. Clin. Endocrinol. Metab.* **96,** E1756–E1760 (2015).
48. Rhee, E.-J. *et al.* Metabolic health is a more important determinant for diabetes development than simple obesity: a 4-year retrospective longitudinal study. *PLoS ONE* **9,** e98369 (2014).
49. Xu, H. *et al.* Uncoupling lipid metabolism from inflammation through fatty acid binding protein-dependent expression of UCP2. *Mol. Cell. Biol.* **35,** 1055–1065 (2015).
50. Wang, F. *et al.* Brd2 disruption in mice causes severe obesity without Type 2 diabetes. *Biochem. J.* **425,** 71–83 (2010).
51. Perry, R. J. *et al.* Reversal of hypertriglyceridemia, fatty liver disease, and

insulin resistance by a liver-targeted mitochondrial uncoupler. *Cell Metabolism* **18,** 740–748 (2013).

52. Wisse, B. E. The inflammatory syndrome: the role of adipose tissue cytokines in metabolic disorders linked to obesity. *J. Am. Soc. Nephrol.* **15,** 2792–2800 (2004).
53. Wellen, K. E. & Hotamisligil, G. S. Obesity-induced inflammatory changes in adipose tissue. *J. Clin. Invest.* **112,** 1785–1788 (2003).
54. Frohnert, B. I. *et al.* Increased adipose protein carbonylation in human obesity. *Obesity (Silver Spring)* **19,** 1735–1741 (2011).
55. Després, J.-P. & Lemieux, I. Abdominal obesity and metabolic syndrome. *Nature* **444,** 881–887 (2006).
56. Milic, I., Melo, T., Domingues, M. R., Domingues, P. & Fedorova, M. Heterogeneity of peptide adducts with carbonylated lipid peroxidation products. *J Mass Spectrom* **50,** 603–612 (2015).
57. Sayre, L. M., Lin, D., Yuan, Q., Zhu, X. & Tang, X. Protein Adducts Generated from Products of Lipid Oxidation: Focus on HNE and ONE*. *Drug Metab. Rev.* **38,** 651–675 (2006).
58. Witz, G. Biological interactions of alpha,beta-unsaturated aldehydes. *Free Radic. Biol. Med.* **7,** 333–349 (1989).
59. Rauniyar, N. & Prokai, L. Detection and identification of 4-hydroxy-2-nonenal Schiff-base adducts along with products of Michael addition using data-dependent neutral loss-driven MS3 acquisition: method evaluation through an in vitro study on cytochrome c oxidase modifications. *Proteomics* **9,** 5188–5193 (2009).
60. Tang, X., Sayre, L. M. & Tochtrop, G. P. A mass spectrometric analysis of 4-hydroxy-2-(E)-nonenal modification of cytochrome c. *J Mass Spectrom* **46,** 290–297 (2011).
61. Long, E. K., Olson, D. M. & Bernlohr, D. A. High-fat diet induces changes in adipose tissue trans-4-oxo-2-nonenal and trans-4-hydroxy-2-nonenal levels in a depot-specific manner. *Free Radic. Biol. Med.* **63,** 390–398

(2013).

62. Curtis, J. M. *et al.* Downregulation of Adipose Glutathione S-Transferase A4 Leads to Increased Protein Carbonylation, Oxidative Stress, and Mitochondrial Dysfunction. *Diabetes* **59,** 1132–1142 (2010).
63. Sies, H. Role of Metabolic H2O2 Generation: REDOX SIGNALING AND OXIDATIVE STRESS. *Journal of Biological Chemistry* **289,** 8735–8741 (2014).
64. Rhee, S. G., Bae, Y. S., Lee, S. R. & Kwon, J. Hydrogen Peroxide: A Key Messenger That Modulates Protein Phosphorylation Through Cysteine Oxidation. *Sci Signal* **2000,** pe1–pe1 (2000).
65. Poole, L. B., Karplus, P. A. & Claiborne, A. PROTEIN SULFENIC ACIDS IN REDOX SIGNALING. *Annu. Rev. Pharmacol. Toxicol.* **44,** 325–347 (2015).
66. Jones, D. P. Radical-free biology of oxidative stress. *Am J Physiol Cell Physiol* **295,** C849–68 (2008).
67. Winterbourn, C. C. & Hampton, M. B. Thiol chemistry and specificity in redox signaling. *Free Radic. Biol. Med.* **45,** 549–561 (2008).
68. Stadtman, E. R. Protein oxidation and aging. *Free Radic. Res.* **40,** 1250–1258 (2006).
69. Morgan, P. E., Dean, R. T. & Davies, M. J. Inactivation of cellular enzymes by carbonyls and protein-bound glycation/glycoxidation products. *Arch. Biochem. Biophys.* **403,** 259–269 (2002).
70. Yan, L. J., Levine, R. L. & Sohal, R. S. Oxidative damage during aging targets mitochondrial aconitase. *Proc. Natl. Acad. Sci. U.S.A.* **94,** 11168–11172 (1997).
71. Dalle-Donne, I., Rossi, R., Giustarini, D., Milzani, A. & Colombo, R. Protein carbonyl groups as biomarkers of oxidative stress. *Clin. Chim. Acta* **329,** 23–38 (2003).
72. Yoo, B.-S. & Regnier, F. E. Proteomic analysis of carbonylated proteins in two-dimensional gel electrophoresis using avidin-fluorescein affinity

staining. *Electrophoresis* **25,** 1334–1341 (2004).

73. Dalle-Donne, I., Rossi, R., Colombo, R., Giustarini, D. & Milzani, A. Biomarkers of oxidative damage in human disease. *Clin. Chem.* **52,** 601–623 (2006).

74. Uchida, K. & Stadtman, E. R. Covalent attachment of 4-hydroxynonenal to glyceraldehyde-3-phosphate dehydrogenase. A possible involvement of intra- and intermolecular cross-linking reaction. *J. Biol. Chem.* **268,** 6388–6393 (1993).

75. Chen, C.-H., Ferreira, J. C. B., Gross, E. R. & Mochly-Rosen, D. Targeting aldehyde dehydrogenase 2: new therapeutic opportunities. *Physiol. Rev.* **94,** 1–34 (2014).

76. Mitchell, D. Y. & Petersen, D. R. Inhibition of rat hepatic mitochondrial aldehyde dehydrogenase-mediated acetaldehyde oxidation by trans-4-hydroxy-2-nonenal. *Hepatology* **13,** 728–734 (1991).

77. Luckey, S. W., Tjalkens, R. B. & Petersen, D. R. Mechanism of inhibition of rat liver class 2 ALDH by 4-hydroxynonenal. *Adv. Exp. Med. Biol.* **463,** 71–77 (1999).

78. Doorn, J. A., Hurley, T. D. & Petersen, D. R. Inhibition of Human Mitochondrial Aldehyde Dehydrogenase by 4-Hydroxynon-2-enal and 4-Oxonon-2-enal †. *Chem. Res. Toxicol.* **19,** 102–110 (2006).

79. Hartley, D. P., Ruth, J. A. & Petersen, D. R. The hepatocellular metabolism of 4-hydroxynonenal by alcohol dehydrogenase, aldehyde dehydrogenase, and glutathione S-transferase. *Arch. Biochem. Biophys.* **316,** 197–205 (1995).

80. Makowski, L. *et al.* Lack of macrophage fatty-acid-binding protein aP2 protects mice deficient in apolipoprotein E against atherosclerosis. *Nat. Med.* **7,** 699–705 (2001).

81. Singh, N. R., Rondeau, P., Hoareau, L. & Bourdon, E. Identification of preferential protein targets for carbonylation in human mature adipocytes treated with native or glycated albumin. *Free Radic. Res.* **41,** 1078–1088

(2007).

82. Cantu-Medellin, N. & Kelley, E. E. Xanthine oxidoreductase-catalyzed reactive species generation: A process in critical need of reevaluation. *Redox Biology* **1,** 353–358 (2013).

83. Berry, C. E. & Hare, J. M. Xanthine oxidoreductase and cardiovascular disease: molecular mechanisms and pathophysiological implications. *The Journal of Physiology* **555,** 589–606 (2004).

84. Nishino, T. & Nishino, T. The conversion from the dehydrogenase type to the oxidase type of rat liver xanthine dehydrogenase by modification of cysteine residues with fluorodinitrobenzene. *J. Biol. Chem.* **272,** 29859–29864 (1997).

85. McMahon, M., Itoh, K., Yamamoto, M. & Hayes, J. D. Keap1-dependent proteasomal degradation of transcription factor Nrf2 contributes to the negative regulation of antioxidant response element-driven gene expression. *J. Biol. Chem.* **278,** 21592–21600 (2003).

86. McMahon, M., Lamont, D. J., Beattie, K. A. & Hayes, J. D. Keap1 perceives stress via three sensors for the endogenous signaling molecules nitric oxide, zinc, and alkenals. *Proceedings of the National Academy of Sciences* **107,** 18838–18843 (2010).

87. Levonen, A.-L. *et al.* Cellular mechanisms of redox cell signalling: role of cysteine modification in controlling antioxidant defences in response to electrophilic lipid oxidation products. *Biochem. J.* **378,** 373–382 (2004).

88. Fang, J. & Holmgren, A. Inhibition of thioredoxin and thioredoxin reductase by 4-hydroxy-2-nonenal in vitro and in vivo. *J. Am. Chem. Soc.* **128,** 1879–1885 (2006).

89. Sharma, R. *et al.* 4-Hydroxynonenal self-limits fas-mediated DISC-independent apoptosis by promoting export of Daxx from the nucleus to the cytosol and its binding to Fas. *Biochemistry* **47,** 143–156 (2008).

90. Sharma, A. *et al.* 4-Hydroxynonenal induces p53-mediated apoptosis in retinal pigment epithelial cells. *Arch. Biochem. Biophys.* **480,** 85–94

(2008).

91. Herman, M. A., She, P., Peroni, O. D., Lynch, C. J. & Kahn, B. B. Adipose tissue branched chain amino acid (BCAA) metabolism modulates circulating BCAA levels. *J. Biol. Chem.* **285,** 11348–11356 (2010).
92. Wang, T. J. *et al.* Metabolite profiles and the risk of developing diabetes. *Nat. Med.* **17,** 448–453 (2011).
93. Newgard, C. B. *et al.* A branched-chain amino acid-related metabolic signature that differentiates obese and lean humans and contributes to insulin resistance. *Cell Metabolism* **9,** 311–326 (2009).
94. Newgard, C. B. Interplay between Lipids and Branched-Chain Amino Acids in Development of Insulin Resistance. *Cell Metab* **15,** 606–614 (2012).
95. Burrill, J. S. *et al.* Inflammation and ER Stress Regulate Branched-Chain Amino Acid Uptake and Metabolism in Adipocytes. *Molecular Endocrinology* **29,** 411–420 (2015).
96. Lackey, D. E. *et al.* Regulation of adipose branched-chain amino acid catabolism enzyme expression and cross-adipose amino acid flux in human obesity. *AJP: Endocrinology and Metabolism* **304,** E1175–87 (2013).
97. Lynch, C. J. & Adams, S. H. Branched-chain amino acids in metabolic signalling and insulin resistance. *Nature Reviews Endocrinology* **10,** 723–736 (2014).
98. Kaplan, R. S., Pratt, R. D. & Pedersen, P. L. Purification and characterization of the reconstitutively active phosphate transporter from rat liver mitochondria. *J. Biol. Chem.* **261,** 12767–12773 (1986).
99. Jahansouz, C. *et al.* Roux-en-Y Gastric Bypass Acutely Decreases Protein Carbonylation and Increases Expression of Mitochondrial Biogenesis Genes in Subcutaneous Adipose Tissue. *Obes Surg* (2015).
100. Møller, I. M., Rogowska-Wrzesinska, A. & Rao, R. S. P. Protein carbonylation and metal-catalyzed protein oxidation in a cellular

perspective. *J Proteomics* **74,** 2228–2242 (2011).

101. Guéraud, F. *et al.* Chemistry and biochemistry of lipid peroxidation products. *Free Radic. Res.* **44,** 1098–1124 (2010).
102. Furukawa, S. *et al.* Increased oxidative stress in obesity and its impact on metabolic syndrome. *J. Clin. Invest.* **114,** 1752–1761 (2004).
103. Hahn, W. S. *et al.* Proinflammatory cytokines differentially regulate adipocyte mitochondrial metabolism, oxidative stress, and dynamics. *AJP: Endocrinology and Metabolism* **306,** E1033–E1045 (2014).
104. Grimsrud, P. A., Xie, H., Griffin, T. J. & Bernlohr, D. A. Oxidative Stress and Covalent Modification of Protein with Bioactive Aldehydes: FIGURE 1. *Journal of Biological Chemistry* **283,** 21837–21841 (2008).
105. Ayyadevara, S. *et al.* Lifespan and stress resistance of Caenorhabditis elegans are increased by expression of glutathione transferases capable of metabolizing the lipid peroxidation product 4-hydroxynonenal. *Aging Cell* **4,** 257–271 (2005).
106. Shearn, C. T., Orlicky, D. J., Saba, L. M., Shearn, A. H. & Petersen, D. R. Increased hepatocellular protein carbonylation in human end-stage alcoholic cirrhosis. *Free Radic. Biol. Med.* **89,** 1144–1153 (2015).
107. Wong, C.-M., Cheema, A. K., Zhang, L. & Suzuki, Y. J. Protein carbonylation as a novel mechanism in redox signaling. *Circ. Res.* **102,** 310–318 (2008).
108. Student, A. K., Hsu, R. Y. & Lane, M. D. Induction of fatty acid synthetase synthesis in differentiating 3T3-L1 preadipocytes. *J. Biol. Chem.* **255,** 4745–4750 (1980).
109. Rappsilber, J., Mann, M. & Ishihama, Y. Protocol for micro-purification, enrichment, pre-fractionation and storage of peptides for proteomics using StageTips. *Nature Protocols* **2,** 1896–1906 (2007).
110. Cox, J. & Mann, M. MaxQuant enables high peptide identification rates, individualized p.p.b.-range mass accuracies and proteome-wide protein quantification. *Nat. Biotechnol.* **26,** 1367–1372 (2008).

111. Huang, D. W., Sherman, B. T. & Lempicki, R. A. Bioinformatics enrichment tools: paths toward the comprehensive functional analysis of large gene lists. *Nucleic Acids Research* **37,** 1–13 (2009).
112. Huang, D. W., Sherman, B. T. & Lempicki, R. A. Systematic and integrative analysis of large gene lists using DAVID bioinformatics resources. *Nature Protocols* **4,** 44–57 (2009).
113. Mi, H. *et al.* PANTHER version 11: expanded annotation data from Gene Ontology and Reactome pathways, and data analysis tool enhancements. *Nucleic Acids Research* **45,** D183–D189 (2017).
114. Schwartz, D. & Gygi, S. P. An iterative statistical approach to the identification of protein phosphorylation motifs from large-scale data sets. *Nat. Biotechnol.* **23,** 1391–1398 (2005).
115. Chou, M. F. & Schwartz, D. Biological sequence motif discovery using motif-x. *Curr Protoc Bioinformatics* **Chapter 13,** Unit 13.15–24 (2011).
116. Bruenner, B. A., Jones, A. D. & German, J. B. Direct characterization of protein adducts of the lipid peroxidation product 4-hydroxy-2-nonenal using electrospray mass spectrometry. *Chem. Res. Toxicol.* **8,** 552–559 (1995).
117. Zhu, X., Tang, X., Anderson, V. E. & Sayre, L. M. Mass spectrometric characterization of protein modification by the products of nonenzymatic oxidation of linoleic acid. *Chem. Res. Toxicol.* **22,** 1386–1397 (2009).
118. Chavez, J. D., Wu, J., Bisson, W. & Maier, C. S. Site-specific proteomic analysis of lipoxidation adducts in cardiac mitochondria reveals chemical diversity of 2-alkenal adduction. *J Proteomics* **74,** 2417–2429 (2011).
119. Vigilanza, P., Aquilano, K., Baldelli, S., Rotilio, G. & Ciriolo, M. R. Modulation of intracellular glutathione affects adipogenesis in 3T3-L1 cells. *J. Cell. Physiol.* **226,** 2016–2024 (2011).
120. Galinier, A. *et al.* Adipose tissue proadipogenic redox changes in obesity. *J. Biol. Chem.* **281,** 12682–12687 (2006).
121. Dixon, S. J. *et al.* Ferroptosis: an iron-dependent form of nonapoptotic

cell death. *Cell* **149,** 1060–1072 (2012).

122. Frohnert, B. I., Long, E. K., Hahn, W. S. & Bernlohr, D. A. Glutathionylated lipid aldehydes are products of adipocyte oxidative stress and activators of macrophage inflammation. *Diabetes* **63,** 89–100 (2014).

123. Shearn, C. T. *et al.* Deletion of GSTA4-4 results in increased mitochondrial post-translational modification of proteins by reactive aldehydes following chronic ethanol consumption in mice. *Redox Biology* **7,** 68–77 (2015).

124. Wong, H. L. & Liebler, D. C. Mitochondrial protein targets of thiol-reactive electrophiles. *Chem. Res. Toxicol.* **21,** 796–804 (2008).

125. Andringa, K. K., Udoh, U. S., Landar, A. & Bailey, S. M. Proteomic analysis of 4-hydroxynonenal (4-HNE) modified proteins in liver mitochondria from chronic ethanol-fed rats. *Redox Biology* **2,** 1038–1047 (2014).

126. Awada, M. *et al.* Dietary oxidized n-3 PUFA induce oxidative stress and inflammation: role of intestinal absorption of 4-HHE and reactivity in intestinal cells. *J. Lipid Res.* **53,** 2069–2080 (2012).

127. Kristal, B. S., Park, B. K. & Yu, B. P. 4-Hydroxyhexenal is a potent inducer of the mitochondrial permeability transition. *J. Biol. Chem.* **271,** 6033–6038 (1996).

128. Esterbauer, H., Schaur, R. J. & Zollner, H. Chemistry and biochemistry of 4-hydroxynonenal, malonaldehyde and related aldehydes. *Free Radic. Biol. Med.* **11,** 81–128 (1991).

129. Iuchi, S. Three classes of C2H2 zinc finger proteins. *Cell. Mol. Life Sci.* **58,** 625–635 (2001).

130. Ecco, G., Imbeault, M. & Trono, D. KRAB zinc finger proteins. *Development* **144,** 2719–2729 (2017).

131. Urrutia, R. KRAB-containing zinc-finger repressor proteins. *Genome Biol.* **4,** 231 (2003).

132. Kröncke, K.-D. & Klotz, L.-O. Zinc fingers as biologic redox switches? *Antioxidants & Redox Signaling* **11,** 1015–1027 (2009).
133. Pace, N. J. & Weerapana, E. Zinc-binding cysteines: diverse functions and structural motifs. *Biomolecules* **4,** 419–434 (2014).
134. Eichner, L. J. & Giguere, V. Estrogen related receptors (ERRs): a new dawn in transcriptional control of mitochondrial gene networks. *Mitochondrion* **11,** 544–552 (2011).
135. Dixen, K. *et al.* ERRγ enhances UCP1 expression and fatty acid oxidation in brown adipocytes. *Obesity (Silver Spring)* **21,** 516–524 (2013).
136. Kida, Y. S. *et al.* ERRs Mediate a Metabolic Switch Required for Somatic Cell Reprogramming to Pluripotency. *Cell Stem Cell* **16,** 547–555 (2015).
137. Kim, D.-K. & Choi, H.-S. ERRγ: a Junior Orphan with a Senior Role in Metabolism. *Trends in Endocrinology & Metabolism* **28,** 261–272 (2017).
138. Wang, T. *et al.* Estrogen-related receptor α (ERRα) and ERRγ are essential coordinators of cardiac metabolism and function. *Mol. Cell. Biol.* **35,** 1281–1298 (2015).
139. Yoshihara, E. *et al.* ERRγ Is Required for the Metabolic Maturation of Therapeutically Functional Glucose-Responsive β Cells. *Cell Metabolism* **23,** 622–634 (2016).
140. Uchida, K. 4-Hydroxy-2-nonenal: a product and mediator of oxidative stress. *Progress in Lipid Research* **42,** 318–343 (2003).
141. Uchida, K., Szweda, L. I., Chae, H. Z. & Stadtman, E. R. Immunochemical detection of 4-hydroxynonenal protein adducts in oxidized hepatocytes. *Proc. Natl. Acad. Sci. U.S.A.* **90,** 8742–8746 (1993).
142. Hauck, A. K., and Bernlohr, D. A. (2016) Oxidative Stress and Lipotoxicity. *J. Lipid Res.* **57**, 1976–1986.
143. Roberts, C. K. & Sindhu, K. K. Oxidative stress and metabolic syndrome. *Life Sci.* **84,** 705–712 (2009).
144. Hamdy, O., Porramatikul, S. & Al-Ozairi, E. Metabolic obesity: the

paradox between visceral and subcutaneous fat. *Curr Diabetes Rev* **2,** 367–373 (2006).

145. Ilbert, M., Graf, P. C. F. & Jakob, U. Zinc center as redox switch--new function for an old motif. *Antioxidants & Redox Signaling* **8,** 835–846 (2006).
146. Fedotova, A. A., Bonchuk, A. N., Mogila, V. A. & Georgiev, P. G. C2H2 Zinc Finger Proteins: The Largest but Poorly Explored Family of Higher Eukaryotic Transcription Factors. *Acta Naturae* **9,** 47–58 (2017).
147. Garton, M. *et al.* A structural approach reveals how neighbouring C2H2 zinc fingers influence DNA binding specificity. *Nucleic Acids Research* **43,** 9147–9157 (2015).
148. Atsriku, C., Scott, G. K., Benz, C. C. & Baldwin, M. A. Reactivity of zinc finger cysteines: Chemical modifications within labile zinc fingers in estrogen receptor. *J Am Soc Mass Spectrom* **16,** 2017–2026 (2005).
149. Keller, M. P. *et al.* A gene expression network model of type 2 diabetes links cell cycle regulation in islets with diabetes susceptibility. *Genome Res.* **18,** 706–716 (2008).
150. Olefsky, J. M. & Glass, C. K. Macrophages, Inflammation, and Insulin Resistance. *Annu. Rev. Physiol.* **72,** 219–246 (2010).
151. Ros, J., Protein Carbonylation: Principles, Analysis, and Biological Implications. John Wiley & Sons, Inc. (2017).
152. Wong, C.-M. *et al.* Mechanism of protein decarbonylation. *Free Radic. Biol. Med.* **65,** 1126–1133 (2013).
153. Shechter, D., Dormann, H. L., Allis, C. D. & Hake, S. B. Extraction, purification and analysis of histones. *Nature Protocols* **2,** 1445–1457 (2007).
154. INGALLS, A. M., DICKIE, M. M. & SNELL, G. D. Obese, a new mutation in the house mouse. *J. Hered.* **41,** 317–318 (1950).
155. Zhang, Y. *et al.* Positional cloning of the mouse obese gene and its human homologue. *Nature* **372,** 425–432 (1994).

156. Liochev, S. I. Reactive oxygen species and the free radical theory of aging. *Free Radic. Biol. Med.* **60,** 1–4 (2013).
157. Zheng, J., Mutcherson, R. & Helfand, S. L. Calorie restriction delays lipid oxidative damage in Drosophila melanogaster. *Aging Cell* **4,** 209–216 (2005).
158. Zimniak, P. Relationship of electrophilic stress to aging. *Free Radic. Biol. Med.* **51,** 1087–1105 (2011).
159. Ayyadevara, S. *et al.* Life span and stress resistance of Caenorhabditis elegans are differentially affected by glutathione transferases metabolizing 4-hydroxynon-2-enal. *Mech. Ageing Dev.* **128,** 196–205 (2007).
160. Galligan, J. J. *et al.* Stable Histone Adduction by 4-Oxo-2-nonenal: A Potential Link between Oxidative Stress and Epigenetics. *J. Am. Chem. Soc.* **136**, 11864-11866 (2014).
161. Landt, S. G. *et al.* ChIP-seq guidelines and practices of the ENCODE and modENCODE consortia. *Genome Res.* **22,** 1813–1831 (2012).
162. Alessi, M.-C. & Juhan-Vague, I. Metabolic syndrome, haemostasis and thrombosis. *Thromb. Haemost.* **99,** 995–1000 (2008).
163. Saltiel, A. R. & Olefsky, J. M. Inflammatory mechanisms linking obesity and metabolic disease. *J. Clin. Invest.* **127,** 1–4 (2017).
164. James, A. M., Collins, Y., Logan, A. & Murphy, M. P. Mitochondrial oxidative stress and the metabolic syndrome. *Trends in endocrinology and metabolism: TEM* **23,** 429–434 (2012).
165. HARMAN, D. Aging: a theory based on free radical and radiation chemistry. *Journal of gerontology* **11,** 298–300 (1956).
166. Le Lay, S., Simard, G., Martinez, M. C. & Andriantsitohaina, R. Oxidative Stress and Metabolic Pathologies: From an Adipocentric Point of View. *Oxid Med Cell Longev* 1–18 (2014). doi:10.1155/2014/908539
167. Ostan, R. *et al.* Gender, aging and longevity in humans: an update of an intriguing/neglected scenario paving the way to a gender-specific

medicine. *Clin. Sci.* **130,** 1711–1725 (2016).

168. Viña, J., Borrás, C., Gambini, J., Sastre, J. & Pallardó, F. V. Why females live longer than males? Importance of the upregulation of longevity-associated genes by oestrogenic compounds. *FEBS Letters* **579,** 2541–2545 (2005).

169. Huang, H., Sabari, B. R., Garcia, B. A., Allis, C. D. & Zhao, Y. SnapShot: histone modifications. *Cell* **159,** 458–458.e1 (2014).

170. Lu, C. & Thompson, C. B. Metabolic Regulation of Epigenetics. *Cell Metabolism* **16,** 9–17 (2012).

171. Zentner, G. E. & Henikoff, S. Regulation of nucleosome dynamics by histone modifications. *Nat Struct Mol Biol* **20,** 259–266 (2013).

172. Fan, J., Krautkramer, K. A., Feldman, J. L. & Denu, J. M. Metabolic regulation of histone post-translational modifications. *ACS Chem. Biol.* **10,** 95–108 (2015).

173. Sims, R. J., Nishioka, K. & Reinberg, D. Histone lysine methylation: a signature for chromatin function. *Trends Genet.* **19,** 629–639 (2003).

174. Pan, G. *et al.* Whole-genome analysis of histone H3 lysine 4 and lysine 27 methylation in human embryonic stem cells. *Cell Stem Cell* **1,** 299–312 (2007).

175. Zhao, X. D. *et al.* Whole-genome mapping of histone H3 Lys4 and 27 trimethylations reveals distinct genomic compartments in human embryonic stem cells. *Cell Stem Cell* **1,** 286–298 (2007).

176. Black, J. C. & Whetstine, J. R. Chromatin landscape: methylation beyond transcription. *Epigenetics* **6,** 9–15 (2011).

177. Hamanaka, R. B. & Chandel, N. S. Mitochondrial reactive oxygen species regulate cellular signaling and dictate biological outcomes. *Trends Biochem. Sci.* **35,** 505–513 (2010).

178. Liu, W., Porter, N. A., Schneider, C., Brash, A. R. & Yin, H. Formation of 4-hydroxynonenal from cardiolipin oxidation: Intramolecular peroxyl radical addition and decomposition. *Free Radic. Biol. Med.* **50,** 166–178

(2011).

179. Jin, J., He, B., Zhang, X., Lin, H. & Wang, Y. SIRT2 Reverses 4-Oxononanoyl Lysine Modification on Histones. *J. Am. Chem. Soc.* **138,** 12304–12307 (2016).